AN ABSTRACT OF THE THESIS OF

Peter A. Howd for the degree of Doctor of Philosophy in

Oceanography presented on May 6, 1991.

Title: Edge Waves in the Presence of Strong Longshore Currents

Redacted for privacy

Abstract approved:

Robert A. Holman

The wave-induced velocity field in the nearshore is composed of contributions from incident wind waves, surface infragravity waves, and shear waves. Using an alongshore array of current meters located in the trough of a nearshore bar, we investigated the bulk statistical behaviors of these wave bands over a wide range of incident wave conditions. The behavior of each contributing wave type was parameterized in terms of commonly measured or easily predicted variables describing the beach profile, wind waves, and current field.

Incident wave oscillations were limited by depth-dependent saturation over the adjacent bar crest and varied only with the tide. The infragravity wave rms oscillations on this barred beach are best parameterized by the offshore wave height, consistent with previous studies on planar beaches. Comparison with data from four other beaches of widely differing geometries shows the shoreline infragravity amplitude to be a near constant ratio of the offshore wave height, dependent on the Iribarren number, ξ_0 =

$\beta(H/L_0)^{-1/2}$. Shear waves are significantly correlated with a prediction of the seaward-facing shear of the longshore current.

Peculiarities observed in the data lead to the derivation of a form of the linear, inviscid shallow water wave equation which includes arbitrary longshore currents and bathymetry. Interestingly, the current effects can be uniquely accounted for in terms of a modification to the true beach profile, allowing the definition of the 'effective beach profile', $h'(x) = h(x)\left[1 - \frac{V(x)}{c}\right]^{-2}$, where $h(x)$ is the true profile, $V(x)$ is the mean longshore current and c is the edge wave celerity.

The dispersion relationship and the cross-shore shapes of edge waves on a plane beach were solved for under a range of current conditions. Changes to the edge wave alongshore wavenumber, κ, of nearly 100% are found for reasonable current profiles. As expected, as $|\kappa|$ increases (decreases), the cross-shore nodal structure shifts landward (seaward) from the positions found on the test beach in the absence of a current. In addition, the predicted variances away from the nodes, particularly for the alongshore component of edge wave orbital velocity, may change dramatically from the no-current case.

Inclusion of the longshore current also has implications regarding the role of edge waves in the generation of nearshore morphology. The modifications to the wavenumbers of any two phase locked edge wave modes will change the morphology of a potentially resulting sand bar. A more interesting effect is the possibility that modifications to the edge waves due to the presence of a virtual bar in the effective profile could lead to the development of a real sand bar on the true profile. These modifications appear to be only weakly sensitive to frequency, in contrast to the relatively strong dependence of the traditional model for sand bar generation at infragravity wave nodes.

Edge Waves in the Presence of Strong Longshore Currents

by

Peter A. Howd

A THESIS

submitted to

Oregon State University

in partial fulfillment of
the requirements for the
degree of

Doctor of Philosophy

Completed May 6, 1991

Commencement June 1991

APPROVED:

Redacted for privacy

Associate Professor of Oceanography in charge of major

Redacted for privacy

Dean of the College of Oceanography

Redacted for privacy

Dean of Graduate School

Date Thesis Presented May 6, 1991

Typed by Peter A. Howd for Peter A. Howd

ACKNOWLEDGEMENTS

I have been very lucky during the past 15 years, beginning with my undergraduate days, and through two periods each of employment and graduate school, to have been guided by mentors who were not only good scientists, but good people as well. It has made the journey much more enjoyable. Before I start in on my major professor, there are a few other people who were important in my formative years. Over a decade ago, my undergraduate advisor, Bill Fox, encouraged me to apply for a summer job in California with the U.S.G.S. Luckily, Abby Sallenger was looking for someone with a strong back who could swim ropes through the surf zone all day and loose at poker all night. Dr. Fox figured two out of three wasn't bad, so he lied a bit, I went to California, got hooked on nearshore processes and made some extra cash in the evenings.

After graduation, with Abby wanting a chance to recoup some of his losses by playing Acey-Doucey, I went back to California. But after a year or so of enriching the pockets (and minds) of his techs, Abby kicked us all out, muttering something about flinching in the presence of rubber bands and what sounded like "get thee to graduate school". It was then I first met Rob Holman.

There were times in those early years when Rob was getting his program started and establishing himself as one of the leaders in the nearshore community, that if someone had told him "Peter Howd will be your first Ph.D. student, and he won't finish until 1991" he may have given up and fled back to Canada. Luckily he didn't, because the insight he has given me about the art of being a successful research scientist has proven invaluable. I hope the lessons don't end with the submittal this thesis, I still need help with a few of them. So Rob, thanks for taking me on as a student (twice) and giving me a chance. I promise to never embarrass you or use the word "pursuant" again.

Joan Oltman-Shay, with her fountain plots and bountiful enthusiasm, and Tony Bowen, with his incredible insight and a pencil that never seems to dull, have also invested considerable time in my education during the past few years. Curt Mason, Bill Birkemeier, and the rest of the staff at the Field Research Facility in Duck, the best place in the world to acquire field data, hosted the two experiments used in this thesis, and The National Science Foundation, the Office of Naval Research, and the U.S. Geological Survey have all funded me in some way over the course of completing this thesis. And needless to say, none of this work would have been possible without the help of PVO and the guys next door, Chuck, Tom, and Mark, who manage to keep the computers running despite the best efforts of the faculty and students to make it otherwise. I have also had a large and distinguished committee, due to fog in Seattle, sabbatical leaves, and depositions in Miami. I need to thank my permanent members, Joan, Paul Komar, Murray Levine, and Bob Hudspeth for their tolerance, and those that at one time or another filled in on short notice, Bill McDougal, Dudley Chelton, and Vern Kulm. Rob showed up now and again as well.

One of the things that has made Corvallis so enjoyable this time has been the great group of people around the lab who manage to keep their priorities straight. It seemed someone was always ready to either fish, golf, canoe, eat, drink, camp, ski, hike, eat, drink, watch the Ralph Miller and Gary Payton show, go to a gymnastics meet, eat, drink, run the dogs... So thanks to Curt and Carolyn, Mark and Vicki, Todd and Cindy, John and Joan, Dana and David, John and Carla, Dave and ML, Jim and Natalie,Terri and Karl, Jim and Carol, Jon and Jodi, Marcia, Lynn, Linda, all Kathryn's MRM kids, and finally the omnipresent and ever-hungry Tom Lippmann, who can rest assured that I will always remember his birthday is December 3. Y'all made it fun!

Thanks most of all to Kathryn, I never would have made it without you.

TABLE OF CONTENTS

CHAPTER ONE: GENERAL INTRODUCTION 1

CHAPTER TWO: WAVE VARIANCE PARTITIONING IN THE TROUGH OF A BARRED BEACH 7
- Abstract 7
- Introduction 9
- Methods 13
- Results 19
  - *Statistics* 19
  - *Parameterization* 24
- Discussion 36
- Summary 42
- References 44

CHAPTER THREE: EDGE WAVES IN THE PRESENCE OF STRONG LONGSHORE CURRENTS 47
- Abstract 47
- Introduction 49
- Theory 52
- Results 58
  - *Effects on dispersion* 60
  - *Effects on cross-shore structure* 63
- Discussion 71
  - *Implications for field data* 71
  - *Modification of topography* 81
- Summary 89
- References 92

CHAPTER FOUR: INFRAGRAVITY WAVES, LONGSHORE CURRENTS, AND LINEAR SAND BAR FORMATION 95
- Abstract 95
- Introduction 96
- Theory 98
- Field Study 105
- Results 108
- Summary 117
- References 118

CHAPTER FIVE: GENERAL CONCLUSIONS 120

BIBLIOGRAPHY 124

LIST OF FIGURES

Figure		Page
I.1	A schematic representation of the behavior of incident wind waves and infragravity waves in the surf zone.	2
II.1	Plan view of the SUPERDUCK field site at the Coastal Engineering Research Center's Field Research Facility in Duck, North Carolina.	14
II.2	Cyclic alongshore wavenumber ($k = 1/L$) vs. frequency ($f = 1/T$) spectra for with lines showing the bounds of each of the three wave types.	16
II.3	Time series of 4-hour mean statistics for wave parameters at the offshore array pressure sensors and for the current meters/pressure sensor in the surf zone.	22
II.4	The percent contributions made by each band to the total variance of the cross-shore component (top) and the longshore component (bottom)	23
II.5	The magnitude of the incident band rms wave height measured in the trough plotted versus the tide elevation.	26
II.6	u_{IG} (top) and v_{IG} (bottom) plotted versus the offshore wave height, H_{rms}.	27

II.7 The dependence of rms infragravity oscillations on the absolute value of the incident direction, $|\alpha|$, for $H_{rms} > 125$ cm. 30

II.8 u_{SW} (top) and v_{SW} (bottom) plotted versus the absolute value of the measured mean longshore current, $|\langle V \rangle|$. 31

II.9 Model results for H, V_M, and $\partial V_M/\partial x$ on a measured profile. 34

II.10 u_{SW} and v_{SW} plotted versus $|\partial V_M/\partial x|$, the absolute value of the modeled maximum current shear seaward of the bar crest. 35

II.11 Comparison of u_{IG} oscillations from 5 beaches plotted versus the offshore wave height (top) and scaled to estimate the 'equivalent shoreline height' $\hat{H}_{IG} = 2\hat{a}_{IG}$ of the infragravity oscillations (bottom). 38

II.12 Regression slopes for the five beaches (with 95% error bars) as a function of the mean Iribarren number (± 1 st. dev.) for that beach. 41

III.1 Modifications to the nearshore wave guide by the presence of a longshore current is analogous to that of bar and trough topography. 53

III.2 Current profiles used for the test cases 59

III.3 The effective beach profiles for 0.010 Hz mode 0 edge waves for current run 2. 61

III.4 The effect on dispersion, K, for each current group, as a function of frequency for the mode 0 edge waves. 62

III.5 The effect on dispersion for modes 0-4 for current Run 2 64

III.6 K vs. $|\kappa|x(V_{max})$ for the mode 0 edge waves 65

III.7 Cross-shore profiles of surface elevation (top), cross-shore velocity (middle) and longshore velocity (bottom) for the mode 2 edge waves at 0.05 Hz for current Run 2. 67

III.8 A comparison between the cross-shore profiles of η (upper), u (middle), and v (lower), (the dashed lines) in the presence of a current (Run 2) with the solutions assuming a plane beach of slope β_{eff} (solid lines). 68

III.9 $v(x)$ profiles for the first three modes at $f = 0.01$ Hz for current Run 2. 69

III.10 Morphology and sensor locations for October 11, 1990 at the DELILAH experiment 72

III.11 Beach and longshore current profiles used to solve for edge wave characteristics on October 11, 1990. 74

III.12 Frequency-wavenumber spectrum from October 11, 1990 75

III.13 K vs. f for the field data from October 11, 1990 77

III.14 Variance of the longshore component of edge wave flow vs. frequency for the first three modes at the cross-shore location of the array. 79

III.15 Wavenumber spectra for two frequency bands 0.021 Hz (upper

panel) and 0.040 Hz (lower panel). 80

III.16 Profiles of the perturbation topography for edge waves progressing with the current resulting from the introduction of a longshore current. 85

III.17 Total profiles $(h + \hat{h})$ for all edge waves modeled in Run 2 (modes 0 to 4) progressing with the current and with f less than or equal to 0.05 Hz 86

III.18 Same as Figure II.17, but for the edge waves progressing into the current. 87

IV.1 The nearshore wave guide for the simple case of a plane sloping beach. 99

IV.2 Modification of the nearshore wave guide by either sand bars or longshore currents 100

IV.3 Effective beach profiles for a mode 2 edge wave in the presence of a longshore current. 103

IV.4 Layout of the DELILAH instrument array at the FRF. 106

IV.5 Time series of incident wave parameters and wind speed and direction. 109

IV.6 Beach profile evolution 110

IV.7 Evolution of the mean longshore current during the period of active sand bar migration. 112

IV.8 Frequency-wavenumber spectra from late on October 10. 113

IV.9 Evolution of the effective beach profile through the storm. 115

IV.10 The offshore migration of the effective bar crest clearly leads the offshore migration of the true bar crest 116

LIST OF TABLES

Table		Page
II.1	BASIC ENVIRONMENTAL CONDITIONS	20
II.2	BASIC STATISTICS	21
II.3	REGRESSION RESULTS	25
II.4	IRIBARREN REGRESSION RESULTS	29
II.5	DIRECTIONAL DEPENDENCE	29
II.6	INTERCOMPARISON OF BEACHES	39

EDGE WAVES IN THE PRESENCE OF STRONG LONGSHORE CURRENTS

CHAPTER ONE: GENERAL INTRODUCTION

The problem of coastal erosion has become a matter of national concern amid growing speculation of global warming and associated sea-level rise. While the slowly advancing ocean is no doubt partially to blame for the problem, we most commonly associate erosion of the coastline with the passage of major storms or hurricanes. These dramatic events provide the big waves to move the sand. However, as we will see, it is not altogether obvious which waves are responsible for determining where the sand goes.

Incident wind waves, the waves we see approaching the beach from the open ocean, are depth limited in shallow water, giving a linear, empirical relationship between water depth, h, and the wave height, H

$$H = \gamma h \tag{I.1}$$

so that at the shoreline, where $h = 0$ by definition, we expect the incident wave height to be very near zero. The primary effect of increasing the incident wave height during a storm is simply to increase the width of the surf-zone; waves begin to break further offshore (Figure I.1).

As field data were collected from natural beaches, waves with much lower frequencies than the incident waves were discovered. These infragravity waves, with periods generally ranging from 20 to 300 seconds, posess the unique characteristic of having their maximum amplitude at the shoreline (on a plane sloping beach), rather than offshore. The observation that these waves are not depth limited in the manner of inci-

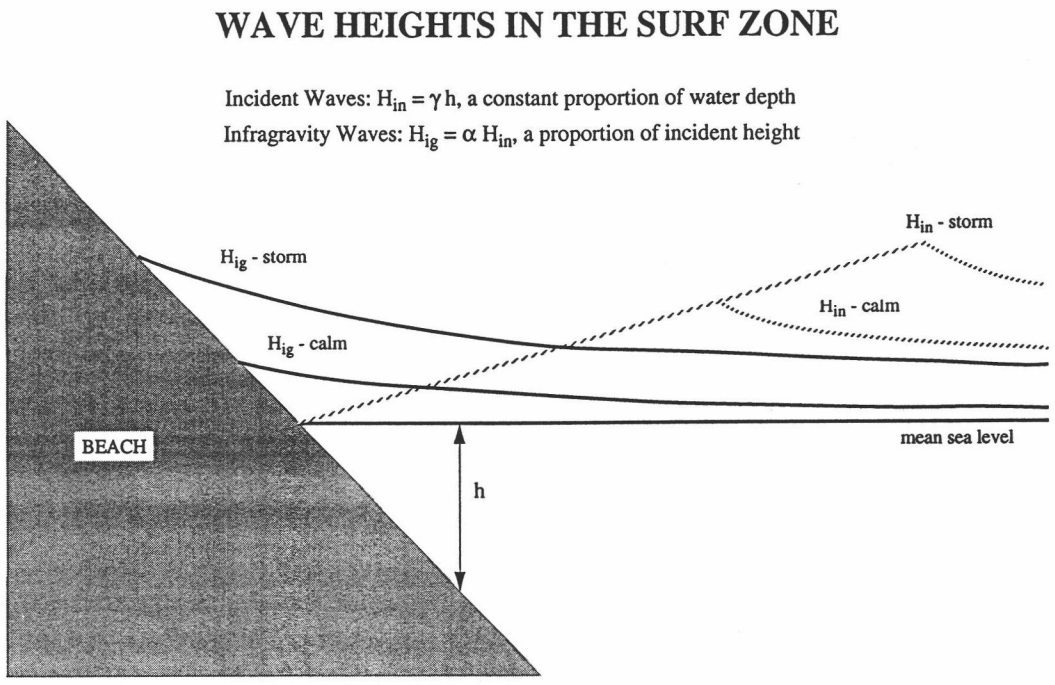

Figure I.1. A schematic representation of the behavior of incident wind waves and infragravity waves in the surf zone. During a storm, the maximum incident height increases, resulting in an increase in surf-zone width and infragravity wave height, but the depth-limited behavior of the incident waves gives an unchanged wave height decay through the inner portion of the breaker zone.

dent waves means that if they become large they may become more important than the incident waves at the shoreline, the biting edge where erosion occurs.

Numerous authors have since proposed that infragravity waves play an important role in a number of specific nearshore processes, including mean circulation patterns [*Bowen and Inman*, 1969], the generation of nearshore morphology [*Holman and Bowen*, 1982], and momentum and energy transfer [*Elgar and Guza*, 1985]. Studies have shown that the shoreline expression of wave energy, the swash, can be dominated by infragravity motions, with magnitudes of up to 70% of the incident gravity waves offshore [*Holman and Sallenger*, 1985]. They are also an energetic part of the wave spectrum in the surf zone, with their amplitudes a nearly linear function of the offshore height of the incident waves [*Holman*, 1981; *Guza and Thornton*, 1985; *Howd et al.*, 1991*a*].

This thesis has three primary objectives. The first is to provide an overview of the contributions of these different waves to the total current variance on a barred beach, concentrating on the infragravity wave field. The second objective is to determine the effects of the longshore current on edge wave dynamics and kinematics. The third objective is to determine if the interaction of the mean longshore current and the edge waves provides a mechanism for the generation or evolution of nearshore bathymetry.

Chapter Two, titled "Wave Variance Partitioning in the Trough of a Barred Beach", has been accepted for publication in the Journal of Geophysical Research [*Howd et al.*, 1991*a*], and is co-authored by Dr. Joan Oltman-Shay, who provided many of the software tools used in the data analysis, and Dr. Rob Holman, who provided a great deal to the evolution of the text into its present form. This chapter provides an introduction to the different bands of wave motion on a beach, followed by a discussion of the partitioning of variance between them on a barred beach. We determine that in-

fragravity waves are an important contributor to the total current variance in the surf zone.

Over the 10 day period, the mean contributions (to the total variance) of the infragravity band at a location approximately 55 m from the shoreline were 14.3% for the alongshore component of flow (mean rms oscillation 20 cm s^{-1}), and 10.9% for the cross-shore component (mean rms oscillations of 32 cm s^{-1}). However, the values varied considerably. The contribution to the alongshore (cross-shore) component of flow ranged from 6.2%-26.6% (2.5%-32.4%). Incident wave oscillations, as expected, were limited by depth-dependent saturation and varied with the tide. The infragravity wave rms oscillations on this barred beach are best parameterized by the offshore wave height, consistent with previous studies on planar beaches.

Chapter Three, titled "Edge Waves in the Presence of Strong Longshore Currents", presents the linear theory for edge waves coexisting with large mean longshore currents. It will be submitted to the Journal of Geophysical Research with co-authors Dr. Tony Bowen and Dr. Rob Holman. Dr. Bowen collaborated on the development of the theory during his sabbatical year at Oregon State University. Dr. Holman kept the numerical approach on target, and his clear thinking helped discussions of the relevant physics.

In this chapter we explore the expectation that longshore currents modify refraction in the nearshore wave guide, changing the dynamics and kinematics of infragravity edge waves. A form of the linear, inviscid shallow water wave equation which includes arbitrary longshore currents and bathymetry is derived. This formulation provides a continuum between gravity waves (either leaky or edge waves) on a longshore current, and the recently discovered shear waves. This thesis will concentrate on gravity wave solutions for which $V/c < 1$, where V is the longshore current, and c is the edge wave

alongshore celerity. Interestingly, for gravity waves, the current effects can be uniquely accounted for in terms of an apparent modification of the true beach profile, allowing the definition of the "effective beach profile", $h'(x) = h(x)\left[1 - \frac{V(x)}{c}\right]^{-2}$, where $h(x)$ is the true profile. The effective profile is particularly useful in conceptualizing the combined effects of longshore currents and variable bottom topography.

To test the sensitivity of edge waves to mean longshore currents, numerical solutions for the dispersion relationship and the cross-shore shapes of edge waves on a plane beach are found under a range of current conditions. Changes to the edge wave alongshore wavenumber, κ, of nearly 100% are found for reasonable current profiles, showing that the departure from plane beach dispersion due to longshore currents can be of the same order as the effect of introducing non-planar topography. These changes are not symmetric as they are for profile changes; $|\kappa|$ increases for edge waves opposing the current flow (a shallower effective profile), but decreases for those coincident with the flow (a deeper effective profile). The cross-shore structure of the edge waves is also strongly modified. As expected, as $|\kappa|$ increases (decreases), the nodal structure shifts landward (seaward) from the positions found on the test beach in the absence of a current. In addition, the predicted variances away from the nodes, particularly for the alongshore component of edge wave orbital velocity, may change dramatically from the no-current case. Failure to account for these changes can lead to incorrect identification of modes and large errors in the estimation of the corresponding shoreline amplitude.

Inclusion of the longshore current also has implications regarding the role of edge waves in the generation of nearshore morphology. The modifications to the wavenumbers of any two phase locked edge wave modes will change the morphology of a potentially resulting sand bar. For example, in the absence of a current, two phase locked

edge waves of equal frequency and mode progressing in opposite directions are expected to produce a crescentic bar. However, in the presence of a current, the wavenumbers would differ, stretching the expected crescentic bar into a welded bar. A more interesting effect is the possibility that modifications to the edge waves due to the presence of a virtual bar in the effective profile could lead to the development of a real sand bar on the true profile. These modifications appear to be only weakly sensitive to frequency, in contrast to the relatively strong dependence of the traditional model for sand bar generation at infragravity wave nodes.

Chapter Four, titled "Infragravity Waves, Longshore Currents, and Linear Sand Bar Formation", which will appear in the Proceedings of Coastal Sediments '91 [*Howd et al.*, 1991*b*], looks at beach profile evolution during a large field experiment in light of the model presented in Chapter Two. The findings, while preliminary, support the new model. The paper relies on the techniques and models of Chapters One and Two, and is thus co-authored by Drs. Bowen, Holman, and Oltman-Shay.

CHAPTER TWO:

WAVE VARIANCE PARTITIONING IN THE TROUGH OF A BARRED BEACH

Abstract

The wave-induced velocity field in the nearshore is composed of contributions from incident wind waves ($f > 0.05$ Hz), surface infragravity waves ($f < 0.05$ Hz, $|\kappa| < (\sigma^2/g\beta)$ and shear waves ($f < 0.05$ Hz, $|\kappa| > \sigma^2/g\beta$), where f is the frequency, $\sigma = 2\pi f$, κ the radial alongshore wavenumber ($2\pi/L$, L being the alongshore wavelength), β is the beach slope, and g is the acceleration due to gravity. Using an alongshore array of current meters located in the trough of a nearshore bar (mean depth ≈ 1.5 m), we investigate the bulk statistical behaviors of these wave bands over a wide range of incident wave conditions. The behavior of each contributing wave type is parameterized in terms of commonly measured or easily predicted variables describing the beach profile, wind waves, and current field.

Over the 10 day period, the mean contributions (to the total variance) of the incident, infragravity and shear wave bands were 71.5%, 14.3% and 13.6% for the alongshore component of flow (mean rms oscillations of 44 cm s^{-1}, 20 cm s^{-1}, and 19 cm s^{-1} respectively), and 81.9%, 10.9%, and 6.6% for the cross-shore component (mean rms oscillations of 92 cm s^{-1}, 32 cm s^{-1}, and 25 cm s^{-1}, respectively). However, the values varied considerably. The contribution to the alongshore (cross-shore) component of flow ranged from 44.8%-88.4%, (58.5%-95.8%) for the incident band, 6.2%-26.6% (2.5%-32.4%) for the infragravity band, and 3.4%-33.1% (0.6%-14.3%) for the shear wave band.

Incident wave oscillations were limited by depth-dependent saturation over the

adjacent bar crest and varied only with the tide. The infragravity wave rms oscillations on this barred beach are best parameterized by the offshore wave height, consistent with previous studies on planar beaches. Comparison with data from four other beaches of widely differing geometries shows the shoreline infragravity amplitude to be a near constant ratio of the offshore wave height. The magnitude of the ratio is found to be dependent on the Iribarren number, $\xi_0 = \beta(H/L_0)^{-1/2}$. Shear waves are, as previous observation and theory suggest [*Oltman-Shay et al.*, 1989*a*; *Bowen and Holman*, 1989], significantly correlated with a prediction of the seaward-facing shear of the longshore current.

Introduction

For nearly two decades one of the primary interests in the study of nearshore processes has been the characterization of two frequency bands of gravity waves, incident wind waves (0.33 Hz > f > 0.05 Hz) and infragravity waves (f < 0.05 Hz). The recent discovery of a third "band", shear waves, [*Oltman-Shay et al.*, 1989*a*; *Bowen and Holman*, 1989] has added a new twist to the difficult problem of quantifying wave energy in the nearshore.

This chapter has two primary objectives. The first is to provide an overview of the variance contributions of these different waves in the trough of a barred beach. Of particular interest is the contribution of shear waves, which has not been previously quantified. The second objective is to examine the lowest order controls of infragravity wave variance on a barred beach with strong longshore currents and compare our findings with those of previous studies. In the remainder of this section we will review some of the relevant literature concerning the three wave types and their behaviors in the surf zone. We then discuss the acquisition and analysis techniques for the present data, followed by the presentation of our findings and a comparison with other field data.

It has been consistently shown that statistical measures of incident wind wave height become depth-limited in the inner surf zone of natural beaches, and thus independent of the offshore wave height, according to the linear relation

$$H_{rms} = \gamma h \qquad \text{(II.1)}$$

where $H_{rms} = (8s^2)^{1/2}$, where s^2 is the incident wave variance, and h is the local water depth. For monochromatic laboratory waves *Galvin and Eagleson* [1965] found γ to have a value ranging from 0.7 to 1.2. For field data, *Thornton and Guza* [1982] found

γ to be much lower, approximately 0.42. Many researchers have reported γ to be a function of beach slope and/or wave steepness [*Bowen et al.*, 1968; *Weishar and Byrne*, 1978; *Sallenger and Holman*, 1985*b*]. Statistical representations of random waves from field experiments include both broken and unbroken waves, one reason why the saturation value of γ is significantly lower for field data than for monochromatic laboratory waves.

Infragravity waves are traditionally considered to be those surface gravity waves which result from the second order interaction of incident wind waves. Under most conditions in surf zones on coasts open to the ocean, these waves have frequencies ranging from 0.005 to 0.05 Hz. The free infragravity waves can be broken into two distinct groups, a discrete set of edge wave modes which are trapped to the shoreline, and a continuum of leaky waves which reflect from the shoreline and radiate energy back out of the nearshore zone. Bound waves, the forced displacement of the free water surface by the structure of wave groups [*Longuet-Higgins and Stewart*, 1964], also contribute to infragravity wave energy [*Guza et al.*, 1985; *Elgar and Guza*, 1985].

Edge waves on a plane beach of slope β have a discrete set of possible alongshore wavenumbers, κ, in the range $\sigma^2/g \leq |\kappa| \leq \sigma^2/g\beta$ satisfying the relationship $\sigma^2 = g|\kappa|(2n+1)\beta$ [*Eckart*, 1951], while for leaky waves there is a continuum with $|\kappa| < \sigma^2/g$ [*Suhayda*, 1974; *Guza and Bowen*, 1976]. Bound waves have no constraint on κ. Analytic solutions to the linear, shallow water equations of motion on a plane sloping beach give the free wave velocity potential, Φ, as

$$\Phi = ag/\sigma \cos(\kappa y - \sigma t)\, \phi(x) \qquad \text{(II.2)}$$

where x is the cross-shore coordinate, y the alongshore coordinate, and a is the wave amplitude at the shoreline [*Eckart*, 1951; *Suhayda*, 1974; and *Guza and Bowen*, 1976].

The cross-shore nodal structure, $\phi(x)$, follows

$$\phi(x) = \begin{cases} e^{-\kappa x} L_n(2\kappa x) & \text{edge waves} \\ J_0\left(\frac{4\sigma^2 x}{g\beta}\right)^{1/2} & \kappa=0 \quad \text{leaky wave} \end{cases} \tag{II.3}$$

with L_n being the Laguerre polynomial of order n (where n is the mode number of the edge wave) and J_0 is the zeroth order Bessel function. The cross-shore structure of the higher mode edge waves ($n > 2$) and the normally incident leaky wave are very similar near the shoreline and can be represented by the J_0 solution for approximate calculations [*Holman*, 1981; *Sallenger and Holman*, 1985*a*].

The cross-shore structure of infragravity waves has made frequency spectra of surf-zone currents difficult to interpret and compare between beaches. Wavenumber-frequency spectra estimated from cross-shore currents are also difficult to interpret, being dominated by some unresolved combination of high mode edge waves, leaky waves, phase-locked edge waves, and bound waves [*Elgar and Guza*, 1985; *Oltman-Shay and Guza*, 1987; *Huntley*, 1988; *Haines and Bowen*, 1988]. However, wavenumber-frequency spectra of the alongshore component of currents have been shown to be particularly useful in determining the progressive low mode edge wave content of the infragravity wave field [*Huntley et al.*, 1981; *Oltman-Shay and Guza*, 1987].

Past field studies have shown a dependence between the magnitude of the local infragravity wave oscillations, u_{IG} and a_{IG} (the cross-shore oscillation and the wave amplitude), and the offshore wind wave height [*Holman*, 1981; *Guza and Thornton*, 1985]. *Holman and Sallenger* [1985] and *Sallenger and Holman* [1985*a*] concluded that the dependence was also function of the deep water Iribarren number, $\xi_0 = \beta/(H/L_0)^{1/2}$, where H and L_0 are representative of the deepwater height and wavelength of the incident waves, and of the dimensionless cross-shore distance, $\chi = \sigma^2 x/g\beta$, to the

location of the measurements

$$u_{IG} = m_u(\chi, \xi_0) H \tag{II.4}$$

and

$$a_{IG} = m_a(\chi, \xi_0) H \tag{II.5}$$

where m is the slope of the linear regression.

Shear waves, a new class of nearshore wave, are distinguished by large wavenumbers, well outside the wavenumber range of gravity waves, $|\kappa| > \sigma^2/g\beta$ [*Oltman-Shay et al.*, 1989*a*]. On the one beach studied to date, a typical energetic period is 200 s with an alongshore wavelength of 200 m. This distinctive signature permits their contribution to total current variance to be separated in wavenumber-frequency space. *Bowen and Holman* [1989] show theoretically that these waves may be an instability of the mean longshore current which conserves potential vorticity. The cross-shore shear of the mean longshore current provides the background vorticity (the role of Coriolis in larger scale flows). Using a simple model, they show there is a frequency range where a perturbation to the mean current (the shear wave) will grow exponentially at a rate which depends on the magnitude of the shear on the seaward face of the current ($\partial V/\partial x|_{SEAWARD}$). While only the growth rate is predicted, we will test the assumption that the rms velocities of the shear waves also scale as the maximum seaward shear of the longshore current

$$u_{SW} = m_{SW} \left.\frac{\partial V}{\partial x}\right|_{SEAWARD} \tag{II.6}$$

Methods

In this section we first briefly describe the field site, the instrumentation used in this study, and the data sampling. Then we present the analysis techniques and the sensitivity of these techniques to different processing options.

The data used for this study were collected as part of the SUPERDUCK experiment [*Crowson et al.*, 1988] hosted by the Coastal Engineering Research Center's Field Research Facility (FRF) in Duck, North Carolina during October, 1986 (Figure II.1). The beach is located near the center of a 100-km-long barrier island. The mean slope is approximately 1 in 10 on the foreshore, decreasing offshore to 1 in 100. Sand bars are consistently present, most commonly in a 3-dimensional configuration which becomes linear during most storm events [*Lippmann*, 1989]. The extreme tide range during the experiment was 137 cm.

An array of 10 Marsh-McBirney bidirectional electromagnetic current meters was deployed approximately 55 m seaward of the mean shoreline position in the trough of a nearshore bar system. The depth ranged from ~0.5 m to ~2.5 m over the course of this study. Only the 7 southernmost sensors were used in this study to minimize spatial inhomogeneity. The sampled array was thus 290 m in length, sufficient to resolve typical wavelengths at this site [*Oltman-Shay et al.*, 1989*a*]. Sensors were oriented such that their axes coincided with the longshore (+v currents flow north) and cross-shore (+u currents flow offshore) directions. All gages remained submerged at low tide.

Complementary data were collected by other investigators. A pressure sensor (maintained by Asbury Sallenger, Jr., U. S. Geological Survey) was located 3 m south of the central current meter. The wind wave climate was sampled in 8-m depth using a 255-m-long array of bottom mounted pressure sensors as part of the routine monitoring

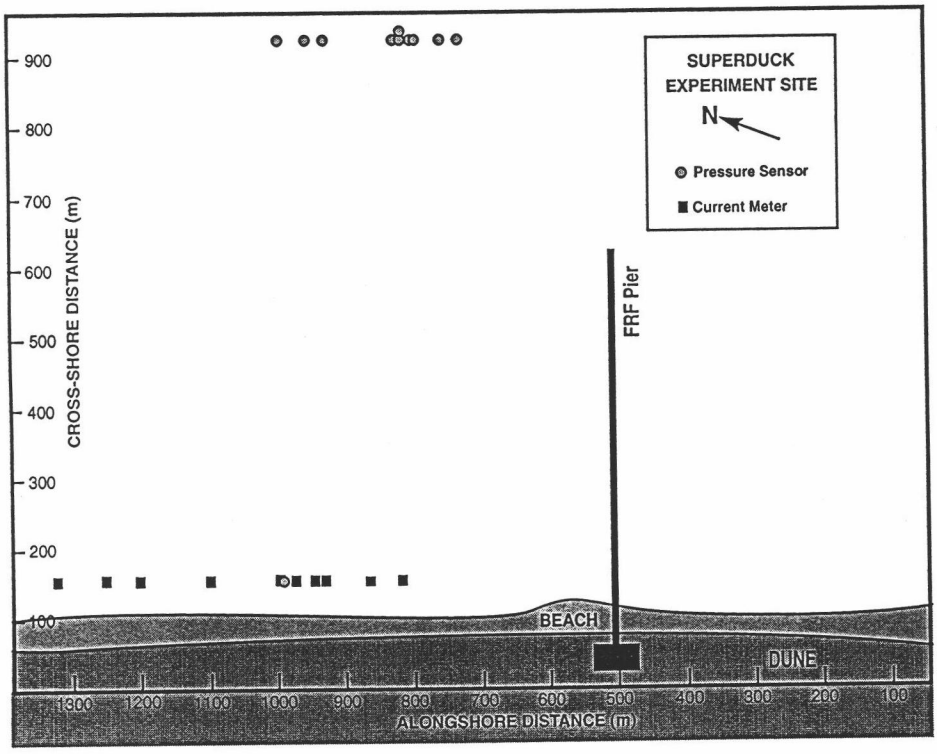

Figure II.1. Plan view of the SUPERDUCK field site at the Coastal Engineering Research Center's Field Research Facility in Duck, North Carolina. Shown are the nearshore current meter array, the nested pressure sensor and the offshore wind wave directional array relative to the location of the pier. All measurements were made outside the known region of the pier's influence.

program of the FRF. The surf-zone morphology was measured using the FRF CRAB (Coastal Research Amphibious Buggy, *Birkemeier and Mason*, 1984).

All current meters and pressure sensors were hard-wired to the data collection system. Gages were sampled at 2 Hz for 4 hours centered on high and low tides. High quality data from the majority of the gages were collected for 10 days, with the exception of approximately 22 hours lost due to a power failure. Each time series was exhaustively checked for reliability in both time and frequency domains. Suspect gages were excluded from further analysis as were time periods marked by large spatial inhomogeneities or temporal non-stationarity. From a total of 36 collections, 21 were processed further.

The current meter array data were used to calculate the alongshore wavenumber-frequency spectra for both the cross-shore and alongshore components of flow. First, each of the 21 time series was divided into 13 ensembles with 50% overlap, 2048 s in length, demeaned and then detrended (using a least-squares quadratic fit) prior to being tapered with a Kaiser-Bessel window. Wavenumber-frequency spectra were estimated using the Iterative Maximum Likelihood Estimator (IMLE) developed by *Pawka* [1982, 1983] and previously applied to surf zone data by *Oltman-Shay and Guza* [1987] and *Oltman-Shay et al.* [1989*a*].

Variance for each 4-hour run was then partitioned between the three bands in wavenumber-frequency space (Figure II.2). Integrated variances for each band were given by

$$s^2_{INC} = \int_{0.05}^{0.33} \int_{-\kappa_{NY}}^{+\kappa_{NY}} S(\kappa, f)\, d\kappa df \qquad \text{(II.7)}$$

$$s^2_{IG} = \int_{0}^{0.05} \int_{(-\kappa_0 - \delta)}^{(\kappa_0 + \delta)} S(\kappa, f)\, d\kappa df \qquad \text{(II.8)}$$

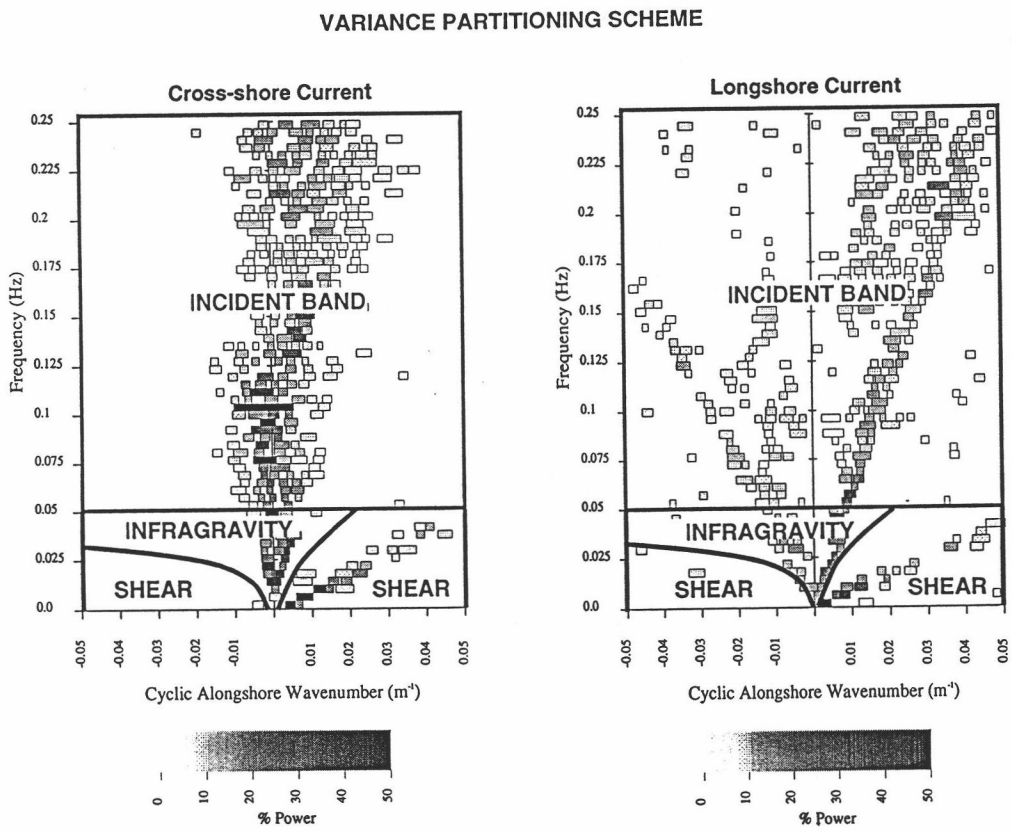

Figure II.2. Cyclic alongshore wavenumber ($k = 1/L$) vs. frequency ($f = 1/T$) spectra for with lines showing the bounds of each of the three wave types. The boxes represent peaks in $S(k,f)$ with the darkness indicating the percent of variance in that frequency band contained in that peak. The width of the box indicates the half- power wavenumber bandwidth. The array was designrd for infragravity frequencies, thus the incidend band is shown for reference only. Left: Estimate from cross-shore (u) current. Right: Estimate from longshore (v) current.

$$s^2_{SW} = \int_0^{0.05} \int_{-\kappa_{NY}}^{\kappa_{NY}} S(\kappa, f)\, d\kappa df - s^2_{IG} \qquad \text{(II.9)}$$

where s^2 is the integrated variance for each of the bands, κ_{NY} is the nyquist radial wavenumber of the array, $\pm\kappa_0$ are the estimated mode zero wavenumbers, δ is a constant wavenumber offset used to account for wavenumber bandwidth of the mode 0 spectral peak (set at 0.0094 m^{-1} in radial units; this accounts for the variation in κ from the bottom of the frequency bin to the top, see *Oltman-Shay and Guza*, 1987) and $S(\kappa,f)$ is the spectral density. The subscripts refer to the incident (INC), infragravity (IG), and shear wave (SW) bands, respectively.

The incident band integration limits (in frequency) were chosen based on the spectral characteristics of the offshore pressure gage array data. The upper limit, 0.33 Hz, was the highest frequency for which the depth attenuated wave signals reliably exceeded instrument noise. The lower limit (0.05 Hz) was chosen such that all wind wave variance would be excluded from estimates of the infragravity motions (but not the opposite). Examination of spectra from the 8 m array showed no energetic swell at frequencies below 0.05 Hz. The 0.05 Hz cutoff results in a small underestimate of the infragravity band variance.Varying the cutoff from 0.04 to 0.06 Hz resulted in typical changes of ±5% of the total variance, with the trade always being between incident and infragravity regimes. The results were not sensitive to reasonable choices for δ.

The wavenumber limits for the infragravity band calculation are based on estimates of $\pm\kappa_0$, the largest wavenumbers possible for free surface gravity waves (the plus and minus signs indicating direction of propagation). We have assumed $\pm\kappa_0$ can be closely approximated by the plane beach solution with a simple correction for the mean longshore current

$$\pm\kappa_0 = \frac{(\sigma - (\pm\kappa_0)\, V)^2}{g\beta} \qquad \text{(II.10)}$$

Kenyon [1972] demonstrated that the dispersion curve for the mode 0 edge wave, in the presence of a current with constant shear, behaves as if it were Doppler shifted, as above, by the longshore current at an offshore distance of $L/4\pi$, which is approximately 33 m for the 'typical' mode 0 edge wave in this study. This behavior has also been reported by *Oltman-Shay and Guza* [1987] for field data. Values chosen for the beach slope and mean longshore current at $x = 33$ m were based on average values over the length of the alongshore array. A constant β was chosen to match the observed mode 0 dispersion lines.

Tests were conducted concerning the sensitivity of the analysis to different data windows and ensemble length, detrending, and changes in the wavenumber/frequency partitioning scheme. There were no statistically significant differences from varying the ensemble and window characteristics. As expected, detrended data contained less total variance than data with trends, but the differences occurred only in the lowest frequency bin.

Results

Statistics. Tables II.1 and II.2 and Figures II.3 and II.4 present a summary of basic wave and current statistics. In all cases, the root mean square (rms) statistics, calculated as $(8s^2)^{1/2}$, are presented for wave heights and current oscillations. Because of the processing techniques, rms current oscillations represent the average over the array. Percent contributions always refer to the percent of total variance contributed by the band.

The data cover a wide range of conditions, with H_{rms} in 8 m-water-depth ranging from 30 cm to over 215 cm (significant heights in excess of 300 cm), the peak period varying from 4.4 s to 12.0 s, and the mean longshore current averaged over the current meter array, $\langle V \rangle$, ranging from -159 cm s^{-1} (southward) to +31 cm s^{-1} (northward).

Statistics for the rms oscillations in each band are found in Table II.2. Mean values (±1 standard deviation) over the experiment for u_{INC} and v_{INC} are 92 ± 11 cm s^{-1} and 44 ± 9 cm s^{-1} with maxima of 108 cm s^{-1} and 61 cm s^{-1} respectively. Mean values of the u and v infragravity wave oscillations (u_{IG} and v_{IG}) were 32.1 ± 16.0 cm s^{-1} and 20.2 ± 7.8 cm s^{-1} with maxima of 62.5 cm s^{-1} and 32.6 cm s^{-1}, respectively. The mean shear wave oscillations were 25.1 ± 10.6 cm s^{-1} and 19.5 ± 7.3 cm s^{-1} for u_{SW} and v_{SW}. Maxima were 41 cm s^{-1} and 35 cm s^{-1} respectively.

The percent contributions of each band to the total variance are shown in Figure II.4. The incident band oscillations on average provided 71.5% of the alongshore current variance and 81.9% of the cross-shore current variance. The percent contribution of the infragravity band waves ranged from 6.2% to 26.6% of the longshore variance and from 2.5% to 32.4% of the cross-shore variance at the surf zone location of the alongshore array. Shear wave oscillations contributed up to 33.1% of the total long-

TABLE II.1

BASIC ENVIRONMENTAL CONDITIONS

Run/Day/Time/Tide	H (cm)	T (s)	α (o)	H_{INC} (cm)	$\langle U \rangle$ (cm/s)	$\langle V \rangle$ (cm/s)
1 9 0930 H	57.8	6.4	-31.9		- 4.5	16.3
2 9 2200 H	35.8	5.8	-29.9	19.6	2.8	3.6
3 10 1030 H	184.2	7.3	24.3	53.5	31.5	-159.3
4 10 1700 L	205.5	7.9	16.0	36.4	12.9	-114.4
5 10 2320 H	216.5	8.9	8.9	55.8	22.2	-88.1
6 11 0540 L	216.2	9.7	4.2	35.0	7.5	-52.7
7 11 1200 H	213.7	9.7	4.9	69.4	23.6	-41.3
8 11 1820 L	190.3	10.0	0.3	35.7	3.6	-13.0
9 12 0040 H	172.6	11.9	-3.7	61.3	14.4	30.5
10 13 0130 H	126.2	12.0	-10.4	57.2	16.4	29.1
11 14 1500 H	57.1	9.7	-25.3	49.6	4.8	21.4
12 15 0330 H	110.5	5.5	36.1	63.3	8.9	-87.1
13 15 0945 L	96.2	6.0	25.0	23.3	5.9	-91.1
14 15 1600 H	71.3	6.4	22.7	49.8	5.0	-35.5
15 15 2200 L	71.4	4.4	25.8	20.2	2.8	-64.2
16 16 0400 H	79.3	4.6	27.9	50.5	5.0	-40.0
17 16 1630 H	75.8	5.2	24.4	45.3	4.9	-35.3
18 16 2240 L	69.1	5.5	16.5	21.4	3.8	-52.8
19 17 0450 H	75.5	5.1	18.4	48.5	5.2	-29.5
20 17 1100 L	70.1	5.8	6.6	21.4	3.7	-40.7
21 18 0530 H	91.3	9.7	20.4	51.8	9.6	-45.3

Day - Day of the month October 1986
Time - Hours Eastern Standard Time
Tide - H = High L = Low
H - Incident Root Mean Square wave height in 8 m depth
T - Peak spectral period in 8 m water depth
α - Median spectral direction in 8 m water depth (CCW from shore normal)
H_{INC} - Incident Root Mean Square wave height in the surf zone (from pressure)
$\langle U \rangle$ - Mean cross-shore current averaged over the array of current meters
$\langle V \rangle$ - Mean longshore current averaged over the array of current meters

TABLE II.2

BASIC STATISTICS

	MEAN	ST. DEV.	MAXIMUM	MINIMUM
OFFSHORE				
H_{rms} (cm)	118.4	61.1	216.5	35.8
T (s)	7.5	2.3	12.0	4.4
α (^{o})	-8.3	19.1	6.1	-31.9
SURF-ZONE				
H_{INC} (cm)	43.5	15.4	69.4	19.6
u_{INC} (cm s^{-1})	92.0	11.0	108.5	74.2
u_{IG} (cm s^{-1})	32.1	16.0	62.5	15.0
u_{SW} (cm s^{-1})	25.1	10.6	40.6	6.0
v_{INC} (cm s^{-1})	44.4	8.8	60.8	27.5
v_{IG} (cm s^{-1})	20.2	7.8	32.6	8.4
v_{SW} (cm s^{-1})	19.5	7.3	34.8	8.4
% u_{INC}	81.9	11.8	95.8	58.5
% u_{IG}	10.9	8.5	32.4	2.5
% u_{SW}	6.6	4.1	14.3	0.6
% v_{INC}	71.5	11.2	88.4	48.8
% v_{IG}	14.3	6.0	26.6	6.2
% v_{SW}	13.6	6.7	33.1	3.4

MEAN - The mean value of the variable for the 21 data runs.
ST. DEV. - The standard deviation about that mean value.
MAXIMUM - The maximum value of the variable for these 21 runs.
MINIMUM - The minimum value of the variable for these 21 runs.

Note: The mean value for each run is the result of an average of many sensors, with the exception of H_{INC}, which is calculated from a single pressure gage.

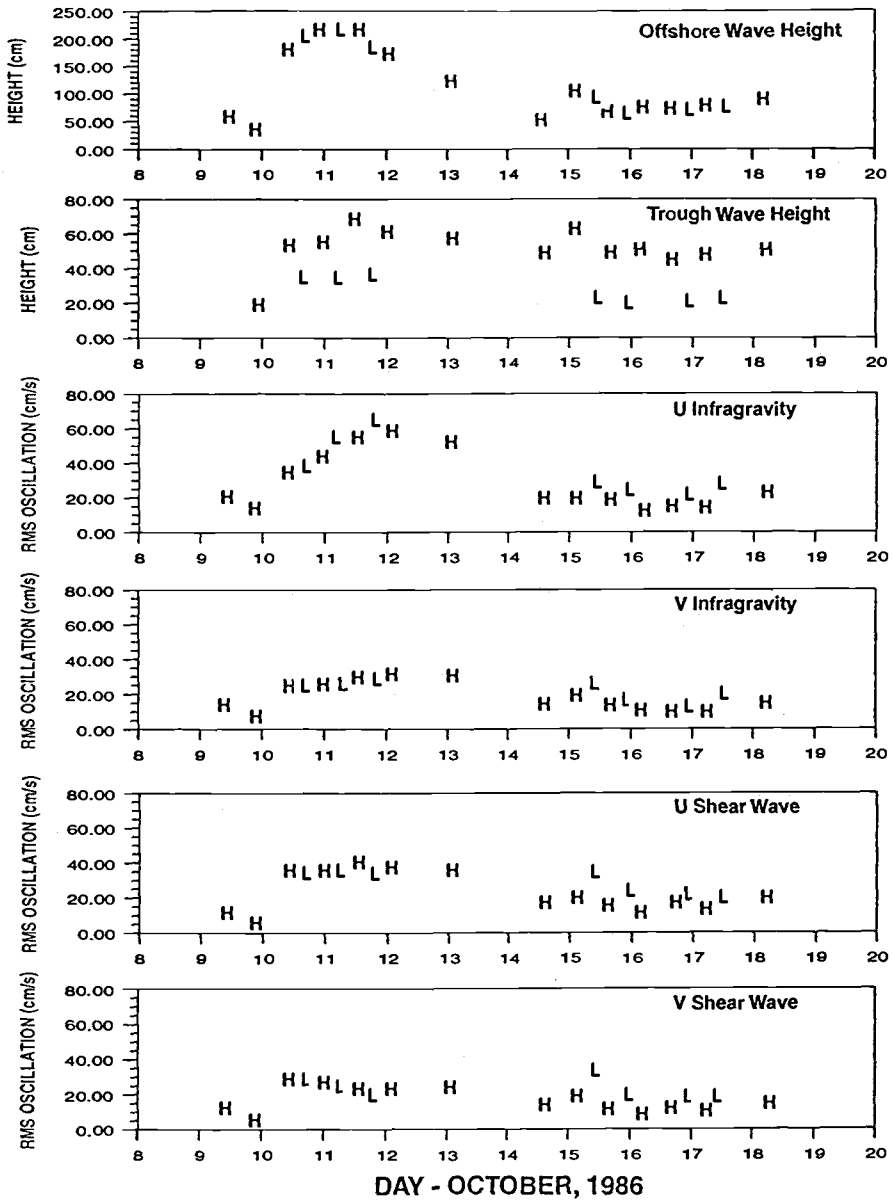

Figure II.3. Time series of 4-hour mean statistics for wave parameters at the offshore array pressure sensors and for the current meters/pressure sensor in the surf zone. *H* and *L* refer to the tide stage. See the text for details of how the variances were partitioned between wave types.

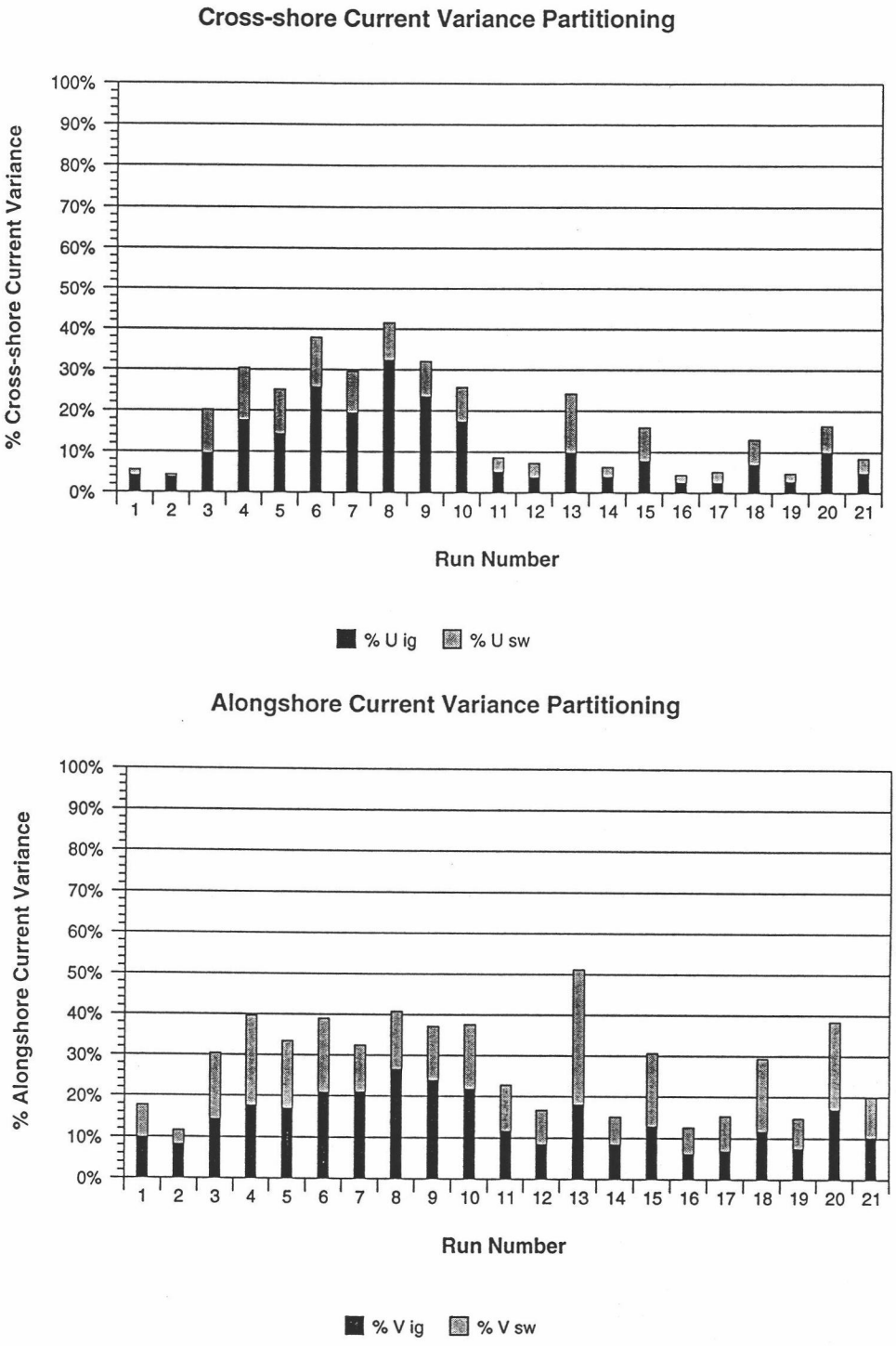

Figure II.4. The percent contributions made by each band to the total variance of the cross-shore component (top) and the longshore component (bottom). The incident band contribution brings the total to100%. The incident band is clearly dominant at this cross-shore location for both the alongshore and cross-shore flows.

shore current variance, but only up to 14.3% of the cross-shore variance.

Parameterization. Incident band rms current oscillations, u_{INC} and v_{INC}, and wave heights, H_{INC}, in the bar trough were observed to be depth limited, but not saturated, in agreement with the previous observations of *Wright et al.* [1986]. However, there was evidence for saturation seaward of the array, as there was a lack of statistically significant correlations between the incident wave heights in the trough and the offshore wave height (Table II.3). The oscillations were, however, significantly correlated with the tide (Table II.3, Figure II.5), clearly showing that the incident band was typically limited by depth, presumably at the bar crest. Given that the surf-zone instruments were in the trough of the nearshore bar for much of the experiment, it is no surprise that the local mean value of γ (0.20 ± 0.03) was considerably lower than saturation value (0.30 ± 0.01) previously predicted for this beach at the bar crest [*Sallenger and Holman*, 1985b].

The percent contributions of u_{IG} and v_{IG} were found to be significantly correlated with the offshore wave height (Figures II.6a and II.6b), in agreement with current meter data from similar water depths on three other beaches [*Holman*, 1981; *Guza and Thornton*, 1985]. Comparison with these data sets will be presented in the discussion. *Holman and Sallenger* [1985] and *Guza et al.* [1985] also found that, for the infragravity band, the slopes of the regression lines for swash amplitude versus offshore wave height depended on the Iribarren number (larger slopes for larger ξ_0). To test this dependence for the velocity oscillations, we have divided the data set into two subsets ($\xi_0 < 0.40$ and $\xi_0 > 0.40$) and calculated the regression slope for each group (Table II.4). While there is an increase in slope for the higher ξ_0, the difference is not statistically significant for this small sample.

TABLE II.3

REGRESSION RESULTS

(19 DOF) Y = mX + b + error

Y	X	m ± 95% Conf.	b	r^2
H_{INC}	H_{RMS}	0.100 ± 0.111	31.3	0.158
H_{INC}	Tide	0.261 ± 0.063	30.0	0.798
u_{IG}	H_{RMS}	0.224 ± 0.064	5.6	0.729
v_{IG}	H_{RMS}	0.110 ± 0.030	7.1	0.746
% u_{IG}	H_{RMS}	0.001 ± 0.0004	-0.023	0.641
% v_{IG}	H_{RMS}	0.059 ± 0.001	0.007	0.526
u_{SW}	$\lvert\langle V\rangle\rvert$	0.143 ± 0.117	17.7	0.245
v_{SW}	$\lvert\langle V\rangle\rvert$	0.130 ± 0.071	12.7	0.419
% u_{SW}	$\lvert\langle V\rangle\rvert$	0.0007 ± 0.0004	0.032	0.342
% v_{SW}	$\lvert\langle V\rangle\rvert$	0.0009 ± 0.0007	0.088	0.260
u_{SW}	$\partial V_M/\partial x$	868.7 ± 388.9	13.9	0.521
v_{SW}	$\partial V_M/\partial x$	637.7 ± 249.2	11.2	0.587
% u_{SW}	$\partial V_M/\partial x$	3.491 ± 1.457	0.021	0.555
% v_{SW}	$\partial V_M/\partial x$	4.172 ± 2.981	0.083	0.300

$r^2 > 0.185$ correlation different from 0 at 95% level
$r^2 > 0.303$ correlation different from 0 at 99% level

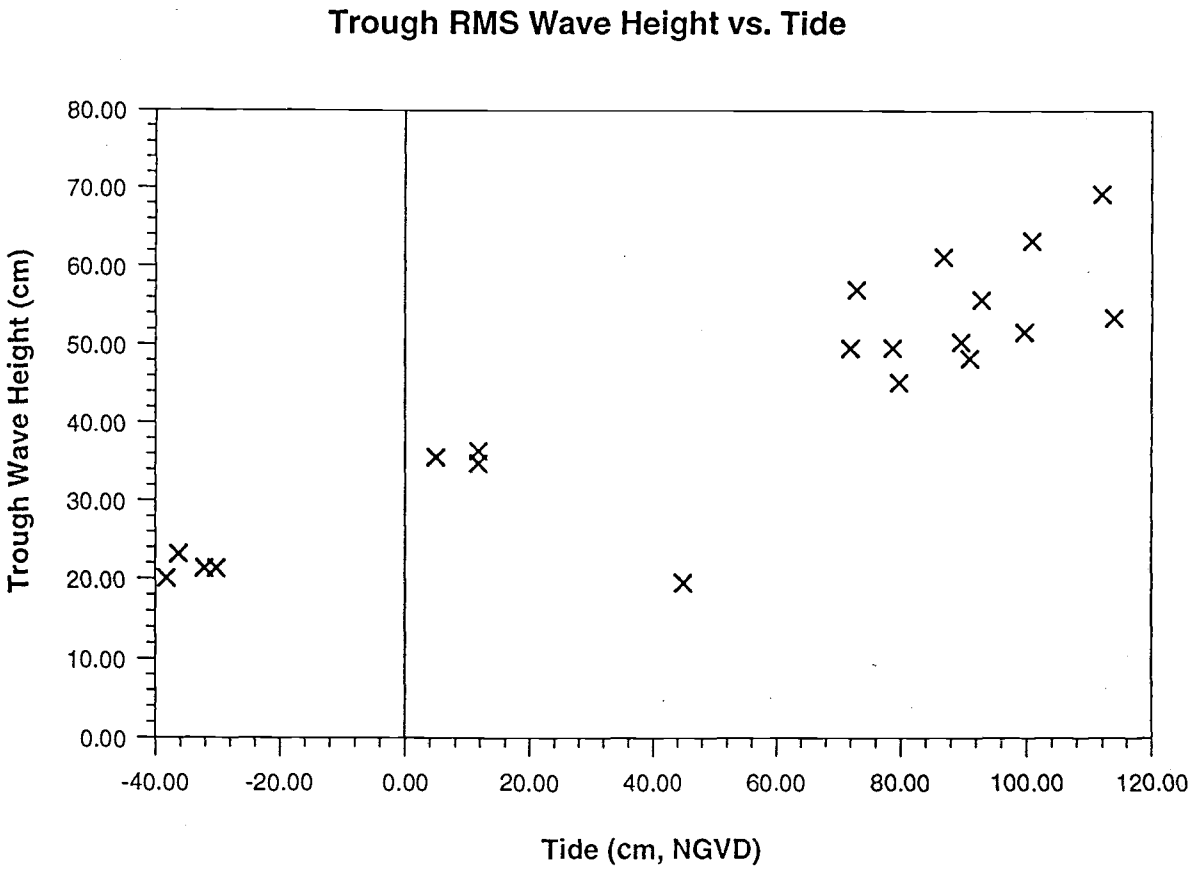

Figure II.5. The magnitude of the incident band rms wave height measured in the trough plotted versus the tide elevation. This, combined with the lack of correlation between offshore wave height and rms oscillation, indicates the incident band is depth-limited during the majority of the experiment. The one outlier represents the lowest wave conditions (October 9 2200 EST) when oscillations were not depth limited.

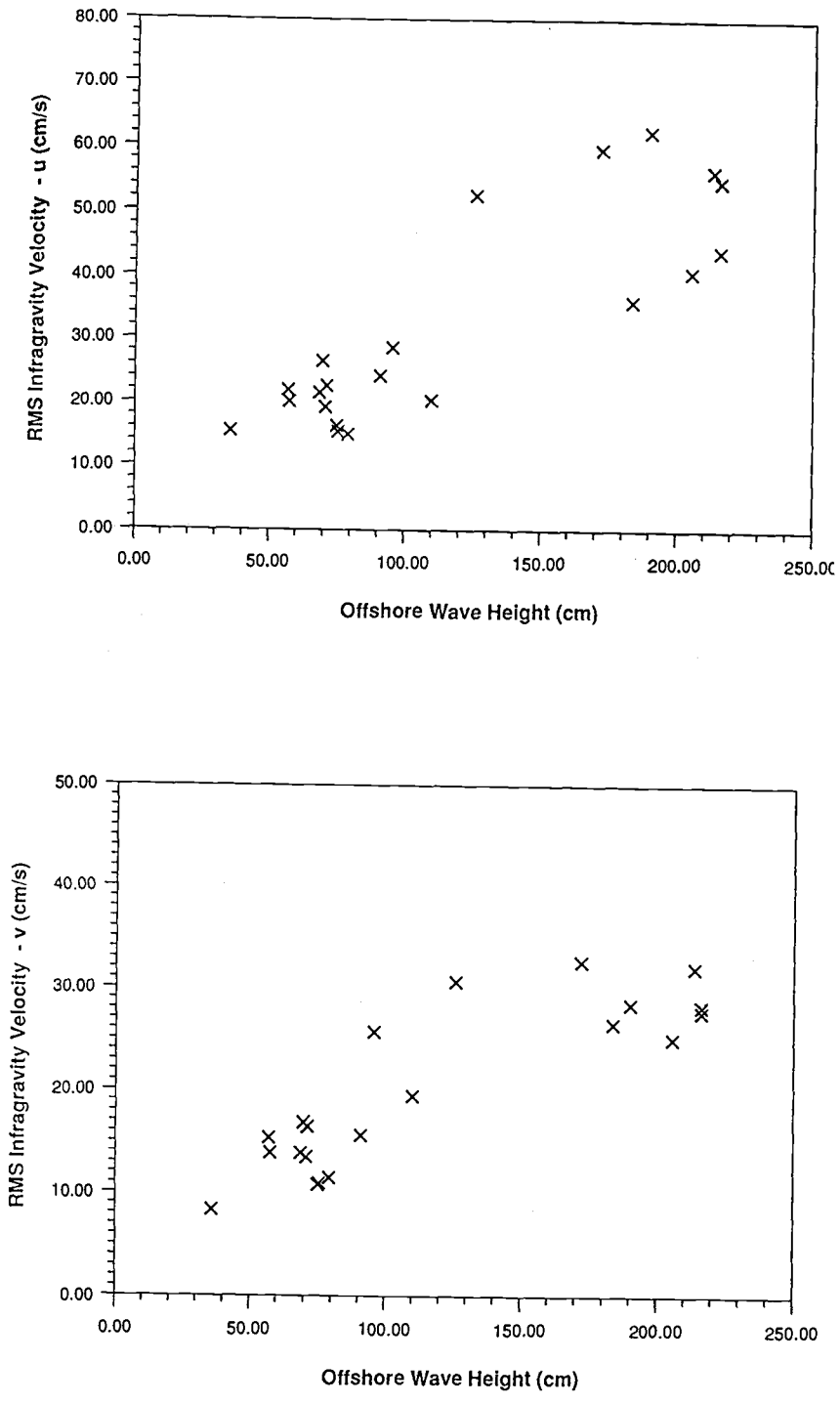

Figure II.6. u_{IG} (top) and v_{IG} (bottom) plotted versus the offshore wave height, H_{rms}. Both show a linear relationship with increasing wave height as has been seen on other beaches.

The large range of conditions experienced during SUPERDUCK also allowed examination of the impact of the wind wave incident angle on infragravity band variance levels. Multiple regression analysis shows a significant negative relation between u_{IG} and $|\alpha|$, while there is not a significant relationship between v_{IG} and $|\alpha|$ (Table II.5). The directional dependence is most clearly illustrated (Figure II.7) during the passage of the storm (October 10 to 12) when the direction of wave approach was highly variable, but the wave height was nearly constant. The u_{IG} oscillations clearly decrease as $|\alpha|$ increases, while the v_{IG} oscillations are essentially constant. Preliminary analysis suggests that u_{IG} oscillations in the presence of a large $|\alpha|$ (low u_{IG}) are dominated by high mode edge waves, while the low $|\alpha|$ u_{IG} oscillations are dominated by more energetic leaky or bound waves [*Elgar et al.*, 1989; *Oltman-Shay et al.*, 1989*b*].The v_{IG} oscillations are expected to be dominated by low mode edge waves regardless of the leaky/ high mode contributions to u_{IG}.

Shear waves are hypothesized to scale with the longshore current shear (Eq. II.5), but no measurements of the longshore current shear were obtained for extended periods of the experiment. Thus, based on the observations of *Oltman-Shay et al.* [1989*a*], we assume the absolute value of the measured mean longshore current, $|\langle V \rangle|$, is a proxy for the dynamically important shear (Figures II.8a and II.8b). The mean current, $\langle V \rangle$, was estimated as the mean of the 4-hour averages of the current meters used in the wavenumber-frequency spectral analysis. u_{SW} and v_{SW} were significantly correlated with $|\langle V \rangle|$, but with considerable scatter.

In an attempt to better parameterize the shear waves, we have modeled the longshore current, and its theoretically important shear, based on the work of *Thornton and Guza* [1983, 1986]. Wave heights in the surf zone were assumed to be Rayleigh distributed with a probability, p, of

TABLE II.4

IRIBARREN REGRESSION RESULTS

(8 DOF) $Y = mX + b + error$

Y	X	m ± 95% Conf.	b	r^2
u_{IG} ($\xi_0 < 0.40$)	ξ_0	0.157 ± 0.054	8.26	0.808
u_{IG} ($\xi_0 > 0.40$)	ξ_0	0.256 ± 0.076	6.14	0.872
v_{IG} ($\xi_0 < 0.40$)	ξ_0	0.093 ± 0.046	8.00	0.677
v_{IG} ($\xi_0 > 0.40$)	ξ_0	0.121 ± 0.043	7.00	0.819

$r^2 > 0.400$ correlation different from 0 at 95% level
$r^2 > 0.585$ correlation different from 0 at 99% level

TABLE II.5

DIRECTIONAL DEPENDENCE

$Y = m_1X_1 + m_2X_2 + b + error$

Y	X	m ± 95% Conf.	b	r^2	mean square error
u_{IG}					
	H_{RMS} alone	0.22 ± 0.06	5.62	0.73	76.70
	H_{RMS}	0.14 ± 0.06			
	$\|\alpha\|$	-0.74 ± 0.38			
			28.80	0.85	43.38
v_{IG}					
	H_{RMS} alone	0.11 ± 0.02	7.14	0.75	17.08
	H_{RMS}	0.10 ± 0.04			
	$\|\alpha\|$	-0.14 ± 0.24			
			11.44	0.76	16.74

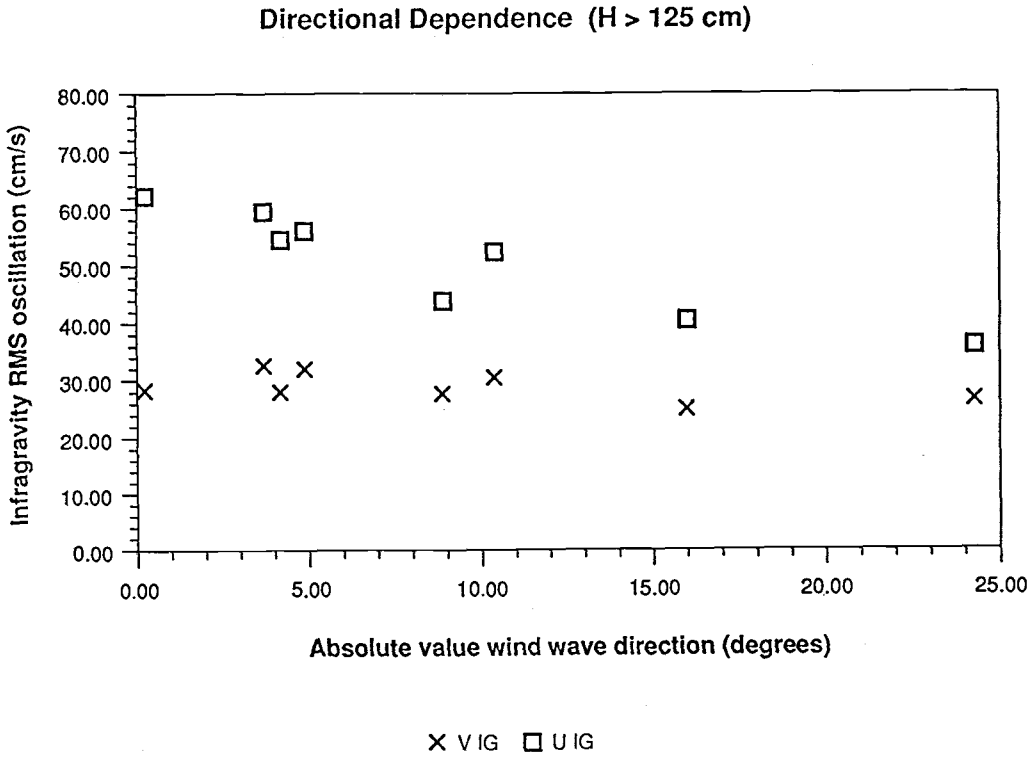

Figure II.7. The dependence of rms infragravity oscillations on the absolute value of the incident direction, $|\alpha|$, for $H_{rms} > 125$ cm.

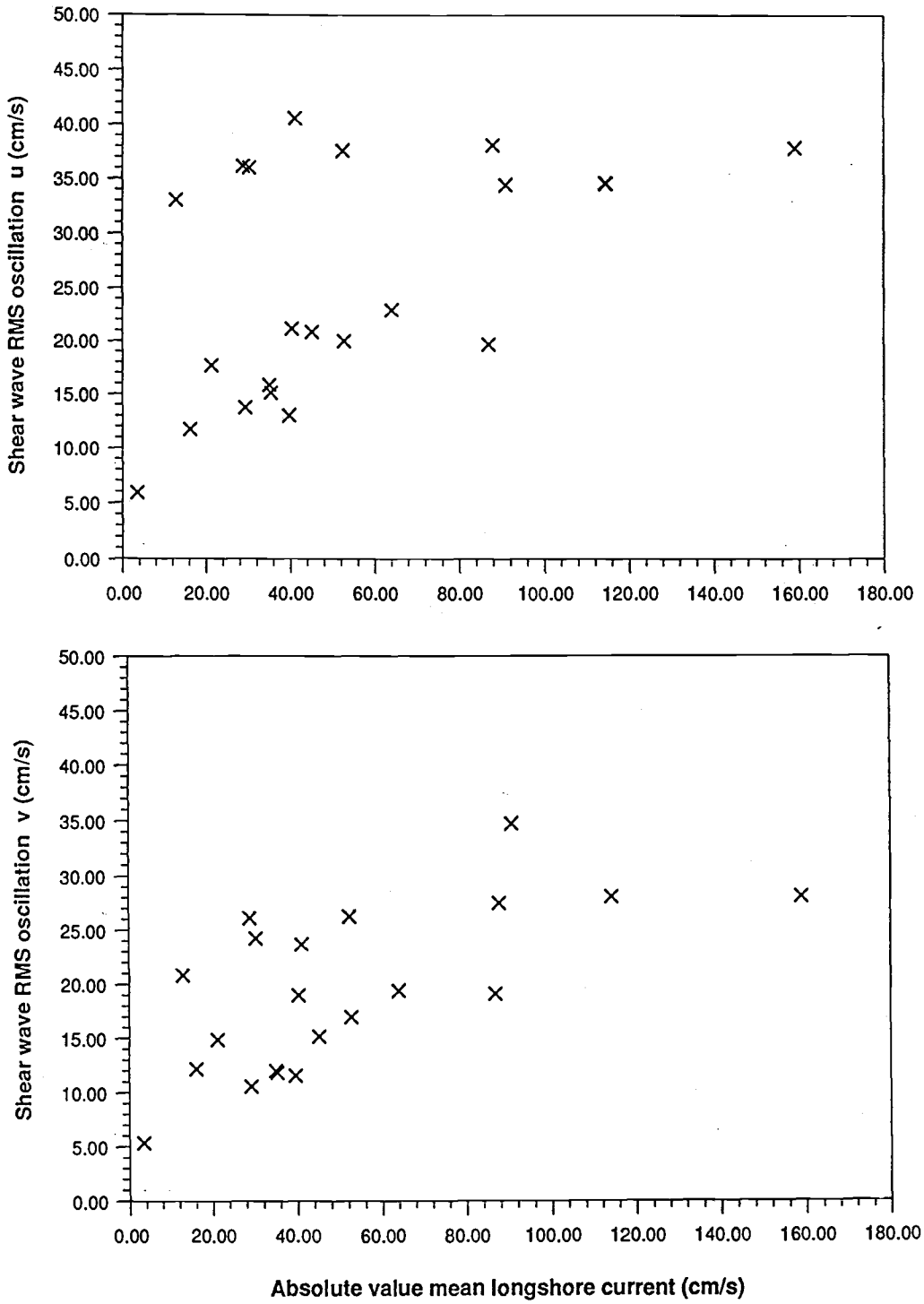

Figure II.8. u_{SW} (top) and v_{SW} (bottom) plotted versus the absolute value of the measured mean longshore current, |<*V*>|.

$$p(H) = \frac{2H}{H_{RMS}} e^{-\left(\frac{H}{H_{rms}}\right)^2} \qquad \text{(II.11)}$$

This distribution is modified by a weighting function to provide a statistical estimate of those waves which are breaking. The mean dissipation due to wave breaking, <ε>, (integrated through the wave height distribution) is given by

$$<\varepsilon> = \left(\frac{3\pi^{1/2}}{16}\right) \rho g B^3 f \left(\frac{H_{RMS}^5}{\gamma_{RMS}^2 h^3}\right) \left[1 - \left\{ \frac{1}{\left(1 - \left(\frac{H_{RMS}}{\gamma_{RMS} h}\right)^2\right)^{5/2}} \right\}\right] \qquad \text{(II.12)}$$

where ρ is the density of water, B is an empirical coefficient representing the portion of the bore face actively breaking, and f is the peak incident frequency. It is then simple to step shoreward from the input conditions at the 8 m array calculating wave height based on energy flux balance with the incident angle varied according to Snell's law of linear wave refraction.

The wave height and dissipation profiles across the surf zone were then used to predict longshore current following *Thornton and Guza*, [1986]

$$V_M(x) = \left[\frac{\sin(\alpha(x))}{\rho u(x) C(x) c_f}\right] <\varepsilon> \qquad \text{(II.13)}$$

where c_f is an empirical drag coefficient, $\alpha(x)$ is defined as in *Thornton and Guza* [1986], C is the phase velocity of the incident waves and u is given for a Rayleigh distribution by

$$u(x) = \left[\frac{g}{4\pi h(x)}\right]^{1/2} H_{RMS}(x) \qquad \text{(II.14)}$$

We have assumed the bottom stress to be linear, ignored the turbulent Reynold's stresses and assumed constant values for $\gamma = 0.45$, $B = 1.0$, and $c_f = 0.009$.

A typical output of the model is shown in Figure II.9. The predicted maximum longshore current was significantly correlated with the observed current ($r^2 = 0.942$). We assume the model does a reasonable job of predicting the relative changes (between the 21 data collections) in the cross-shore structure of the longshore current in the absence of the mixing induced by the shear waves and Reynold's stresses. No attempt was made to further tune the model to match conditions observed in the surf zone.

The dependence of shear wave magnitude on the maximum of the modeled shear on the seaward face of the longshore current is shown in Figure II.10. The correlations are not significantly improved over that with the mean velocity measured in the trough (Table II.3). Clearly more field data are needed to better define the forcing of this new phenomenon.

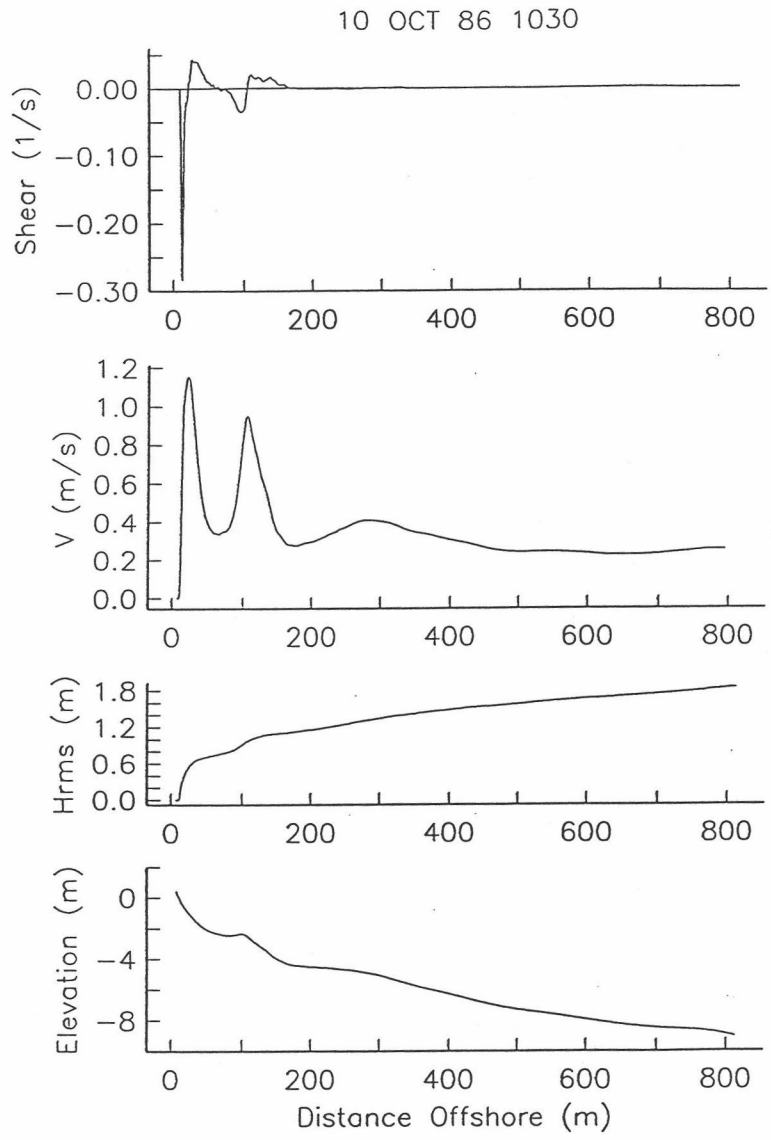

Figure II.9. Model results for H, V_M, and $\partial V_M/\partial x$ on the measured profile. The input values for H and α were those measured at the offshore array at the offshore boundary of the model. Two jets are seen in the current, one over the bar, and one at the shoreline. The shoreline jet is large due to the assumption that all incident energy is dissipated (no reflection). Shear wave theory predicts that the shear on the seaward face of the bar is the dynamically important variable.

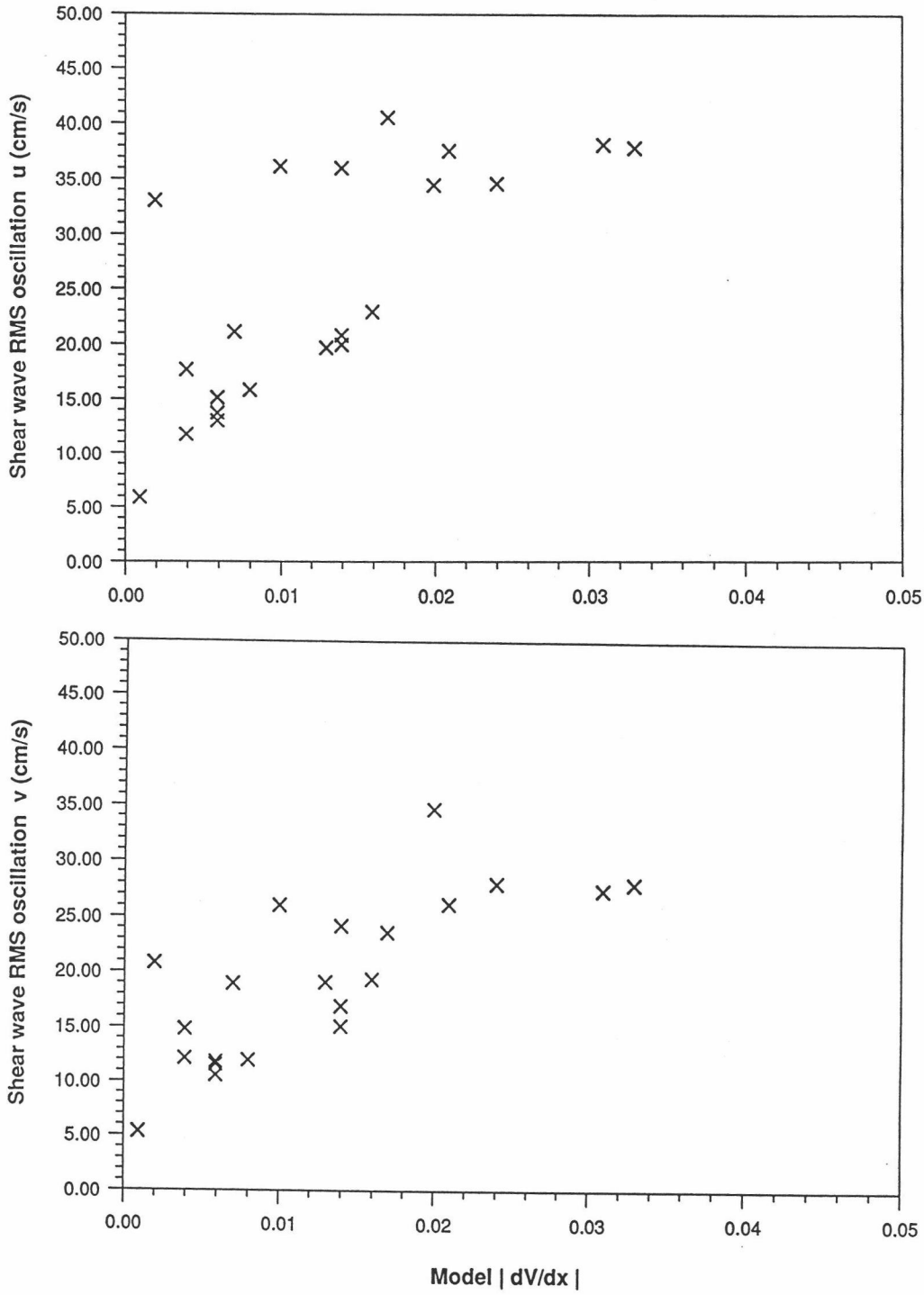

Figure II.10. u_{SW} and v_{SW} plotted versus $|\partial V_M/\partial x|$, the absolute value of the modeled maximum current shear seaward of the bar crest. The scatter, of unknown origin, is not significantly reduced. Compare with Figure II.8. A. u_{SW}. B. v_{SW}.

Discussion

The SUPERDUCK data, collected in the trough of a barred beach, have a 'process signature' which qualitatively agrees with the results of *Wright and Short* [1983], and *Wright et al.* [1986]. They presented distinctive ratios between the different components of the flow field based on the morphodynamic state of the beach. The SUPERDUCK data clearly fall into the intermediate (longshore bar and trough/rhythmic bar and beach) state between fully dissipative and fully reflective. The signature is characterized by low frequency oscillations in the surf zone approximately half the magnitude of the incident band oscillations.

Four large data sets of u_{IG} oscillations and incident wave heights are available for quantitative comparison with the SUPERDUCK data. *Guza and Thornton* [1985] presented data from the NSTS experiments at two non-barred beaches of very different slopes, Torrey Pines (TP) and Santa Barbara (SB). These data represent the variance integrated over the frequency range 0.005 - 0.05 Hz and averaged over a variable number of current meters positioned at depths between 1 m and 2 m. The authors note that less than 10% of the energy lay at frequencies below 0.005 Hz. *Wright et al.* [1986] reported statistics for 8 moderate to high energy ($H > 160$ cm) data runs of 2 to 4 sensors between 1 m and 2m depth (with highly variable cross-shore locations) from a barred section of Ninety Mile Beach in southeast Australia (AU). We chose one representative sensor for each data run (rather than average different cross-shore locations) and combined the subharmonic and infragravity bands (their infragravity band was $f < 0.03$ Hz). *Holman* [1981] presented data from a single sensor at 2 m depth, integrated from 0 to 0.05 Hz, on Martinique Beach (MA). The SUPERDUCK (SD) variances for this comparison include contributions from all wavenumbers in the frequency band 0 to 0.05 Hz. All data were converted to rms oscillations.

Figure II.11a shows these five data sets of u_{IG} oscillations plotted versus offshore H. The four North American locations show statistically significant positive regression slopes (Table II.6) even while these slopes vary between the different beaches (except between TP and SB). This is reflected in the low skill (r^2) of linear regression models between u_{IG} and offshore H for the beaches as a group, but the high r^2 for each beach individually. The regression slope for the Australian data is negative, a result of the highly variable cross-shore location of the chosen sensors (no one sensor was operational for all runs).

These results are not unexpected because infragravity waves have an offshore decay dependent on β. In an effort to remove complications arising from the cross-shore decay and varying instrument positions for the four data sets, we have calculated an 'equivalent shoreline amplitude', $\hat{a}_{IG}$, by scaling the data from each beach by the predicted u_{IG} variance, s^2_{IGP}, contributed by a white shoreline spectrum of normally incident standing waves

$$s^2_{IGP} = \hat{a}^2_{IG} \int_0^{2\pi(0.05)} \int_0^{2\pi} \left[\frac{\partial}{\partial x} \left[\frac{g \cos(\sigma t)\, \phi(x_i)}{\sigma} \right] \right]^2 dt d\sigma \qquad \text{(II.15)}$$

where x_i is the instrument location and the point at which the derivative with respect to x is evaluated. This approach is very similar to that of *Sallenger and Holman* [1985*a*]. Assuming a white spectrum allows $\hat{a}^2_{IG}$ to be taken outside the integrals. We assume that the cross-shore shape, $\phi(x)$, can be represented by the leaky wave solution given in (3). Substitution and solution for $\hat{a}^2_{IG}$ yields

$$\hat{a}^2_{IG} = \frac{\int_0^{2\pi(0.05)} S(\sigma)\, d\sigma}{\int_0^{2\pi(0.05)} \int_0^{2\pi} \left(\frac{\partial}{\partial x} \left\{ g \cos(\sigma t)\, J_0 \left[\left(\frac{4\sigma^2 x}{g\beta} \right)^{1/2} \right] \right\} \right)^2 dt d\sigma} \qquad \text{(II.16)}$$

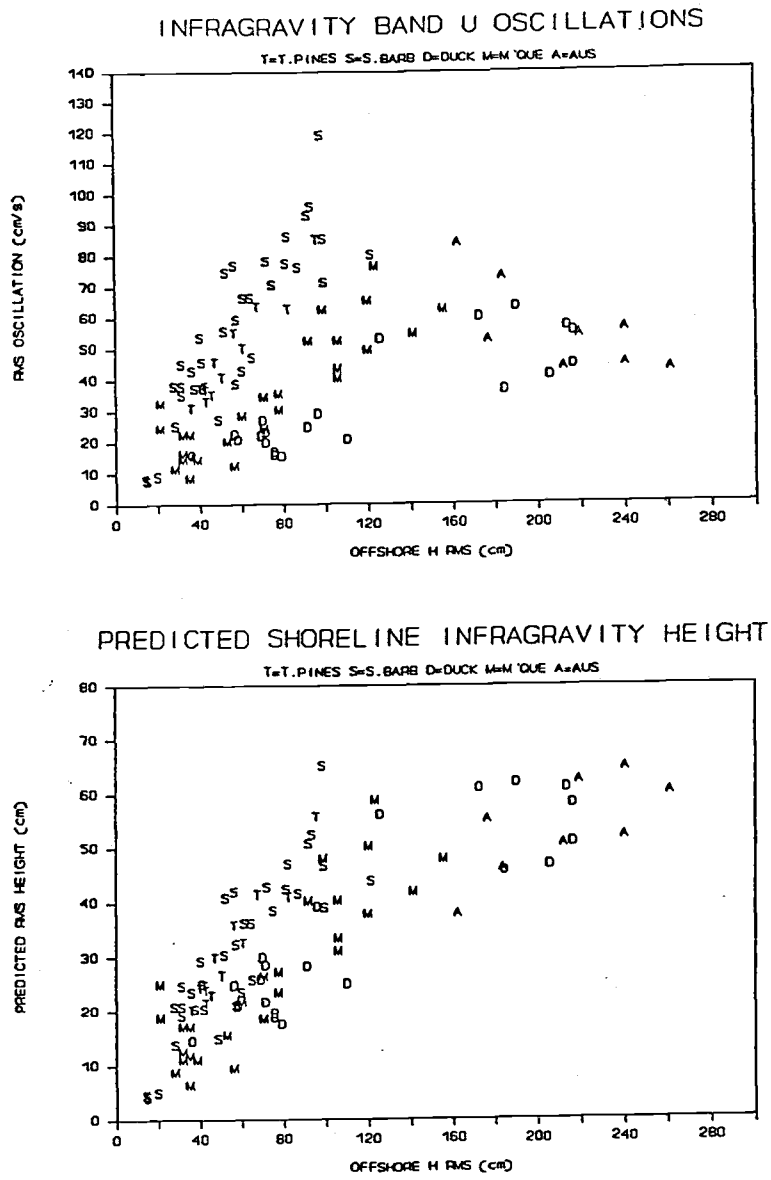

Figure II.11. Comparison of u_{IG} oscillations from 5 beaches plotted versus the offshore wave height (top) and scaled to estimate the 'equivalent shoreline height' $\hat{H}_{IG} = 2\hat{a}_{IG}$ of the infragravity oscillations (bottom). There is considerable scatter in the u_{IG} data as a whole, yet each beach taken by itself is quite well behaved (Table 5). While the scaled data collapse considerably, they are not statistically better correlated with offshore wave height at the 95% level (Table 5).

TABLE II.6

INTERCOMPARISON OF BEACHES

SURF-ZONE u_{IG} RMS OSCILLATIONS vs. OFFSHORE INCIDENT H

BEACH	m ± 95% Conf.	b	r^2	DOF
All Beaches	0.174 ± 0.068	31.26	0.521	102
Torrey Pines	0.847 ± 0.153	0.24	0.924	11
Santa Barbara	0.839 ± 0.162	7.35	0.751	33
Duck	0.272 ± 0.065	8.90	0.790	19
Martinique	0.419 ± 0.095	3.73	0.759	25
Australia	-0.339 ± 0.315	127.69	0.479	6

'EQUIVALENT SHORELINE HEIGHT', $\hat{H}_{IG}$ vs. OFFSHORE INCIDENT H

BEACH	m ± 95% Conf.	b	r^2	DOF
All Beaches	0.215 ± 0.031	13.92	0.646	102
Torrey Pines	0.554 ± 0.100	0.15	0.924	11
Santa Barbara	0.459 ± 0.089	4.02	0.751	33
Duck	0.232 ± 0.027	7.80	0.776	19
Martinique	0.323 ± 0.073	2.87	0.759	25
Australia	0.185 ± 0.157	14.26	0.525	6

* Model: $u_{IG} = m H + b + error$ or $\hat{H}_{IG} = m H + b + error$

This approach is particularly useful method to remove the site-specific nature of point measurements in the surf zone, thus facilitating the comparison of data collected either on different beaches, or at different cross-shore locations on the same beach.

While there is visual improvement in the clustering of the data (Figure II.12b), the improvement in r^2 from 0.521 to 0.646 is not significant at the 95% level. This would seem to imply that, to the lowest order, the magnitude of cross-shore infragravity oscillations are much less sensitive to the details of the incident wave spectrum or the beach topography, than they are to the wave height. The lack of significant dependence on the cross-shore measurement location may be due to the limited range in dimensionless cross-shore space, $\chi = \sigma^2 x/g\beta$, for these measurements. There are indications however (Figure II.12), that there is a ξ_0 dependence for the regression slopes (Eq. II.4) in agreement with the prediction of *Holman and Sallenger* [1985] that infragravity energy levels depend on the Iribarren number.

It is important to note that these new measurements of infragravity and shear wave variances are representative of only one cross-shore distance, that of the array. It is clear that these results are influenced by the array location as *Sallenger and Holman* [1985*a*] have shown u_{IG} to be a strong function of x on this same beach. The shear wave measurements, while clearly showing an important and energetic phenomenon, also need to be taken in the context of some (presently unknown) cross-shore variance structure. Recent measurements made during the 1990 DELILAH experiment should provide a clearer framework for understanding the cross-shore structure of these low frequency motions.

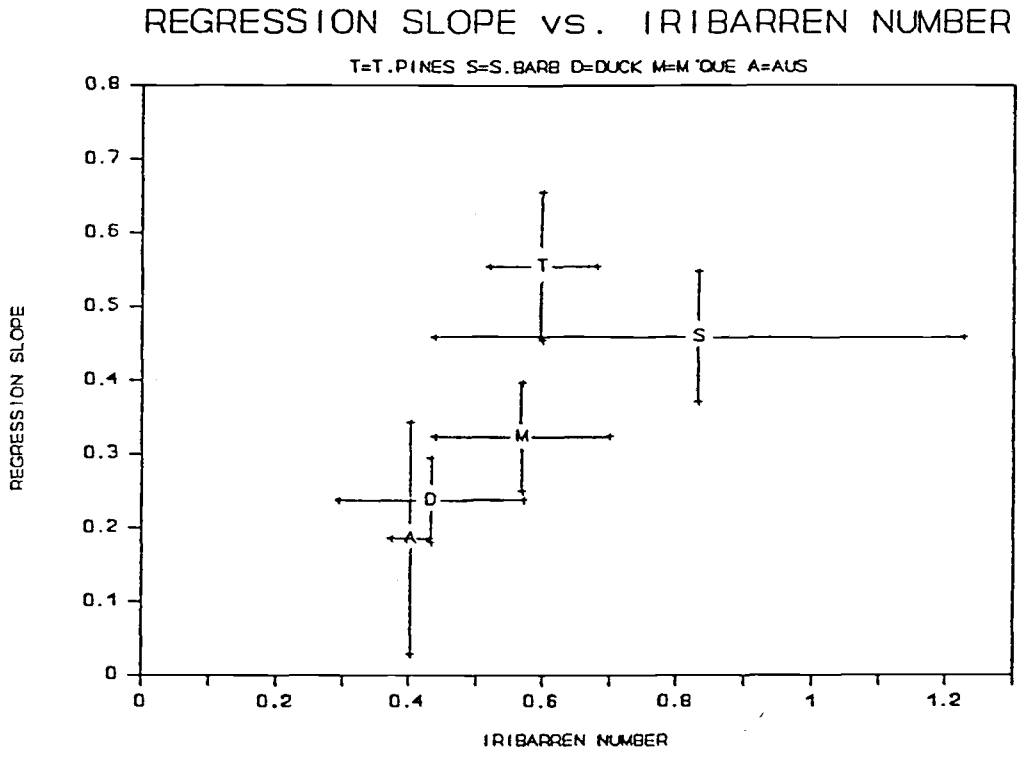

Figure II.12. Regression slopes for the five beaches (with 95% error bars) as a function of the mean Iribarren number (± 1 st. dev.) for that beach. There is a significant increase in regression slope with an increase in Iribarren number, confirming observations that infragravity waves tend to be larger on dissipative beaches than on reflective beaches for a given offshore wave height.

Summary

We have used 21 four-hour data runs collected over a wide range of incident wave conditions to quantify the bulk statistical behaviors of the alongshore and cross- shore flow components of three classes of waves in the trough of a nearshore bar. The incident band oscillations, while not locally saturated, were limited by the presence of a depth minimum at the offshore bar. Thus, the incident band, while not significantly correlated with the offshore wave height, was correlated with the tide elevation. The incident band at this location, approximately 55 m from the shoreline in the bar trough, is the largest contributor to total variance, typically providing 70 to 80%.

The infragravity wave oscillations averaged 20 cm/s and 32cm/s for v_{IG} and u_{IG} respectively and are best parameterized by the offshore wave height. During storms they provided up to 33% of the total variance with an average of approximately 12%. These percentages are expected to be higher at the shoreline. We have also found evidence that u_{IG}, the cross-shore component of infragravity wave oscillation was, to a lesser degree, sensitive to the directional character of the incident waves.

Shear waves were found to be an important contributor to the energetics of this beach, typically comprising approximately 10% of the total variance, but at times contributing up to 35%. The magnitudes of the oscillations exceeded 40 cms^{-1} in the cross-shore and 30 cms^{-1} alongshore. Shear wave magnitudes were correlated with the seaward-facing shear of the longshore current (which was modelled, not measured), as expected from theory. It is difficult to place these measurements in cross-shore context with this data due to the lack of adequate measurement of the cross-shore structure of the longshore current.

Comparison of the cross-shore component of the infragravity band with data col-

lected on other beaches and previously reported in the literature shows that while each experiment's data scales approximately linearly with offshore wave height, the trend of the relationship varies as a function of the Iribarren number. For these data, all collected in a similar depth of water, correcting for the cross-shore location of the sensor provides only a minor improvement in the correlation with the offshore wave height.

References

Birkemeier, W.A. and C. Mason, The CRAB: a unique nearshore surveying vehicle, *J. Surv. Eng.*, Am. Soc. Civ. Eng. 110, 1-7, 1984.

Bowen, A., D. Inman, and V. Simmons, Wave setdown and setup, *J. Geophys. Res.*, 37, 206-215, 1968.

Bowen, A. J. and R. A. Holman, Shear instabilities of the mean longshore current: 1. Theory, *J. Geophys. Res., 94,* 18023-18030, 1989.

Crowson, R., W. Birkemeier, H. Klein, and H. Miller, SUPERDUCK nearshore processes experiment: Summary of studies CERC Field Research Facility, *US Army Tech. Report CERC-88-12,* 1988.

Eckart, C., Surface waves in water of variable depth, *Scripps Inst. of Oc. Ref. 12*, SIO, La Jolla, CA, 94 p., 1951.

Galvin, C. and P. Eagleson, Experimental study of longshore currents on a plane beach, *US Army CERC Tech. Memo. 10*, 1965.

Guza, R. and A. Bowen, Resonant interactions for waves breaking on a beach, *Proc. 15th Conf. Coastal Eng.* 560-579, 1976.

Guza, R. and E. Thornton, Observations of surf beat, *J. Geophys. Res.*, 90, 3161-3172, 1985.

Guza, R., E. Thornton, and R. Holman, Swash on steep and shallow beaches, *19th Coastal Engineering Conference Proceedings*, p. 708-723, 1985.

Elgar, S. and R.T Guza, Observations of bispectra of shoaling surface gravity waves, *J. Fluid Mech.*, 161, 425-448, 1985.

Elgar, S., J. Oltman-Shay, and P.Howd, Observations of infragravity-frequency long waves; I. Coupling to wind waves, *EOS, Trans., Am. Geophys. Union*, 70, 1333, 1989.

Haines, J. and A. J. Bowen, Phase-locking of modes in the nearshore: Field evidence, *Proc. 21st Conf. Coastal Eng.*, 1522-1534, 1988.

Holman, R., Infragravity Energy in the surf zone, *J. Geophys. Res.*, 86, 6442- 6450, 1981.

Holman, R. and A. Sallenger, Setup and swash on a natural beach, *J. Geophys. Res.*, 90, 945-953, 1985.

Huntley, D., R. Guza and E. Thornton, Field observations of surf beat, I. Progressive edge waves, *J. Geophys. Res.*, 86, 6451-6466, 1981.

Huntley, D., Evidence for phase coupling between edge wave modes, *J. Geophys. Res.*, 93, 12393-12408, 1988.

Kenyon, K., Edge waves with current shear, *J. Geophys. Res.*, 77, 6599-6603, 1972.

Lippmann, T., The stability and spatial variability of sand bar morphology, MS thesis, 132 p., Oregon State Univ., 1989.

Lippmann, T. and R. Holman, Quantification of sand bar morphology: A video technique based on wave dissipation, *J. Geophys. Res.*, 94, 995-1011, 1989.

Long, C. and J. Oltman-Shay, 1989, Directional characteristics of waves in shallow water, *US Army CERC Technical Report*, in press.

Longuet-Higgins, M. and R. Stewart, Radiation stress in water waves; a physical discussion, with applications, *Deep Sea Research*, 11, 529-562, 1964.

Oltman-Shay, J. and R. Guza, Infragravity edge wave observations on two California beaches, *J. Phys. Oc.*, 17, 644-663, 1987.

Oltman-Shay, J., P. A. Howd, and W. A. Birkemeier, Shear instabilities of the mean longshore current, 2: Field data, *J. Geophys. Res., 94*, 18031-18042, 1989a.

Oltman-Shay, J., S. Elgar, and P.Howd, Observations of infragravity-frequency long waves; II. Comparisons with a 2-D wave group generation model, *EOS, Trans., Am. Geophys. Union*, 70, 1333, 1989b.

Pawka, S., Wave directional characteristics on a partially sheltered coast, PhD dissertation, 246 p. Scripps Inst. of Oceanography, UCSD, 1982.

Pawka, S., Island shadows in wave directional spectra, *J. Geophys. Res.*, 88, 2579-2591, 1983.

Sallenger, A. and R. Holman, On predicting infragravity energy in the surf zone, *19th Coastal Engineering Conference Proceedings*, p. 1940-1951, 1985a.

Sallenger, A. and R. Holman, Wave energy saturation on a natural beach of variable slope, *J. Geophys. Res.*, 90, 11939-11944, 1985b.

Sallenger, A. and R. Holman, Infragravity waves over a natural barred profile, *J. Geophys. Res.*, 92, 9531-9540, 1987.

Suhayda, J., Standing waves on beaches, *J. Geophys. Res.*, 72, 3065-3071, 1974.

Thornton, E. and R. Guza, Energy saturation and phase speeds measured on a natural beach, *J. Geophys. Res.*, 87, 9499-9508, 1982.

Thornton, E. and R. Guza, Surf zone currents and random waves: Field data and models, *J. Phys. Oc.*, 16, 1165-1178, 1986.

Weishar, L. and R. Byrne, Field study of breaking wave characteristics, *Proc. 16th Coastal Eng. Conf.*, 1978

Wright, L.D. and A.D. Short, Morphodynamics of beaches and surf zones in Australia, in *CRC Handbook of Coastal Processes and Erosion*, Ed. by P.D. Komar, CRC Press, Boca Raton, FL., 1983.

Wright, L.D., P. Nielsen, N.C. Shi, and J.H. List, Morphodynamics of a bar-trough surf zone, *Marine Geology*, 70, 251-285, 1986.

CHAPTER THREE

EDGE WAVES IN THE PRESENCE OF STRONG LONGSHORE CURRENTS

Abstract

It is well known that currents are capable of refracting surface gravity waves in much the same manner as variable water depth. Thus longshore currents are expected to modify refraction in the nearshore wave guide, changing the dynamics and kinematics of edge waves. A form of the linear, inviscid shallow water wave equation which includes arbitrary longshore currents and bathymetry is derived. This formulation provides a continuum between gravity waves (either leaky or edge waves) on a longshore current, and the recently discovered shear waves. In this paper we will concentrate on gravity wave solutions for which $|V/c| < 1$, where V is the longshore current, and c is the edge wave alongshore celerity. Interestingly, for gravity waves, the effects of the current can be uniquely accounted for in terms of a modification to the true beach profile, allowing the definition of the 'effective beach profile', $h'(x) = h(x)\left[1 - \frac{V(x)}{c}\right]^{-2}$, where $h(x)$ is the true profile. The effective profile is particularly useful in conceptualizing the combined effects of longshore currents and variable bottom topography.

To test the sensitivity of edge waves to mean longshore currents, we have numerically solved for the dispersion relationship and the cross-shore shapes of edge waves on a plane beach under a range of current conditions. Changes to the edge wave alongshore wavenumber, κ, of nearly 100% are found for reasonable current profiles, showing that the departure from plane beach dispersion due to longshore currents can be of the same order as the effect of introducing non-planar topography. These changes are not symmetric as they are for profile changes; $|\kappa|$ increases for edge waves opposing the current flow (a shallower effective profile), but decreases for those coincident with the

flow (a deeper effective profile). The cross-shore structure of the edge waves is also strongly modified. As expected, as $|\kappa|$ increases (decreases), the nodal structure shifts landward (seaward) from the positions found on the test beach in the absence of a current. In addition, the predicted variances away from the nodes, particularly for the alongshore component of edge wave orbital velocity, may change dramatically from the no-current case. Failure to account for these changes can lead to incorrect identification of modes and large errors in the estimation of the corresponding shoreline amplitude.

The magnitudes of many of the edge wave responses are related to the ratio V_{max}/c, where V_{max} is the maximum current, and to the dimensionless cross-shore scale of the current, $|\kappa|x(V_{max})$, where $x(V_{max})$ is the cross-shore distance to V_{max}. This is most easily understood in terms of the effective profile and the strong dependence of the edge waves to the details of the inner part of the beach profile.

Inclusion of the longshore current also has implications regarding the role of edge waves in the generation of nearshore morphology. The modifications to the wavenumbers of any two phase locked edge wave modes will change the morphology of a potentially resulting sand bar. For example, in the absence of a current, two phase locked edge waves of equal frequency and mode progressing in opposite directions are expected to produce a crescentic bar. However, in the presence of a current, the wavenumbers would differ, stretching the expected crescentic bar into a welded bar. A more interesting effect is the possibility that modifications to the edge waves due to the presence of a virtual bar in the effective profile could lead to the development of a real sand bar on the true profile. These modifications appear to be only weakly sensitive to frequency, in contrast to the relatively strong dependence of the traditional model for sand bar generation at infragravity wave nodes.

Introduction

Numerous authors have proposed that edge waves play an important role in a number of nearshore processes, including mean circulation patterns [*Bowen and Inman*, 1969], the generation of nearshore morphology [*Holman and Bowen*, 1982], and momentum and energy transfer [*Elgar and Guza*, 1985]. Studies have shown that the shoreline expression of wave energy, the swash, can be dominated by infragravity motions with up to 70% the variance of the incident gravity waves offshore [*Holman and Sallenger*, 1985]. They are also an energetic part of the wave spectrum in the surf zone [*Holman*, 1981; *Guza and Thornton*, 1985; *Howd et al.*, 1991*a*].

Much of the interest in edge waves arises from the observation that their length scales were similar to those of sand bar systems, both in the cross-shore [*Short*, 1975; *Bowen*, 1981], and in the longshore for three-dimensional systems [*Bowen and Inman*, 1971; *Holman and Bowen*, 1982]. In all these cases, the sand bars are hypothesized to result from the nodal structure of the infragravity wave drift velocities. Unlike reflected incident waves, which have nodes every 10-20 m in the cross-shore, infragravity wave nodes are typically spaced at 50-100 m intervals, closely matching the observed scales of sand bars.

The description of edge wave dynamics on beaches began with the consideration of two analytically tractable cases, the plane sloping profile, $h(x) = \beta x$, [*Eckart*, 1951], and the exponential profile, $h(x) = h_0(1 - e^{-\alpha x})$, [*Ball*, 1967]. *Holman and Bowen* [1979] and *Kirby et al.* [1981] used numerical models to predict the dispersion relation and cross-shore shape of edge waves on arbitrary topography. *Holman and Bowen* [1979] showed that assuming a profile shape for which an analytic result exists may lead to errors of up to 100% in κ for predictions of the dispersion relationship. Numerical solu-

tions in both studies show two related kinematic effects, the relative change of edge wave amplitudes away from the shoreline (compared to the plane beach case) and the associated movement of the nodal structure. *Kirby et al.* [1981] found that, over a limited frequency range, distortion of edge wave shapes occurred such that elevation antinodes were attracted to the cross-shore location of a bar crest. The complexity of these numerical approaches is great however, and many later researchers have simply assumed one of the analytic forms of the beach profile to be adequate [*Holman and Bowen*, 1984; *Sallenger et al.*, 1984; *Howd et al.*, 1991*a*].

Kenyon [1972] considered the influence of longshore currents on edge waves, analytically modelling the case of a plane beach with a longshore current constantly increasing in the offshore direction ($V(x) = \vartheta_1 x$). He found systematic variations in edge wave dispersion, although his theory was only valid for a current, $V(x)$, that remained very small compared to the celerity of the edge wave. While this approximation may hold for shelf-scale phenomena, it is routinely violated in the nearshore, both in terms of the constant shear and the magnitude of $V(x)$ relative to the edge wave celerity.

To test hypotheses regarding the generation of edge waves (for instance, *Gallagher* [1971]) and to correctly interpret measurements made in the field, the dispersion relationship and the cross-shore structure of the edge waves must be well understood. Because many measurements are made in the surf zone, and the data transformed to predict the shoreline amplitudes of the edge waves, it is important that the cross-shore shape of the edge waves be accurately predicted. It is necessary to be able not only to determine the edge wave mode through the dispersion relationship, but also to be able to relate the variance at any cross-shore location to the reference value at the shoreline. It will be shown that incorporation of both bathymetric and current effects are required for this task.

In the next section we will explore the role of the cross-shore structure of the mean longshore current, $V(x)$, in modifying edge waves in the nearshore. A conceptual framework for understanding the longshore current effects is followed by the derivation of the governing equations for low frequency waves in the presence of arbitrary topography, $h(x)$, and longshore current, $V(x)$. While the equation is valid for all low frequency motions (edge waves, leaky waves, and the recently discovered shear waves), we will concentrate for the remainder of this paper on edge waves. Results from a series of synthetic tests designed to examine the role currents play in modifying edge wave properties will be presented. Implications of these effects are then discussed. The improvements in describing edge wave dispersion and the cross-shore variance structure by the inclusion of longshore currents are shown using data collected during a large field experiment. Finally, we will present a new hypothesis for the generation of sand bars based on changes in sediment transport resulting from edge wave modification by a strong longshore current.

Theory

The nearshore, where shallow water wave celerities are a function of the water depth, $\sqrt{gh}$, has the possibility of trapping wave motions through refraction offshore and reflection at the shoreline (where the depth goes to zero). This behavior can be viewed as a wave guide, in direct analogy to other geophysical wave guides.The discrete set of resonant motions trapped in the nearshore wave guide are called edge waves, while leaky waves are those free waves which, upon reflection from the shoreline, escape the nearshore wave guide to deep water. A critical value of the alongshore wavenumber, $\kappa = 2\pi/L_y$, of the motion separates the two regimes. The sign of κ determines the direction of wave progression.

Two major modifications to the properties nearshore wave guide are sand bars and longshore currents (Figure III.1). A comparison of their refractive effects is instructive. Sand bars modify the wave guide by changing the water depth. The sand bar crest, a depth minimum, is the location of a local celerity minimum and provides a focussing of wave rays at that location. A bar trough, meanwhile, is a local celerity maximum and leads to divergence of wave rays. While topography may be generally expected to change the cross-shore structure and wavenumber of an edge wave, the changes should be symmetric for waves progressing either direction along the coast. A longshore current modifies the wave guide in a similar manner. Edge wave travelling into the current experience refractive focussing of the wave rays at the cross-shore location of the maximum longshore current, the location where opposition to their progression is the greatest. This response is the same as we expect for the sand bar. In contrast, the wave rays of edge waves travelling with the current diverge at the longshore current maximum, behavior that would also be expected over trough topography. The current has added asymmetry to the edge wave field.

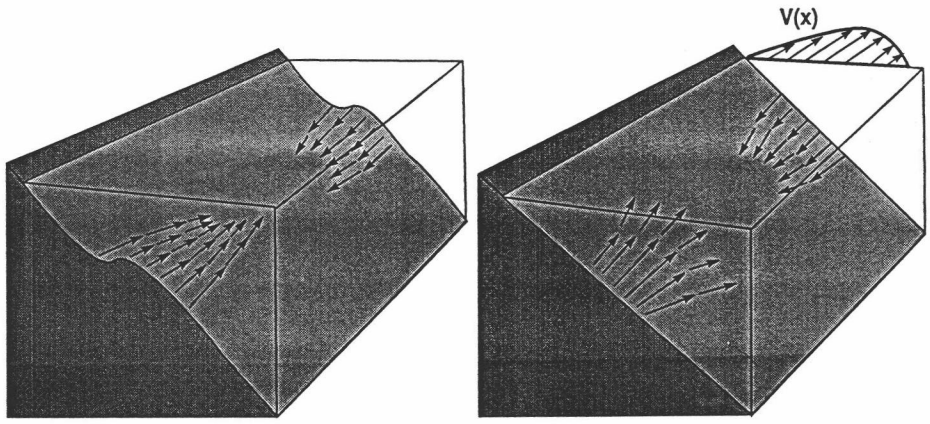

Figure III.1. Modifications to the nearshore wave guide by the presence of a longshore current is analogous to that of bar and trough topography. The edge wave response to a sand bar is independent of the direction of edge wave propagation, wave rays refract and focus on the crest and diverge in the deeper trough. In the case of the longshore current, the effects are opposite for the different directions of edge wave propagation. Edge wave rays progressing into the current are refracted to focus on the current maximum (as if it were a bar), while those progressing with the current diverge as if they were in the trough of a bar.

General changes in the dispersion relationship due to longshore currents can also be predicted. We expect that edge wave travelling into (with) a current will have larger (smaller) $|\kappa|$ values than those on the same beach in the absence of a longshore current. The current acts to either decrease or increase (edge waves travelling with the current) the observed celerity at any frequency. To summarize, we expect there to be a relationship between longshore currents and apparent modifications to the beach profile seen by the edge waves. These changes are no longer the same for both directions of edge wave progression, introducing dynamical asymmetry to the problem.

This conceptual treatment of the nearshore as a wave guide can be formalized in a theoretical description of edge wave behavior by inclusion of variable topography and longshore currents in the inviscid shallow water equations for conservation of momentum and mass with the total velocity vector $U(x,y,t) = (u(x,y,t), v(x,y,t)+V(x))$. We will assume the edge wave velocity components, u and v are small, $u, v << V$ and the depth, $h = h(x)$ only. Retaining only those terms that are linear in u and v gives

$$u_t + Vu_y = -g\eta_x \tag{III.1}$$

$$v_t + uV_x + Vv_y = -g\eta_y \tag{III.2}$$

$$\eta_t + \nabla\,(\eta + h)\,U = 0 \tag{III.3}$$

Subscripts indicate partial differentiation, and ∇ is the horizontal gradient operator. The x axis is taken positive in the offshore direction and h is positive downward from mean sea level. Taking the form $f(x,y,t) = f(x)e^{i(\kappa y - \sigma t)}$ for u, v, and η and substituting in (1) to (3) yields

$$u(x) = \Re\left[\frac{-g\eta_x}{i(-\sigma + \kappa V)}\right] \tag{III.4}$$

$$v(x) = \Re\left[\frac{(-ig\kappa\eta - V_x u)}{(i(-\sigma+\kappa V))}\right] \tag{III.5}$$

$$\eta(x) = \Re\left[\frac{-(hu)_x - i\kappa hv}{i(-\sigma+\kappa V)}\right] \tag{III.6}$$

where subscripts indicate differentiation, $\Re$ indicates the real portion, and the x-dependencies on the right hand sides of the equations are understood. These equations can be manipulated to give a second order differential equation in terms of either η

$$\left[\frac{gh\eta_x}{(-\sigma+\kappa V)^2}\right]_x + \eta\left[1 - \frac{\kappa^2 gh}{(-\sigma+\kappa V)^2}\right] = 0 \tag{III.7}$$

or u,

$$\left[\frac{\gamma^2}{(1-\gamma^2)}\left[\frac{hu}{(-\sigma+\kappa V)}\right]_x\right]_x - \gamma^2\kappa^2\left[\frac{hu}{-\sigma+\kappa V}\right] = 0 \tag{III.8}$$

where

$$\gamma^2 = \frac{(-\sigma+\kappa V)^2}{\kappa^2 gh} \tag{III.9}$$

is a measure of the divergence of the motion.

In the non-divergent case ($\gamma^2 \to 0$), (III.8) reduces to Equation 8 of *Bowen and Holman* [1989] for nondivergent shear waves. For $V(x) = 0$, (III.7) reduces to the classical edge wave equation in the absence of a current (for instance, *Holman and Bowen*, 1979)

$$\left[\frac{gh\eta_x}{\sigma^2}\right]_x + \eta\left[1 - \frac{\kappa^2 gh}{\sigma^2}\right] = 0 \tag{III.10}$$

Of particular interest is the observation that if we make the substitution in (III.7) of

$$h'(x) = \frac{h(x)}{\left[1 - \frac{V(x)}{c}\right]^2} \tag{III.11}$$

where $h'(x)$ is defined as the effective beach profile and $c = \sigma/\kappa$ is the edge wave celerity (and carries the sign of κ), we get the result

$$\left[\frac{gh'\eta_x}{\sigma^2}\right]_x + \eta\left[1 - \frac{\kappa^2 gh'}{\sigma^2}\right] = 0 \tag{III.12}$$

which is functionally identical to the classical edge wave equation (III.10). The term $\left[1 - \frac{V(x)}{c}\right]^2$ is not surprising as it also appears in the modification of Snell's Law for the refraction of surface gravity waves by currents [*Kenyon*, 1971]. The concept of the effective beach profile, $h'(x)$, is very useful in gaining a conceptual understanding of the combined role of the current and topography in modifying edge wave characteristics.

Normal mode (edge wave) solutions are obtained by expressing (III.7) as two coupled first order differential equations subject to the boundary conditions that $\eta(0) =$ finite and $\eta(\infty) = 0$. The coupled equations can be solved using a Runge-Kutta technique [*Press et al.*, 1986] starting from initial conditions at the shoreline. These are found by expanding h, V, and η in the form

$$h(x) = \beta_1 x + \beta_2 x^2 + \ldots \tag{III.13}$$

$$V(x) = \vartheta_1 x + \vartheta_2 x^2 + \ldots \tag{III.14}$$

$$\eta(x) = \eta_0(1 + \alpha_1 x + \alpha_2 x^2 + \ldots) \tag{III.15}$$

Substituting in (III.7) and equating terms of like powers of x gives

$$\eta(0) = \eta_0 = given \tag{III.16}$$

$$\eta_x(0) = \frac{-\sigma^2}{g\beta_1}\eta_0 = \alpha_1\eta_0 \tag{III.17}$$

$$\eta_{xx}(0) = \eta_0\left[\frac{1}{2}\left\{\left(\frac{\sigma^2}{g\beta_1}\right)^2 + \kappa\right\} + \frac{\sigma^2}{g\beta_1}\frac{\beta_2}{\beta_1} + \frac{2\kappa\vartheta_1\sigma}{g\beta_1}\right] = \alpha_2\eta_0 \tag{III.18}$$

These are identical to those found by *Holman and Bowen* [1981] with the exception of the ϑ_1 term in (III.18) expressing the added role of the longshore current shear.

As *Holman and Bowen* [1979] report, for any σ, κ pair the trial solution 'blows up' at large x. The values of κ (holding σ constant) for which x is a local maximum represent the set of edge wave modes which satisfy the edge wave dispersion relation and solve III.7. The solution method gives $u(x)$ and $\eta(x)$, while $v(x)$ is calculated from (III.5).

The results of the numerical scheme were tested against the two known analytical solutions for plane and exponential beaches, and against the approximation of *Kenyon* [1972] for very small currents. The dispersion relationship and other edge wave characteristics, such as nodal locations, were reproduced to arbitrary accuracy for the analytic cases, and Kenyon's approximation was found to be valid subject to his stated constraints. The following results satisfy the dispersion relationship to $\pm 0.1\%$ in κ.

Results

A total of 16 test cases were run in order to explore the sensitivity of edge waves to current magnitude and shape. Current profiles were constructed from two regions of constant shear, with the shear discontinuities smoothed using a 10-m wide moving average. Three parameters were used to describe the current: the maximum current, V_{max}, the cross-shore location of the maximum current, $x(V_{max})$, and the width of the current, x_w. Figure III.2 summarizes the different current profiles used in this study. Much of the discussion is based on an example case, Run 2 (which is common to the four groupings in Figure 2), with $V_{max} = 1.00$ m s^{-1} at $x = 50$ m with a width of ~100 m. For each current profile, solutions for modes 0-4 were determined at steps of 0.025 Hz from 0.2 to 0.05 Hz and at steps of 0.0025 Hz from 0.05 to 0.005 Hz.

All simulation runs used the same plane beach profile, $\beta = 0.035$, in order to facilitate comparison and more easily determine the current effects. The shallow water approximation for edge wave dispersion of a plane beach is given by *Eckart* [1951] as

$$\sigma^2 = g|\kappa|\,(2n+1)\,\beta \qquad \text{(III.19)}$$

where n is the edge wave mode number. An effective beach slope felt by the edge waves in the presence of a longshore current, β_{eff}, can therefore be defined as

$$\beta_{eff} \equiv \frac{\sigma^2}{g|\kappa|\,(2n+1)} \qquad \text{(III.20)}$$

allowing qualitative generalizations to be made regarding relative changes between the beach slopes (true and effective) and edge wave characteristics as we introduce different longshore current profiles (changing the effective beach profile).

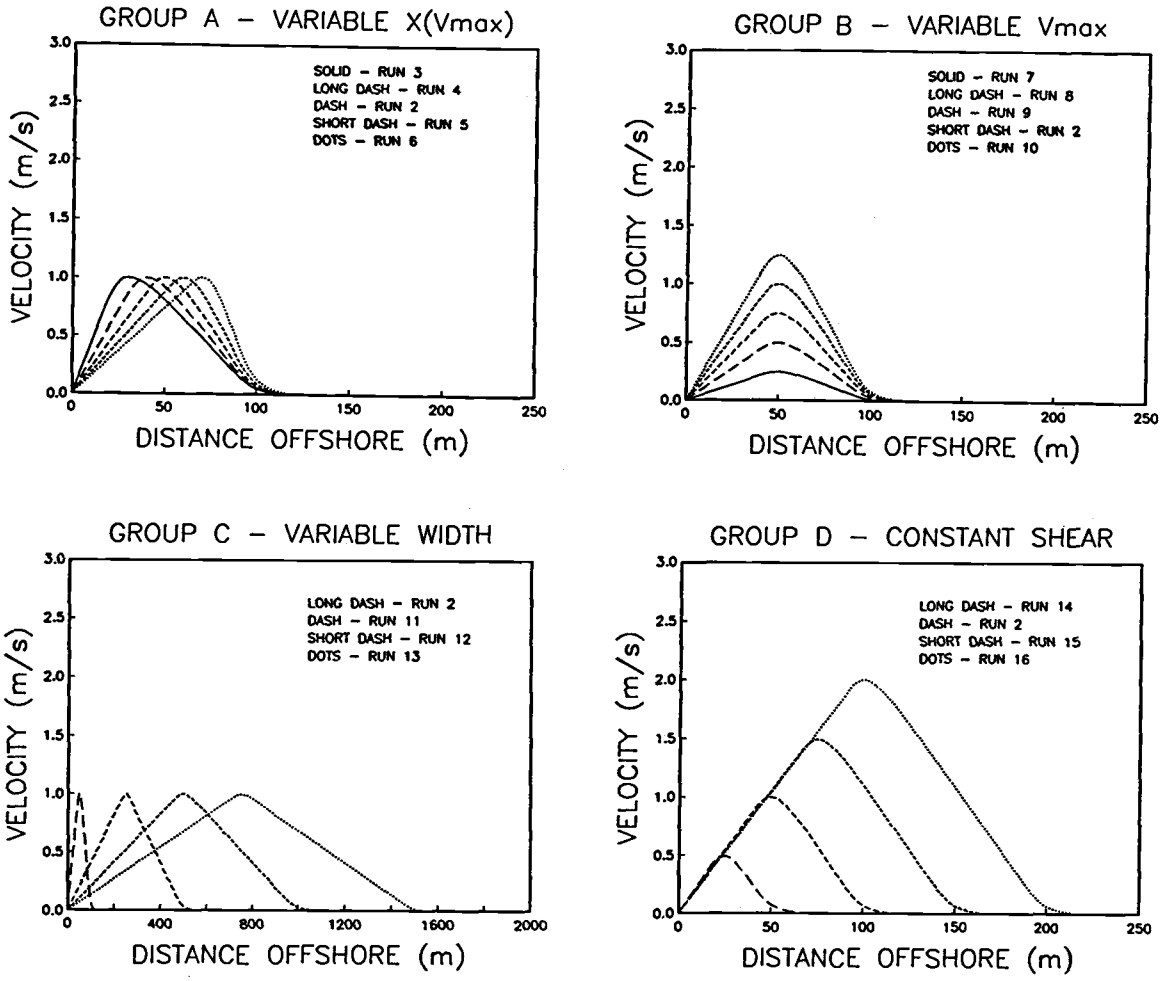

Figure III.2. Current profiles used for the test cases. The 16 runs have been broken into 4 groups. A. Group A holds V_{max} and x_w constant while varying $x(V_{max})$. B. Group B varies V_{max}, holding the width and $x(V_{max})$ constant. C. Group C holds V_{max} and the ratio of $x(V_{max})/x_w$ constant but varies the width and location of the maximum. D. Group D holds the landward face of the current to a constant shear, but varies all three of the current parameters. Note the cross-shore scale is different for C.

Effects on dispersion. Two general predictions can be made about the longshore current effects on edge wave dispersion. First, we expect the response to be asymmetric with regard to the direction of edge wave progression, and second, the maximum effect should occur at an intermediate value of frequency, decreasing for both high and low frequencies. The frequency dependence is related to the cross-shore scales of the edge wave and the current. For high frequencies (high wavenumbers), the edge wave is held tightly to shore and is not expected to see the entire current. For low frequencies, the edge wave extends well beyond the range of the current and sees it as only a small perturbation. The effective beach profile, Eq. III.11, provides a convenient way to address the changes to dispersion (Figure III.3). Edge waves progressing into the current ($V/c < 0$) have an effective profile which is shallower than the true profile, $\beta_{eff} < \beta$, thus $|\kappa|$ should increase. The opposite holds for those waves progressing with the current, the effective profile is deeper, resulting in an expected decrease in $|\kappa|$. We also expect the effects to increase as V increases which increases the departure of the effective profile from the true profile.

Figure III.4 plots the fractional wavenumber shift, K, for mode 0 edge waves as a function of frequency for all cases. We define K as

$$K = \frac{\kappa - \kappa_p}{\kappa_p} \tag{III.21}$$

with κ being the wavenumber in the presence of the current and κ_p being the wavenumber on the beach in the absence of a current. Throughout these synthetic tests the signs of κ and κ_p are negative for edge waves progressing in opposition to the current. Edge waves progressing into the current are modified such that $|\kappa|$ becomes larger (positive K). Those edge wave progressing in the direction of the current are modified such that $|\kappa|$ becomes smaller (negative K).

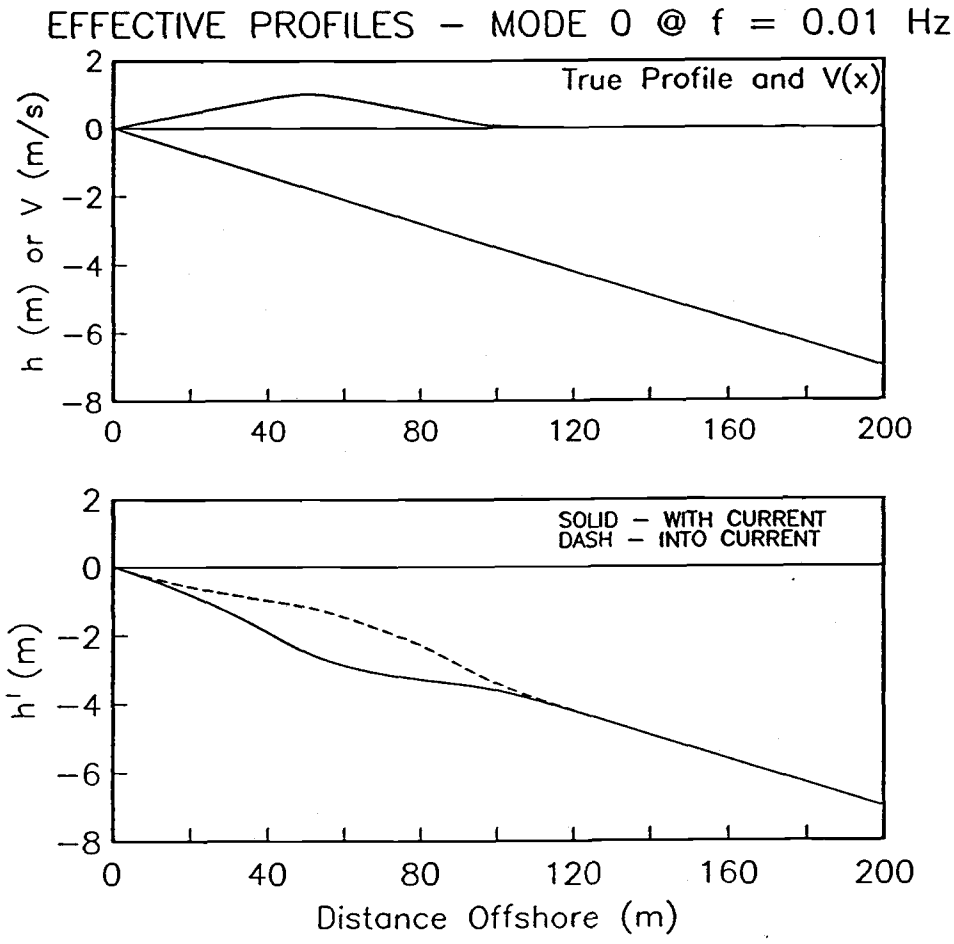

Figure III.3. The effective beach profiles for 0.010 Hz mode 0 edge waves for current run 2. The top panel shows the true beach profile and the current, while the bottom panel plots $h'(x)$. The resemblance of the profiles to either a terrace or bar and trough is unmistakable. The solid line indicates the effective profile for edge waves progressing with the current, the dashed line for edge waves progressing into the current.

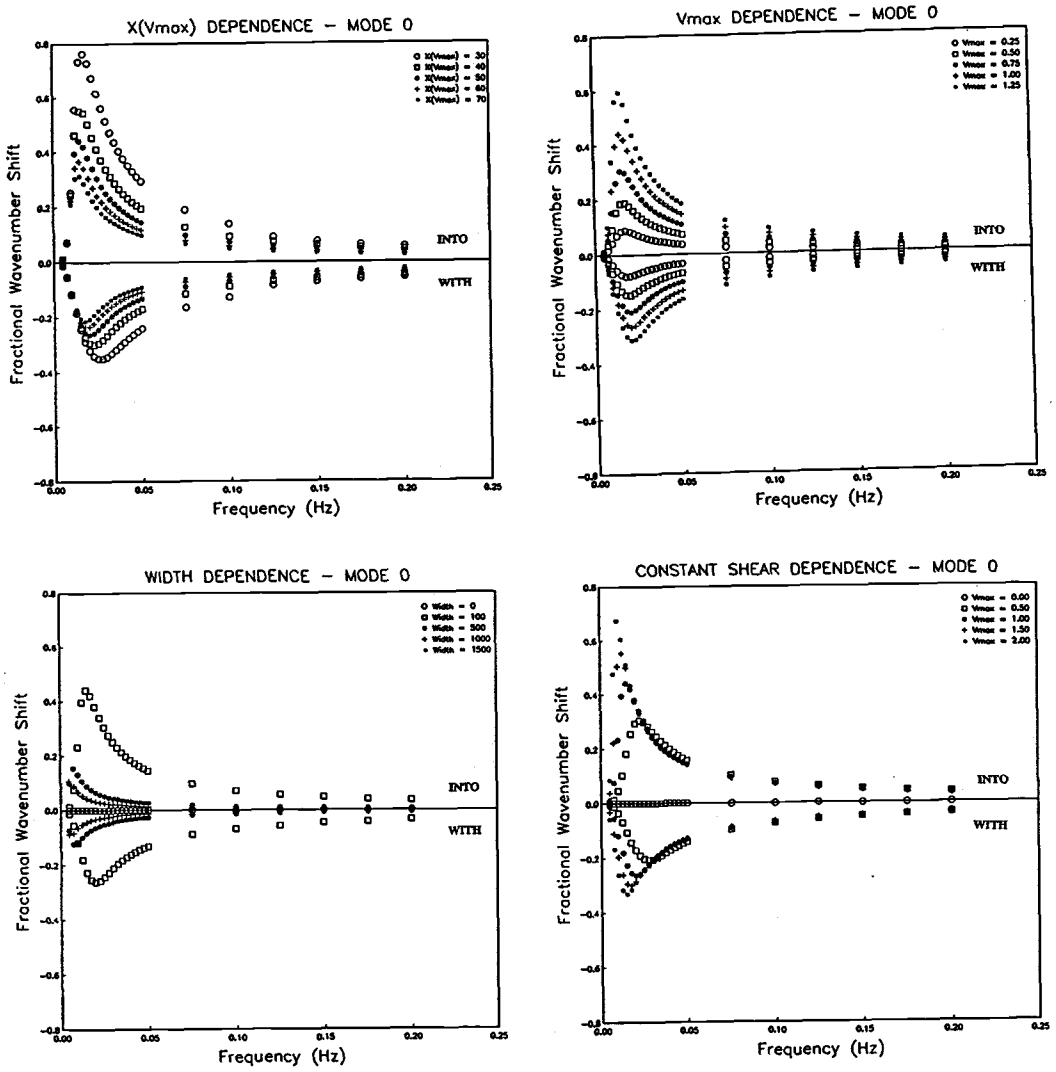

Figure III.4. The effect on dispersion, *K*, for each current group, as a function of frequency for the mode 0 edge waves. Panel letters refer to current groups A-D. In all cases except current run 13, the maximum effect is at an interior frequency. Note that the largest effect, near 80%, is for the current with the greatest shear on its landward face, corresponding to run 3.

Several of the expectations are verified. First, at both high and low frequencies the modification of the dispersion relation is generally small, with the maximum change (of up to 80% for these currents), occurring at an intermediate frequency. Second, the magnitude of the response is clearly asymmetric; the maximum $|K|$ for edge waves progressing into the current is greater, and the frequency at which it occurs is higher. Third, the magnitude of the change is a function of $x(V_{max})$ (Fig. III.4a), as well as the magnitude of V_{max} (Fig. III.4b).

The changes with increasing mode (equivalent to decreasing $|\kappa|$ and increasing the edge wave celerity) are clarified by Figure III.5. The maximum K shifts to higher frequency as the mode increases. The effect on the mode 0 edge wave is greater than for the other modes, for which the maximum effects are roughly equal. Figure III.6 shows the sensitivity to the match between the cross-shore scales of the edge wave and current by plotting K vs. $|k|x(V_{max})$, a dimensionless representation of the scaling between the offshore extent of the edge wave and the current ($k = \kappa/2\pi$). We again see that an interior maximum occurs. For the high frequencies, (large $|k|x(V_{max})$), the edge waves do not extend very far seaward, thus only see a small part of the total width of the current. The effective profile on which they exist does not depart greatly from the true profile. Similarly, for the lowest frequencies, the increase in edge wave celerity (as $|\kappa|$ decreases) acts to decrease the ratio (V/c), thus the departure of $h'(x)$ from the true profile. Throughout equations III.7 - III.11, the dependence on the term $1-V/c$ or $-\sigma+\kappa V$ is apparent.

Effects on cross-shore structure. The cross-shore dependence of an edge wave on a plane beach in the absence of a current, given by *Eckart* [1951], is

$$\phi(x) = A_n e^{-|\kappa|x} L_n(2\kappa x) \qquad \text{(III.22)}$$

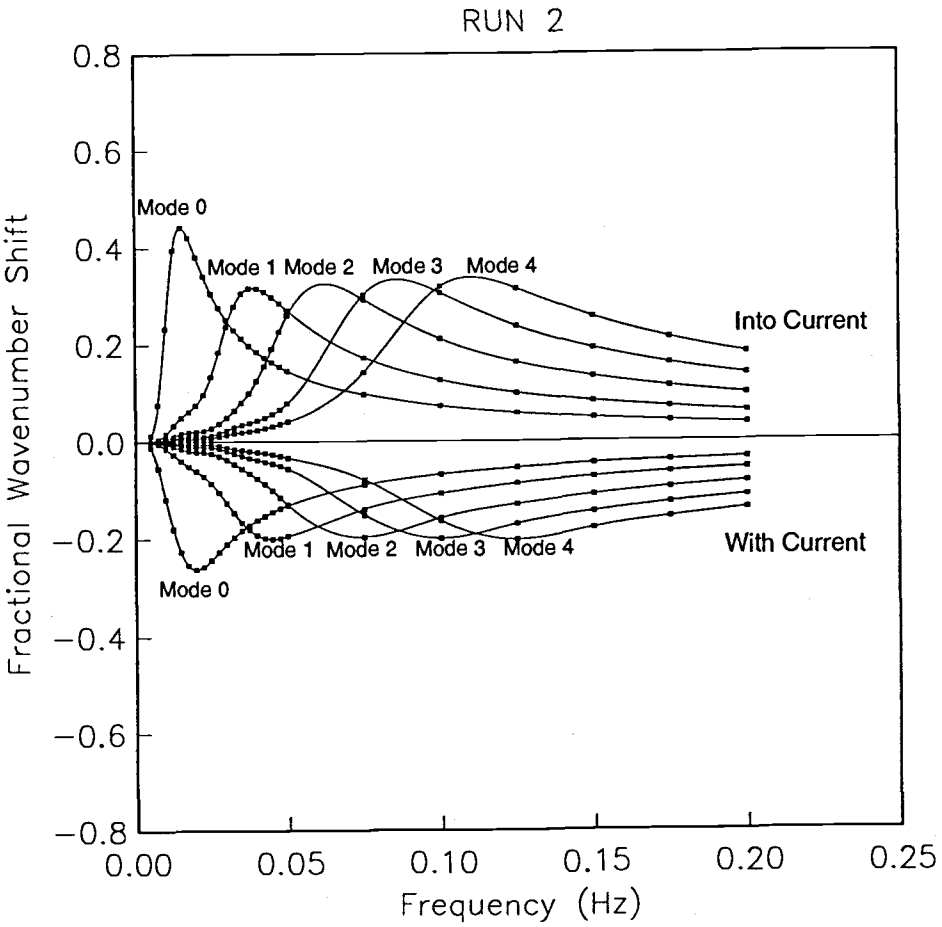

Figure III.5. The effect on dispersion for modes 0-4 for current Run 2. The maximum effects are felt by the mode 0 edge waves. There is a clear increase in the frequency at which the maximum occurs as the mode number increases, suggesting a relationship between the cross-shore extent of the edge wave and the magnitude of the current effect.

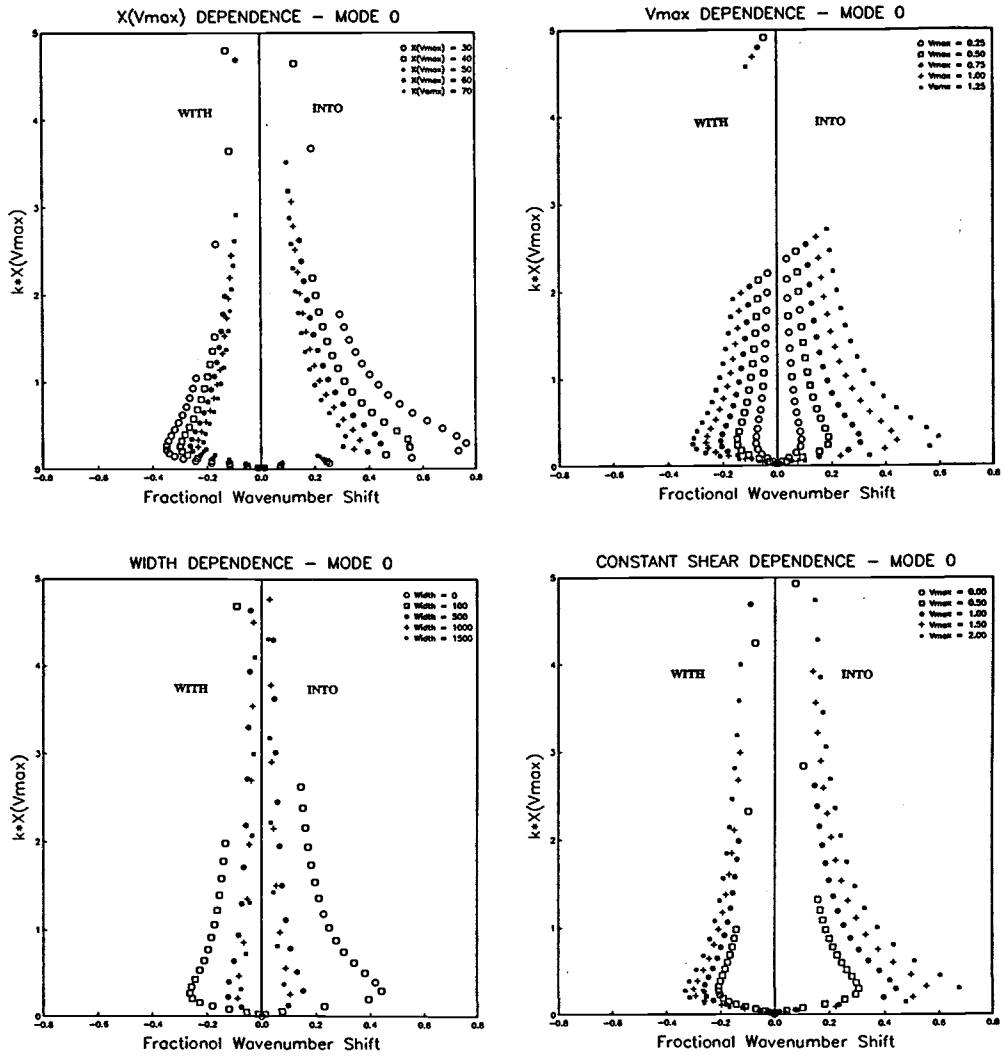

Figure III.6. K vs. $|k|x(V_{max})$ for the mode 0 edge waves.

for $\eta(x)$ and $v(x)$, while $u(x)$ varies as ϕ_x, where A_n is the shoreline value, and L_n is the Laguerre polynomial of order n, (n being the mode number). The cross-shore scale of the edge wave is clearly a function of $|\kappa|$, as $|\kappa|$ increases, the cross-shore scale decreases. As is seen by comparing the different directions of propagation in Figure III.7, the nodal locations are modified as expected; as $|\kappa|$ increases for the edge waves progressing into the current the nodal structure moves closer to shore.

It is also instructive to compare the cross-shore structure in the presence of a current to that found on the plane beach of slope, β_{eff}, which results in the same $\sigma-\kappa$ relationship (Eq. III.20). A sample comparison is shown in Figure III.8. In this case, the nodes for all three profiles (u, v, and η) are shifted landward of their locations on the equivalent plane beach. This figure also illustrates that the amplitudes of the antinodes are also modified by the presence of a current, analogous to the changes reported by *Holman and Bowen* [1979] and *Kirby et al.* [1981].

The impact of the current on the shape of $v(x)$ can become larger than on u or η. Equation III.5 shows that $v(x)$ includes an advective momentum term, uV_x. This term is important, particularly for the lower frequencies, where u remains relatively large at locations of sign changes in V_x. The spatial structure of the $v(x)$ profile is shown for the first three modes at 0.01 Hz in Figure III.9. The regions of large shear in the $v(x)$ profiles correspond with locations where the longshore current shear, V_x, changes sign ($x = 50$ m), and decreases to near zero ($x \sim 100$ m). Note that the variance profile, $v^2(x)$, will be different for the two propagation directions, and that, in the case of the mode 1 edge wave, the uV_x contribution is actually great enough to introduce additional zero crossings into the $v(x)$ profile. The $+\kappa$ edge wave profile now has 3 crossings, while the $-\kappa$ edge wave has two. At the same cross-shore location, it is possible to be at a zero crossing for an edge wave progressing one direction, while near a maximum in variance for

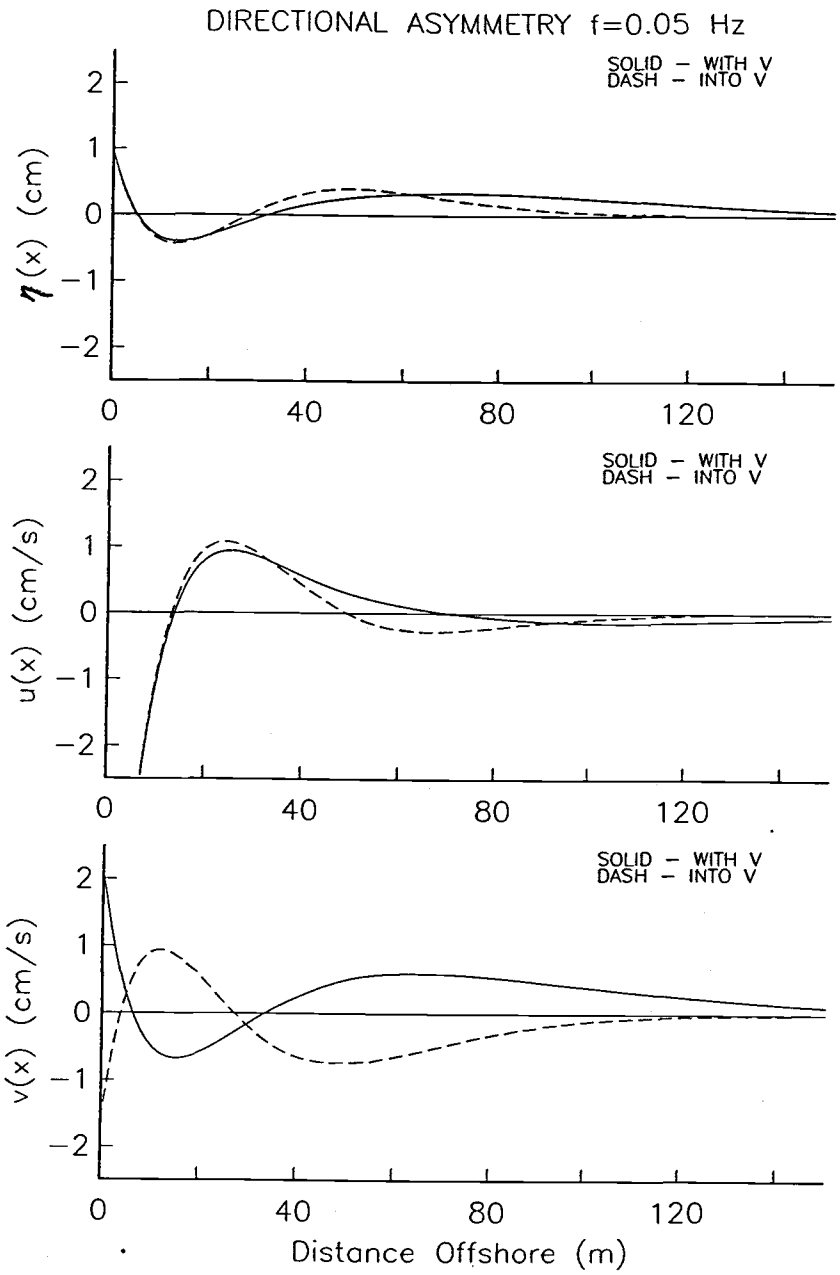

Figure III.7. Cross-shore profiles of surface elevation (top), cross-shore velocity (middle) and longshore velocity (bottom) for the mode 2 edge waves at 0.05 Hz for current Run 2. The nodal locations are shifted landward for the edge waves progressing into the current.

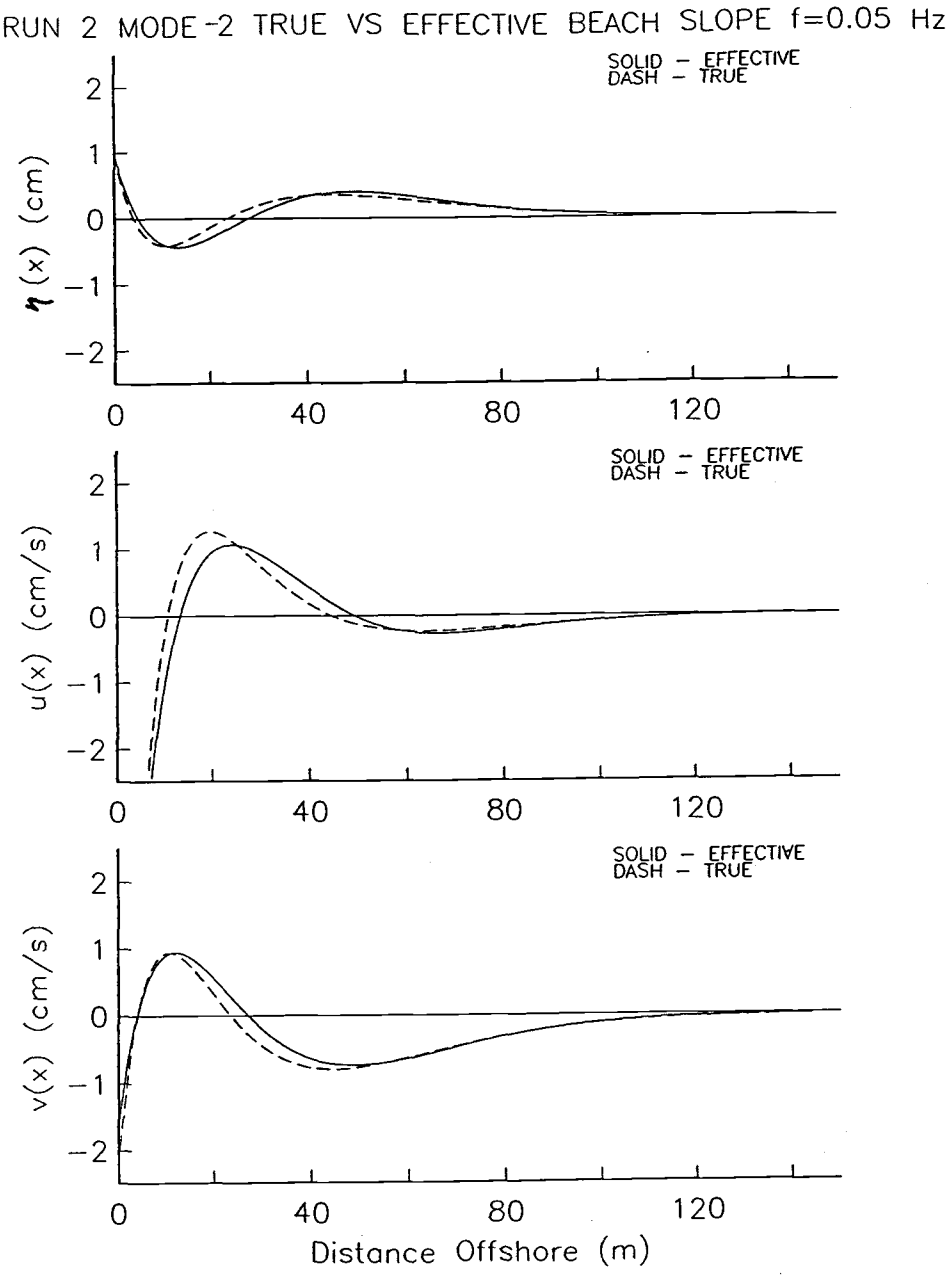

Figure III.8. A comparison between the cross-shore profiles of η (upper), *u* (middle), and *v* (lower), (the dashed lines) in the presence of a current (Run 2) with the solutions assuming a plane beach of slope β_{eff} (solid lines). Example shown is for the 0.05 Hz mode 2 edge wave progressing into the current. The shape of the edge wave is modified from that if the plane beach assumption had been made.

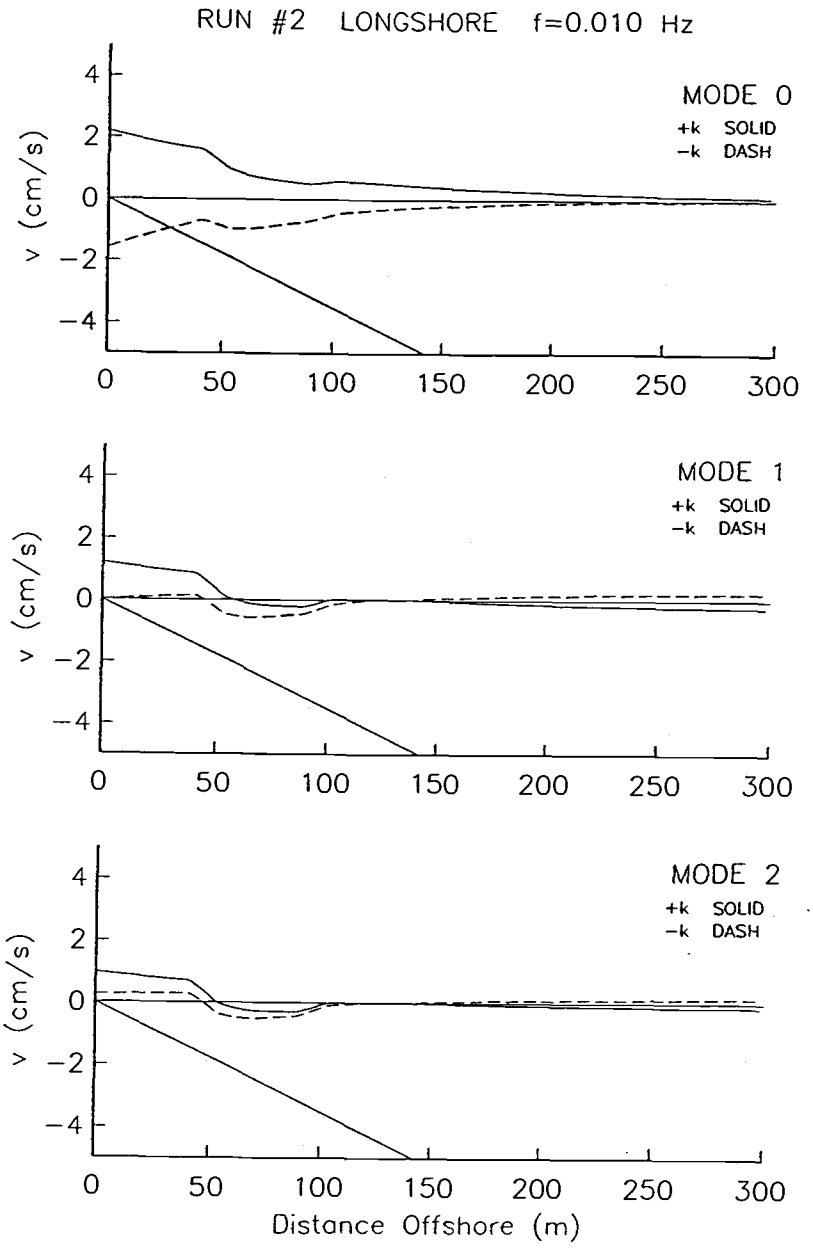

Figure III.9. $v(x)$ profiles for the first three modes at $f = 0.01$ Hz for current Run 2. The 'kinks' in the profiles are the result of the advective momentum term uV_x in Eq. 5 changing sign at $x = 50$, then going to 0. at $x \sim 100$. The effect is to increase the number of zero crossing in this component of flow, and to significantly alter the variance structure (v^2) between edge waves progressing opposite directions. The profiles of η and u (not shown) do not have the additional zero crossings.

the edge wave progressing the other direction. These additional zero crossings are not seen in the surface elevation profile, or in $u(x)$. The asymmetry in the $v(x)$ variance between the two directions of edge waves, obvious from consideration of Figure III.9, will be shown to be important for the correct interpretation of field data in the next section.

Discussion

Implications for field data. The identification of low mode edge waves has recently been shown possible using the longshore component of flow measured by alongshore arrays of bidirectional electromagnetic current meters deployed in the inner surf-zone [Huntley et al., 1981, Oltman-Shay and Guza, 1987]. Critical to the interpretation of these data has been correct prediction of edge wave dispersion, necessary for determination of the mode, as well as the cross-shore structure of the edge waves. These two pieces of information are needed to transform $v^2(\kappa,\sigma)$ measured at the array to the shoreline amplitude (and thus the energy) of the edge wave.

While the effects of longshore currents on edge wave dispersion have been dealt with in the past by common sense and assumption (*Oltman-Shay and Guza*, 1987; *Howd et al.*, 1991*a*), the effects on the cross-shore structure of the edge wave, particularly v(x), have not been considered. A recent experiment, DELILAH, hosted by the Coastal Engineering Research Center's Field Research Facility (FRF) in Duck, North Carolina during October, 1990, provided an opportunity to test the utility of the improved theory.

The study beach is located on the Atlantic coast of the United States in the center of a 100-km long barrier island. The primary source of data for this work was the inner array of current meters deployed in the surf zone, approximately 60 m from the mean shoreline in approximately 2-m water depth, where they remained submerged at all stages of the tide (Figure III.10). Sensors were oriented such that $+V$ currents (alongshore) flow 'south' parallel to the beach. The gages were wired to a computer-based collection system and were sampled at 8 Hz nearly continuously for a three week period. The FRF provided daily bathymetric surveys of the nearshore zone.

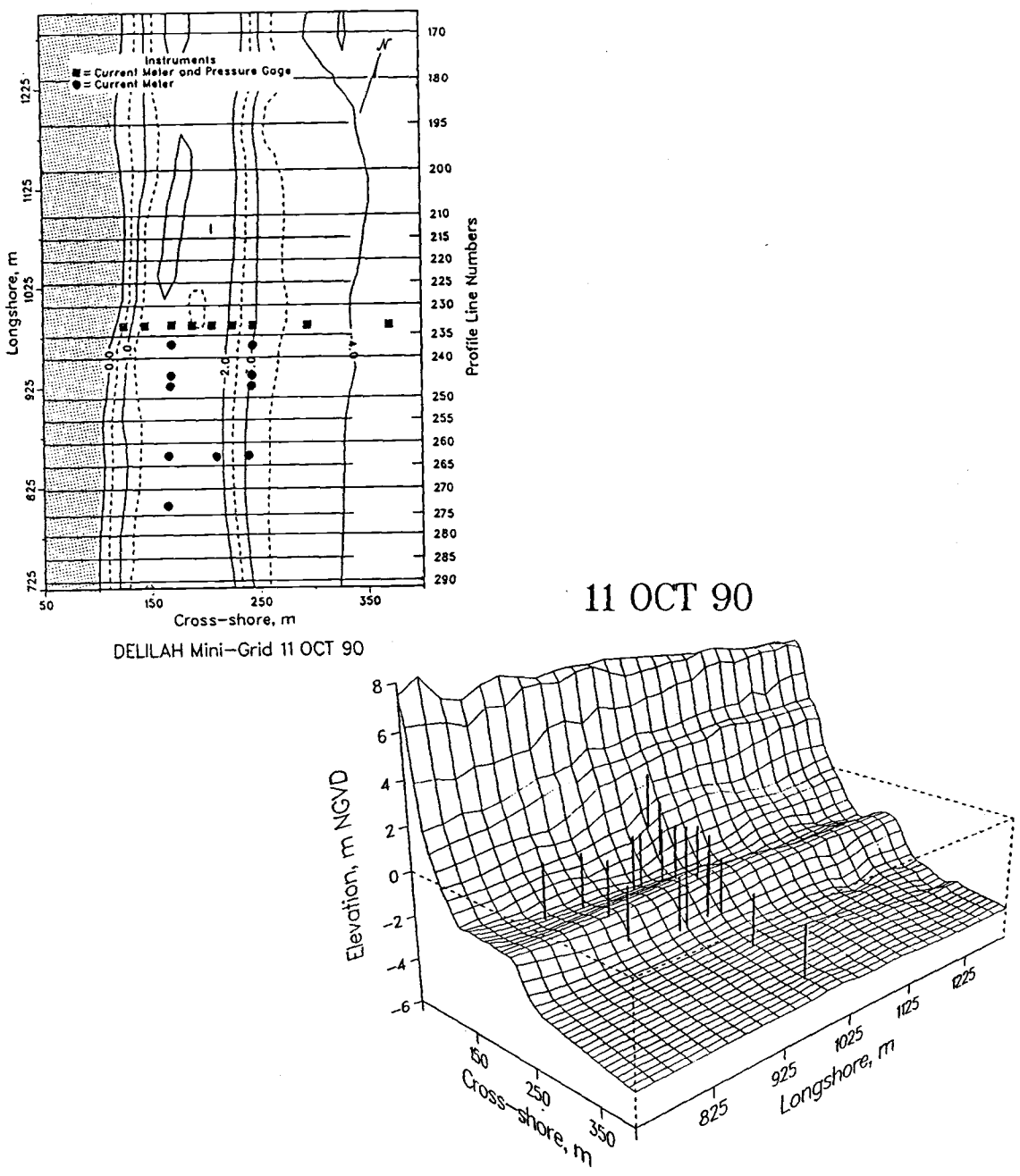

Figure III.10. Morphology and sensor locations for October 11, 1990 at the DELILAH experiment. The inner array of current meters was in the trough of the linear sand bar. The longshore current was to a great extent contained within the cross-shore scale of the array. Figure courtesy of Bill Birkemeier, Chief, CERC Field Research Facility.

A 3-hour time period beginning at 1117 EST on October 11, 1990 and bracketing high tide has been selected to demonstrate the importance of the longshore current on edge wave properties. This period of time was characterized by a stable, linear sand bar, and a steady longshore current. The maximum mean (over the 3-hour period) longshore current was -108 cm s^{-1} (northward) in the trough of the bar, and decreased to -23 cm s^{-1} at the outermost current meter. The current was extrapolated beyond that point and cubic-spline interpolated between the instruments (Fig. III.11).

Alongshore wavenumber-frequency spectra were estimated using the Iterative Maximum Likelihood Estimator (IMLE) previously applied to surf zone data by *Oltman-Shay and Guza* [1987] and *Oltman-Shay et al.* [1989]. The alongshore component of flow was used for the analysis as it provides a natural filter to remove high mode and leaky wave variance as shown by *Oltman-Shay and Guza* [1987]. The first three edge wave modes were modelled for the true morphology both with and without the mean longshore current (Figure III.12). Three areas will be discussed, the improvement in prediction of dispersion, prediction of the transition frequency between modes, and prediction of modal amplitudes.

The asymmetry produced by the current manifests itself in two ways (Fig. III.12b), asymmetric wavenumber shifts (note the difference between the magnitudes of predicted plus and minus mode 0 wavenumbers at 0.05 Hz) and the compression of dispersion lines for the negative wavenumbers (with the current) and the expansion of the dispersion curves for the edge waves progressing against the current (positive wavenumbers). The lower modes are shifted more than the higher modes, be it an increase or decrease in $|\kappa|$. While this makes separation of modes difficult for the edge waves progressing with the current (negative wavenumbers in this case), it improves separation in the direction opposing the current.

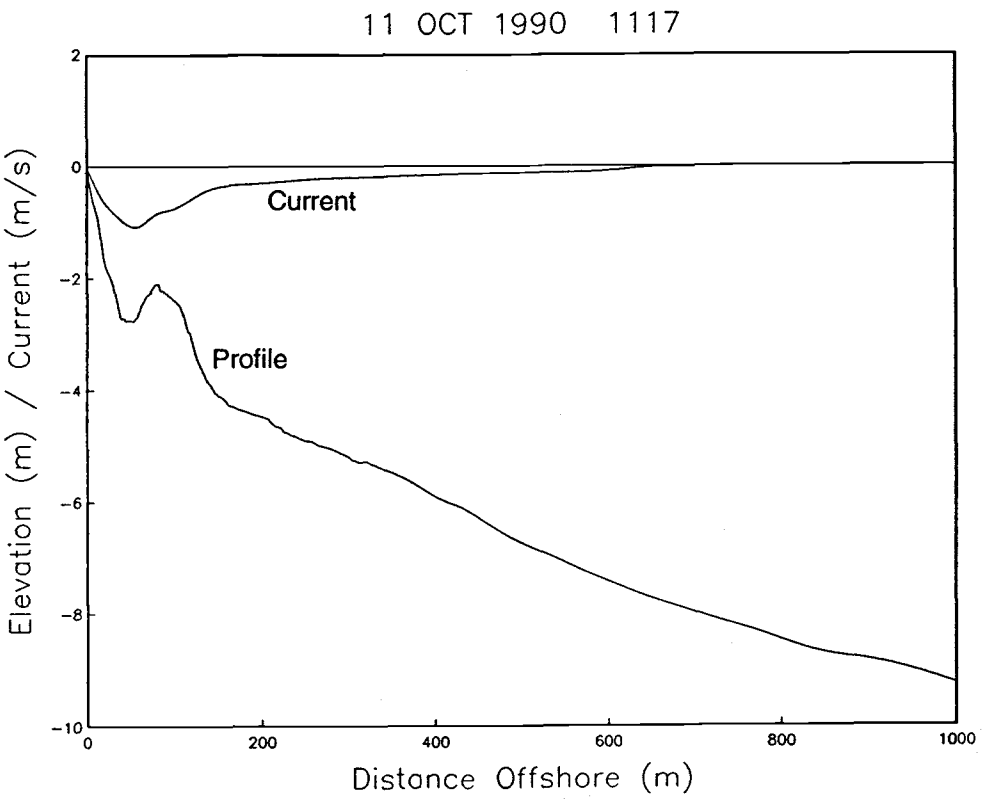

Figure III.11. Beach and longshore current profiles used to solve for edge wave characteristics on October 11, 1990.

Figure III.12. Frequency-wavenumber spectrum from October 11, 1990. The horizontal axis is the cyclic wavenumber ($k = 1/L_y$), the frequency ($f = 1/T$) is shown on the vertical axis. The shaded squares represent concentrations of variance in k-f space, with the darker boxes indicating a greater percent of that frequency band's energy. The height of the boxes is the frequency bandwidth, the width represents the half-power wavenumber bandwidth of the spectral peaks which exceed the noise floor. The left panel shows the numerical solutions, indicated by the $*$, for the dispersion without including the effects of the current, the right panel solutions include the current.

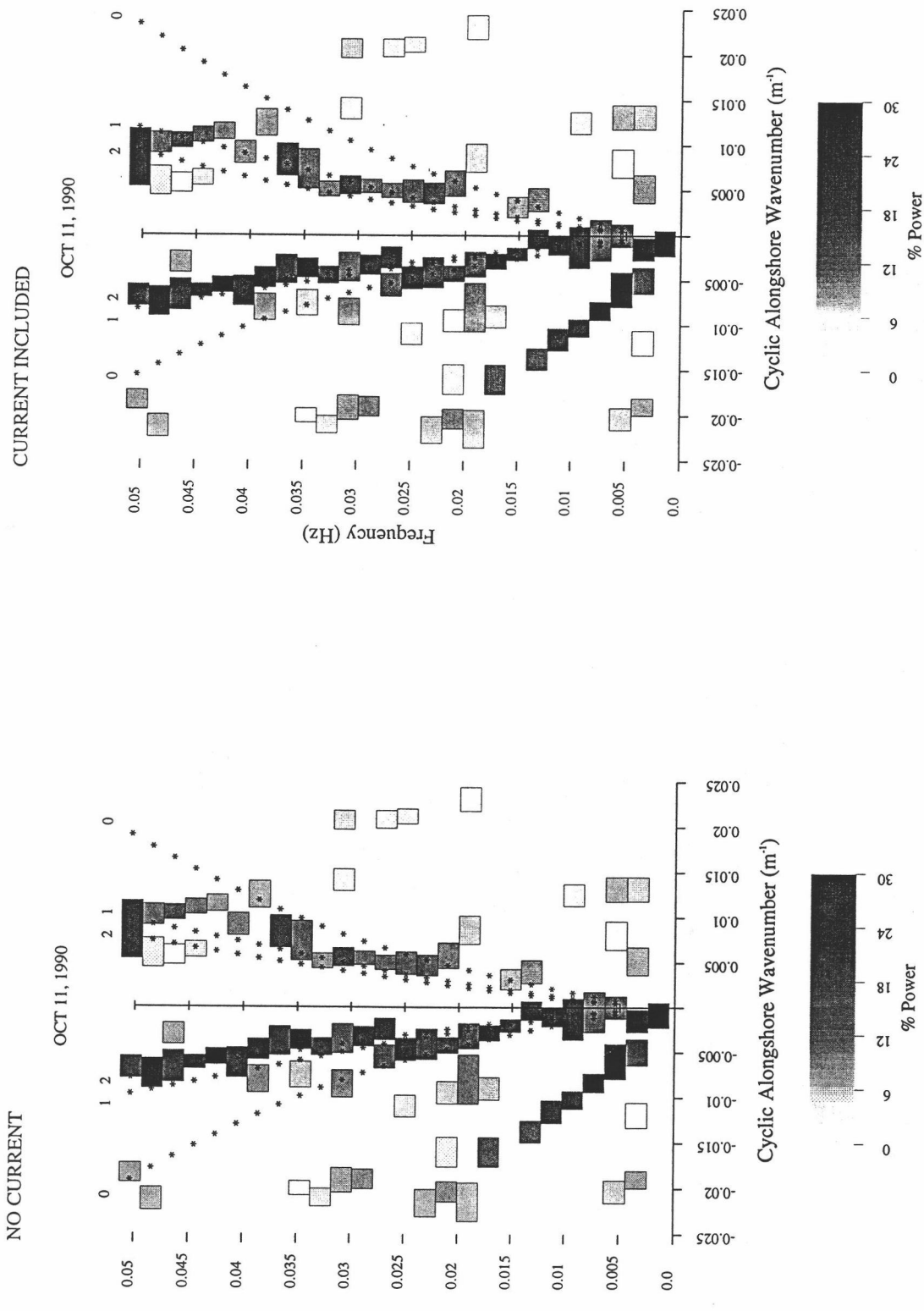

Figure III.12.

Figure III.13 presents K as a function of frequency for the field data. Many of the observations made with the synthetic tests hold here as well. The maximum effect (~30% for the edge waves opposing the current, ~20% for the edge waves progressing with the current) occurs at an intermediate frequency for mode 0. The maximum effect decreases in magnitude and shifts to higher frequencies for the higher modes. In contrast with the synthetic cases, the peak effect is felt over a much broader frequency range.

An excellent example of specific improvement in fitting modes to the data occurs for positive wavenumbers in the frequency range 0.02 to 0.03 Hz. In the absence of the current, (Fig. III.12a), the observed variance peaks fall cleanly between the predicted mode 0 and mode 1 dispersion lines. Inclusion of the current in prediction of the dispersion lines, (Fig. III.12b), indicates that the edge waves are, in fact, mode 1. Similar improvement occurs at other frequencies and wavenumbers, particularly the negative wavenumber mode 0 edge waves.

Close examination of the data presented in Figure III.12 shows some important details that are indicative of directional asymmetry. Most obvious is the dominance of the negative wavenumber edge waves, which contain approximately 1.5 to 2 times the variance of their positive wavenumber counterparts. Also, the mode 0 edge waves dominate the negative wavenumber edge waves up to a frequency of ~ 0.027 Hz where we begin to see evidence for mode 1 or 2 edge waves, while, for the positive wavenumber edge waves, the transition from mode 0 to mode 1 occurs at a lower frequency, 0.023 Hz. The asymmetry may have two causes, differences in the forcing of the modes, or the effects of the longshore current.

The modelled variance structure for mode 0-2 edge waves (all with shoreline amplitudes of 1 cm) as a function of frequency at the cross-shore location of the current

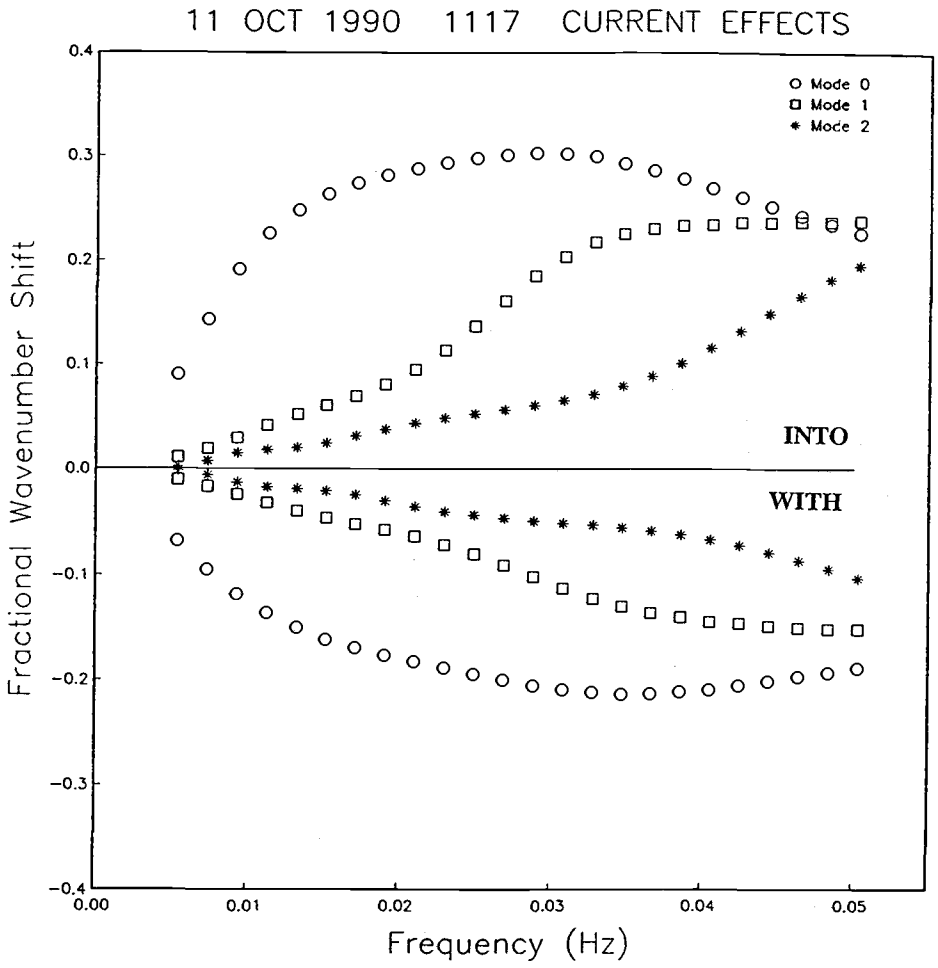

Figure III.13. K vs. f for the field data from October 11, 1990.

meter array addresses the longshore-current-induced asymmetry (Figure III.14). In the absence of a longshore current, the frequency where the mode 0 variance drops below that of modes 1 and 2 would be the same for the two directions of edge wave propagation. The presence of the longshore current has caused shifts in the cross-shore shapes of the edge waves such that the mode 0-1 transition occurs at 0.0275 Hz for negative wavenumbers and at 0.024 Hz for the positive wavenumbers. The asymmetry of mode transition seen in the data (Fig. III.12) is clearly predicted by the inclusion of the longshore current.

As an example of the effect of the longshore current on observed variance levels in the data, we will examine two frequency bands, those centered on 0.021 Hz and 0.040 Hz. Figure III.15 plots the observed wavenumber spectra for these two frequencies. The spectral peaks are clearly associated with the mode 1 (0.040 Hz) and mode 0 (0.021 Hz) edge waves predicted by the model.

The observed ratio between the peak variances of the mode 0 edge waves ($-\kappa/+\kappa$) at 0.021 Hz is 2.52; in the absence of a current we would expect the $-\kappa$ edge wave to have a similarly greater shoreline variance (and lead to the assumption of substantial asymmetry in the forcing). However, the inclusion of the current effects in modelling $v^2(x)$ results in edge waves with identical shoreline elevations having a ratio between their variances of 1.96 at the array location (Fig. III.14). The ratio of these values indicates that the negative mode 0 edge wave should have larger shoreline variance by a factor of only 1.29 (2.52 ÷ 1.96) at the shoreline despite its much larger variance at the array location. Failure to include the effects of the longshore current would result in an overprediction by a factor of ~2 in the relative shoreline variances of these two waves. Indications are that there is less asymmetry in the forcing than would have been previously predicted.

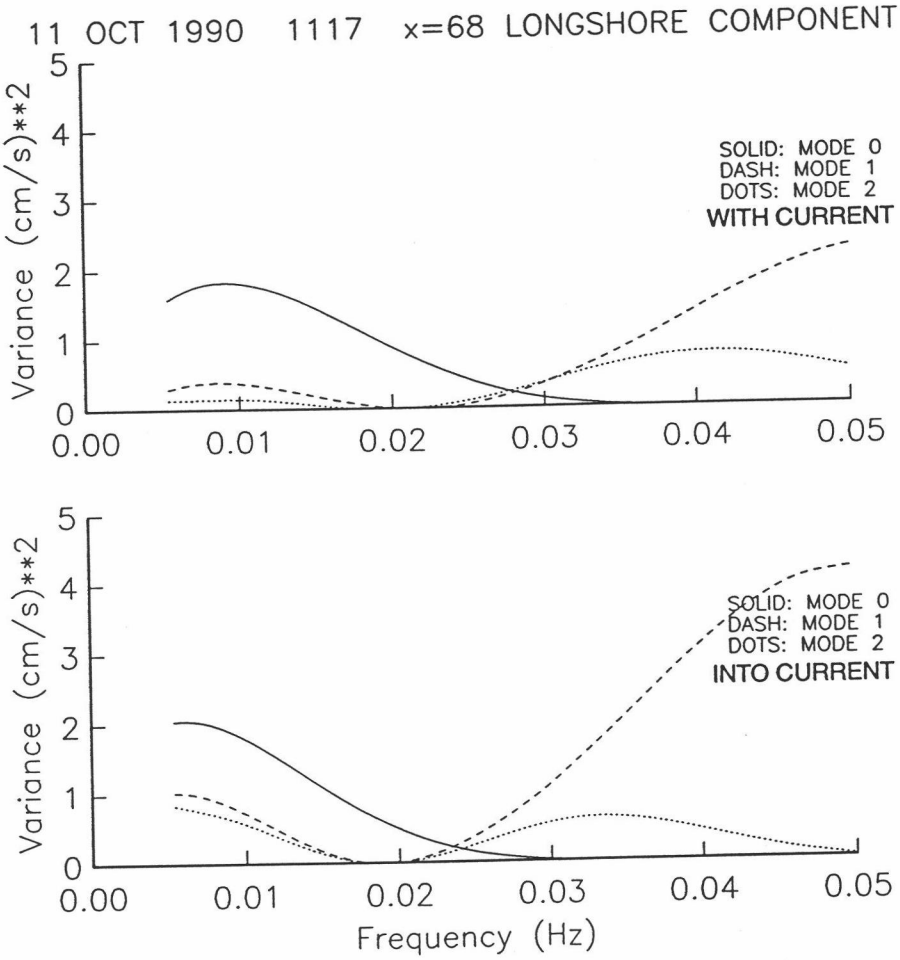

Figure III.14. Variance of the longshore component of edge wave flow vs. frequency for the first three modes at the cross-shore location of the array. Asymmetry introduced by the longshore current is apparent.

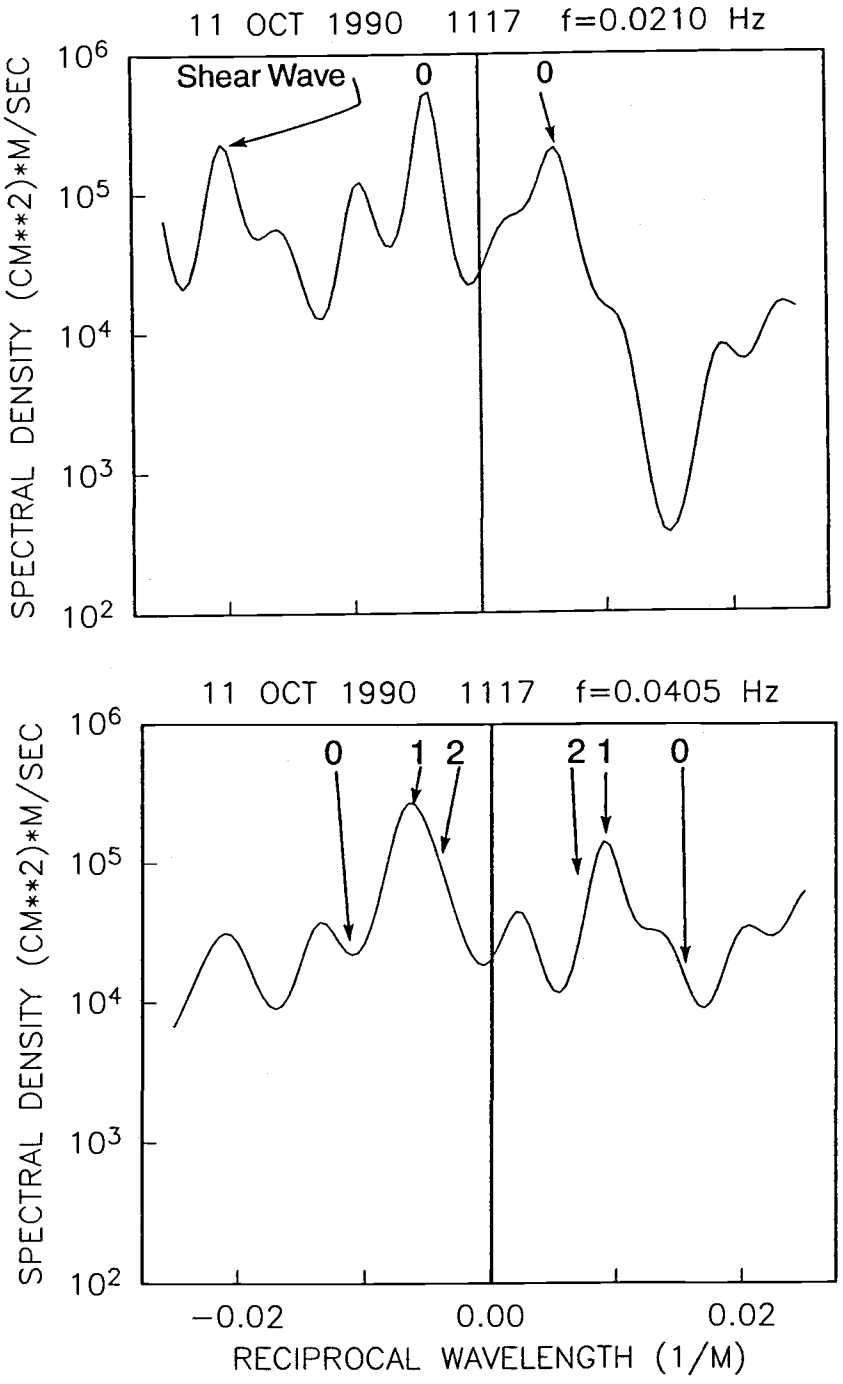

Figure III.15. Wavenumber spectra for two frequency bands 0.021 Hz (upper panel) and 0.040 Hz (lower panel). Peaks correspond with the predicted wavenumbers for edge wave modes in the presence of the longshore current.

A similar situation exits for the mode 1 edge waves at 0.040 Hz. The observed ratio of $-\kappa$ to $+\kappa$ peak variance is 1.90. Again, in the absence of a current, we would assume that this was a direct reflection of different shoreline variances. However, this is misleading, as model results predict a much smaller ratio of 0.45 at the array location for edge waves with equal shoreline amplitudes. In this case, the assumption of no current effect would lead to an underprediction of the relative shoreline variance by a factor of ~4.22. In this case, there is a strong evidence of a much larger directional asymmetry in the edge wave forcing.

The possibility of such strong asymmetry being introduced into the edge wave $v^2(x)$ profiles by the longshore current make it important that the current be adequately measured and accounted for in data analysis if the shoreline amplitudes of the edge waves are required. This topic is discussed further in *Oltman-Shay and Howd*, in prep., in the context of a re-examination of edge wave amplitudes originally presented by *Oltman-Shay and Guza* [1987].

Modification of topography. Perhaps the most obvious impact of the inclusion of the longshore current effects on models for the generation of topography due to edge waves is the modification of the dispersion relationship. Edge waves of the same mode and frequency progressing in opposite directions no longer have equal magnitude wavenumbers. Thus a crescentic sand bar system, predicted for phase-locked edge waves of equal frequency and mode, but opposite directions of progression, by *Bowen and Inman* [1971], could be stretched into the oblique welded bar predicted by *Holman and Bowen* [1982] for the case of two phase locked edge waves of equal frequency but different $|\kappa|$ of opposite sign.

A more interesting role in the evolution of topography is suggested by the shapes of the effective profiles. Recalling Fig. III.3, the effective profiles are very reminiscent

of either bar and trough topography for the edge waves progressing with the current, or of terrace topography for those opposing the current. The possibility of feedback from the effective topography (i.e. due to the longshore current structure) in the determination of the true topography will be briefly explored using one of the synthetic cases presented earlier; a test with field data is beyond the scope of this paper.

Following *Hunt and Johns* [1963] and *Holman and Bowen* [1982], the cross-shore drift velocity of a progressive edge wave at the top of the bottom boundary layer, $\hat{u}(x)$, can be expressed as

$$\hat{u}(x) = \frac{-1}{4\sigma}(3uu_x - \kappa uv) \tag{III.23}$$

and the x-dependencies on the R.H.S. are understood. We will examine the drift velocity defect, $\Delta\hat{u}(x)$, defined as

$$\Delta\hat{u}(x) = \hat{u}(x) - \hat{u}_p(x) \tag{III.24}$$

where $\hat{u}_p(x)$ is the drift velocity on a plane beach in the absence of a current.

If the existing profile results from the balance between gravity (always working down slope), the edge wave drift velocities, and the incident waves, we can conceptualize the changes which will result from the modification of the edge waves (due to the addition of a longshore current) in terms of the differential transport, which, after *Holman and Bowen* [1982], should be of a form similar to

$$\Delta i_x = \frac{\varepsilon_s C_d \rho}{w}\frac{16}{15\pi}\left(5u_0^3\Delta\hat{u} + \frac{u_0^5}{w}\frac{d\hat{h}}{dx}\right) \tag{III.25}$$

where Δi_x is the differential suspended transport in the cross-shore direction, u_0 is a characteristic incident wave orbital velocity, ρ and w are the sediment density and fall

velocity, and ε_s and C_d are an efficiency and drag coefficient, respectively, and finally, $\hat{h}$ is the perturbation to the bed away from its old equilibrium position. The new equilibrium profile is defined by the condition $\Delta i_x = 0$ for all x giving

$$\frac{d}{dx}\hat{h}(x) = \frac{-5w\Delta\hat{u}}{u_o^2} \qquad \text{(III.26)}$$

Integrating from deep water toward the shoreline gives the perturbation profile. The u_o profile is specified as in [*Holman and Bowen*, 1982] for shallow water theory seaward of the breakpoint (u_o increases slowly to the breakpoint). A depth-dependent breaking region with decreasing velocity has been added from the breakpoint to the shoreline. Because u_o goes to zero at the shoreline, the integration of Eq. III.26 is invalid very close to shore. However, the tendency of the perturbation transport will be toward $\hat{h}$, thus a true bar or terrace on the beach profile will be reinforced if the perturbation profile assumes the shape of the effective profile.

There are two primary contributions to $\Delta\hat{u}(x)$, thus to the perturbation topography, the shift of the nodal structure as κ changes (due to the dispersion effects of the longshore current) and the 'kinks' in the $v(x)$ profiles introduced by the longshore current shear (Fig. III.9, Eq. III.5). It is important to note that while the cross-shore location of the nodal structure will change (and with it the preferred location of the sand bar) with frequency and mode, perturbations to $v(x)$ (and through Eq. III.23, $\hat{h}(x)$) resulting from the longshore current shear change only in magnitude and have a fixed cross-shore location (Eq. III.5). This should provide a consistent cross-shore scale for the perturbation topography (for one direction of edge wave progression) even in the presence of a broad-banded edge wave field (where the nodes are not at a constant cross-shore distance).

Figure III.16 presents the perturbation profile for three (randomly selected) edge waves progressing with the current. Recall the effective profiles for these edge wave should look like a bar and trough (Fig. III.3) . This figure serves to show the contributions of the two different current effects. The two low-frequency edge waves (the lower panels) are modified strongly by the shear in the current, and predict a bar-like feature ~100 m offshore. For the higher frequency edge wave (upper panel), the pattern is dominated by shifts in the nodal positions. The value of $u(x)$ is near zero at $x = 50$ and 100 m where V_x changes sign. Thus, the uV_x contribution to the perturbation drift velocity is small for this edge wave (Eq. III.5 and III.23).

A logical test of the robust nature of this hypothesis is presented in Figure III.17 which shows the result of adding the perturbation profiles for all the modelled edge waves, modes 0 to 4, with $\kappa > 0$, for the frequency range 0.05 to 0.005 Hz. The total perturbation profile predicts the formation of a sand bar 100 m offshore, the same location predicted by the effective profile (Eq. III.11). The longshore current effects may in fact provide a positive feedback mechanism, through the effective beach profile, for the evolution of the true profile. These results should not be interpreted as quantitative, rather as a qualitative prediction of the tendency for sediment transport by edge waves perturbed by a longshore current. Obviously the total transport of sediment in the surf zone is much more complicated than allowed by the simple model presented here.

For the case of edge waves opposing the current, $\kappa < 0$, the total perturbation profile is indicative of a bar or terrace, much closer to the shoreline, as expected (Figure III.18). Note that for the net perturbation profile to look like either a bar and trough, or a terrace, the edge wave field must be dominated by the "correct" direction of progression. Field data seem to indicate this is a more plausible senario than having the edge wave field dominated by a single frequency as required by previous models for linear

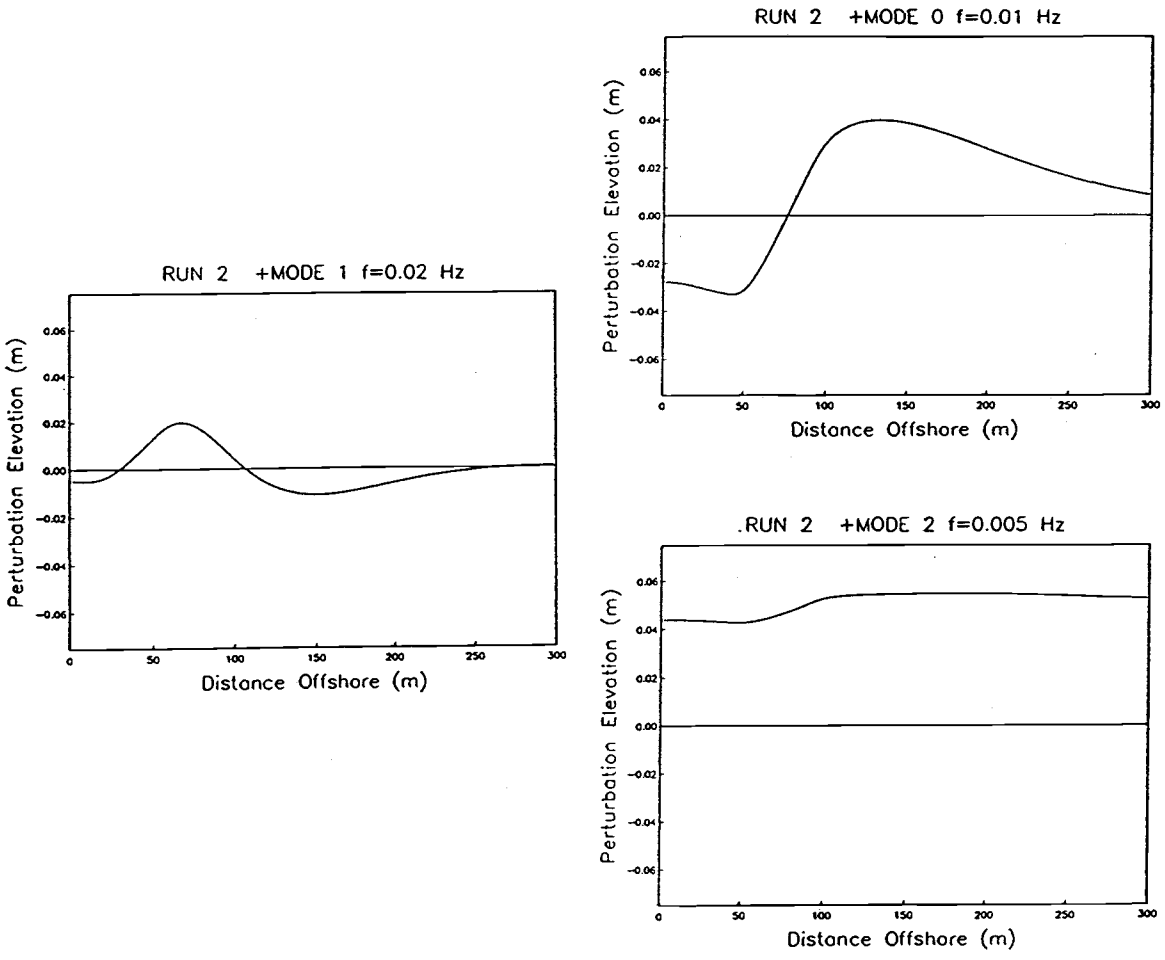

Figure III.16. Profiles of the perturbation topography for edge waves progressing with the current resulting from the introduction of a longshore current. The left panel shows the profile for a 0.02 Hz mode 1 edge wave; the top right panel mode 0 at 0.01 Hz; the lower, mode 2 at 0.005 Hz.

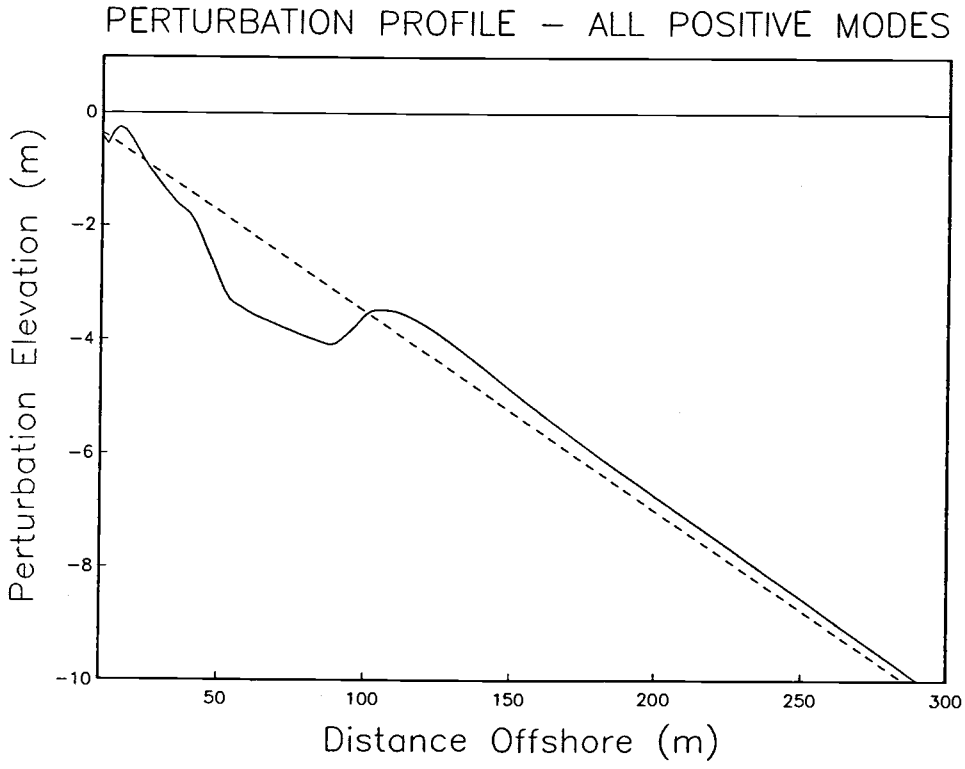

Figure III.17. Total profiles $(h + \hat{h})$ for all edge waves modeled in Run 2 (modes 0 to 4) progressing with the current and with f less than or equal to 0.05 Hz. Bar and trough topography with the same cross-shore scale as the effective profile (Figure 3) is predicted. The perturbation topography has been arbitrarily scaled (for ease of visibility) to correspond with an edge wave shoreline amplitude of 50 cm.

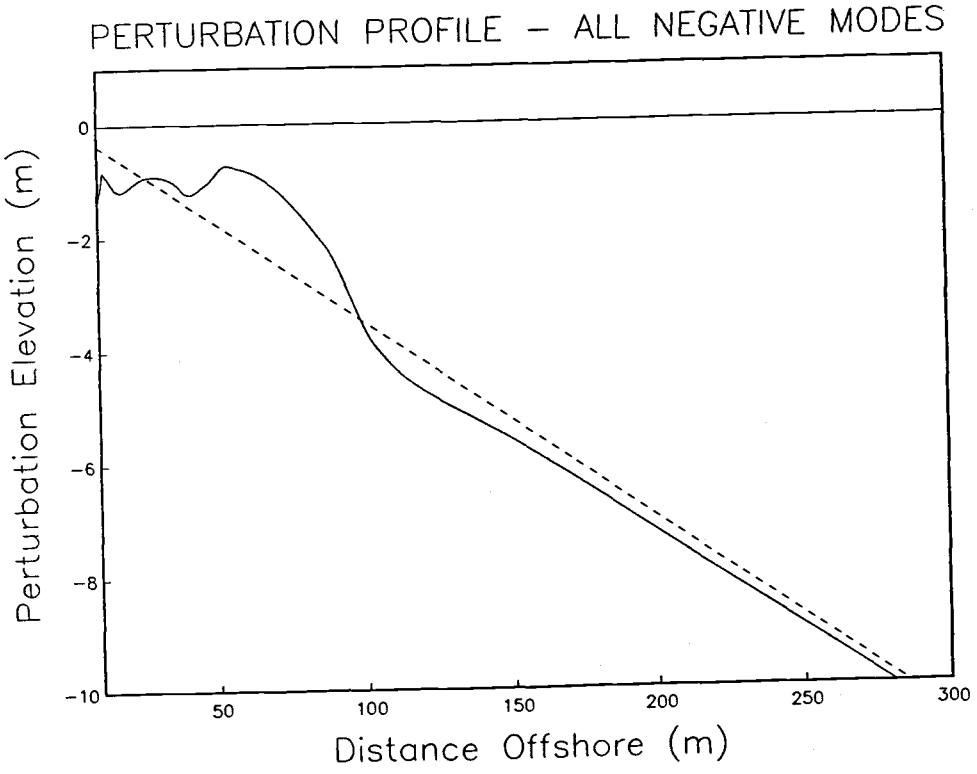

Figure III.18. Same as Figure III.17, but for the edge waves progressing into the current. A terrace is predicted.

sand bar formation. *Howd et al.* [1991*b*] present an initial look at field data showing the evolution of a linear bar during a storm and report that there are indications of the effective profile providing positive feedback to the evolution of the true profile.

Summary

We have shown that longshore currents modify refraction in the nearshore wave guide, changing the dynamics and kinematics of edge waves. A form of the linear, inviscid shallow water wave equation, which includes arbitrary longshore currents and bathymetry, was derived. This equation provides a continuum of solutions between gravity waves (either leaky or edge waves) and the recently discovered shear waves. For edge waves and leaky waves, the current effects can be uniquely accounted for in terms the effective beach profile, $h'(x) = h(x)\left[1 - \frac{V(x)}{c}\right]^{-2}$. The effective profile is particularly useful in conceptualizing the combined effects of longshore currents and variable bottom topography provided $V/c < 1$.

Numerical solutions have shown the edge wave dispersion relationship and the cross-shore shapes of edge waves to be sensitive to the presence of a current. Changes to the edge wave alongshore wavenumber, κ, of up to 80% are found for reasonable current profiles, showing that the departure from plane beach dispersion due to longshore currents can be of the same order as the effect of introducing non-planar topography. Unlike non-planar topography, the longshore current introduces anisostropy into the edge wave dispersion relationship, with $|\kappa|$ increasing for edge waves opposing the current flow, and decreasing for those edge waves coincident with the flow. The cross-shore structure of the edge waves is also strongly modified. As expected, as $|\kappa|$ increases (decreases), the nodal structure shifts landward (seaward) from the positions in the absence of a current. In addition, the predicted variances away from the nodes, particularly for the alongshore component of edge wave orbital velocity, may change dramatically from the no-current case. Failure to account for these changes can lead to incorrect identification of modes and large errors in the estimation of the corresponding shoreline amplitude.

The magnitudes of many of the edge wave responses are related to the ratio V_{max}/c, where V_{max} is the maximum current, and to the dimensionless cross-shore scale of the current, $|\kappa|x(V_{max})$, where $x(V_{max})$ is the cross-shore distance to V_{max}. This is most easily understood in terms of the effective profile and the strong dependence of the edge waves to the details of the inner part of the beach profile.

Examination of field data supports the importance of correct modelling of longshore current effects. Inclusion of the current was needed for correct identification of the different edge wave modes, and accurate estimates of their shoreline variances. For the case discussed, the longshore current (maximum mean velocity of -108 cm s^{-1}) produced shifts in the dispersion relationship in excess of 20% over much of the infragravity band. Errors of greater than a factor of 4 in relative shoreline variance were shown possible if the current effects were not properly accounted for in interpreting data collected from a current meter array located in the surf zone.

Inclusion of longshore current effects also has strong implications regarding the role of edge waves in the generation of nearshore morphology. The most obvious of these is the result of changes to the dispersion relationship. In the absence of a current, up and down coast edge waves of equal frequency and mode have the same $|\kappa|$. If the waves are phase locked, a crescentic bar is expected to result [*Bowen and Inman*, 1971]. However, in the presence of a current, the $|\kappa|$ magnitudes differ and presumably a more complicated pattern would result, perhaps resembling the welded bar result of *Holman and Bowen* [1982].

The most interesting effect is the positive feedback between the effective topography and the true profile. The cross-shore component of the edge wave drift velocity is modified in such a way that the effective topography is enhanced in the true profile. The perturbation profile results from two effects, the shifting of the nodal structure as

the current changes the dispersion relationship, and the importance of the longshore current shear on the $v(x)$ profile of the edge wave. Because the longshore current profile is assumed fixed in time and space, it provides a consistent perturbation regardless of edge wave frequency or mode. This is attractive because it provides an independent cross-shore scale for edge wave generation of sand bars, requiring only that one direction of progression be dominant.

References

Ball, F. K., Edge waves in an ocean of finite depth, *Deep Sea Res.,14*,79-88, 1967.

Bowen, A. J., Simple models of nearshore sedimentation; beach profiles and longshore bars, in *Proceedings of the Coastlines of Canada Conference*, p. 1-11, 1981.

Bowen, A. J., and D. L. Inman, Rip currents: 2. Laboratory and field observations, *J. Geophys. Res., 74*, 5479-5490, 1969.

Bowen, A. J. and D. L. Inman, Edge waves and crescentic bars, J. *Geophys. Res., 76,* 8662-8671, 1971.

Bowen, A. J. and R. A. Holman, Shear instabilities of the mean longshore current: 1. Theory, *J. Geophys. Res., 94,* 18023-18030, 1989.

Eckart, C., Surface waves on water of variable depth, *Wave Rep. 100, Ref. 51-12*, 99 pp., Scripps Inst. of Oceanogr., Univ. of Calif., La Jolla, 1951.

Elgar, S. and R.T Guza, Observations of bispectra of shoaling surface gravity waves, *J. Fluid Mech.*, 161, 425-448, 1985.

Gallagher, B., Generation of surf beat by non-linear wave interactions, *J. Fluid Mech., 49*, 1-20, 1971.

Guza, R. T. and D. L. Inman, Edge waves and beach cusps, *J. Geophys. Res., 80,* 2997-3012, 1975

Guza, R. T. and E. B. Thornton, Observations of surf beat, *J. Geophys. Res., 90*, 3161-3172, 1985.

Holman, R.A. and A. J. Bowen, Edge waves on complex beach profiles, *J. Geophys. Res., 84,* 6339-6346, 1979.

Holman, R. A., Infragravity wave energy in the surf zone, *J. Geophys. Res., 86,* 6422-6450, 1981.

Holman, R. A. and A. J. Bowen, Bars, bumps, and holes: Models for the generation of

complex beach topography, *J. Geophys. Res., 84,* 457-468, 1982.

Holman, R. A. and A. J. Bowen, Longshore structure of infragravity wave motions, *J. Geophys. Res., 89,*6446-6452,1984.

Holman, R. A. and A. H. Sallenger, Setup and swash on a natural beach, *J. Geophys. Res., 90,* 945-953, 1985.

Howd, P. A., J. Oltman-Shay, and R. A. Holman, Wave variance partitioning in the trough of a barred beach, *J. Geophys. Res., in press,* 1991a.

Howd, P. A., A. J. Bowen, R. A. Holman, and J. Oltman-Shay, Infragravity waves, longshore currents and linear sand bar formation, *Proceedings, Coastal Sediments '91,* 1991b.

Hunt, J. N., and B. Johns, Current induced by tides and gravity waves, *Tellus, 15,* 343-351, 1963.

Huntley, D. A., R. T. Guza, and E. B. Thornton, Field observations of surf beat, 1. Progressive edge waves, *J. Geophys. Res., 86,* 6451-6466, 1981.

Kenyon, K. E., Wave refraction in ocean currents, *Deep Sea Res., 18,* 1023-1034, 1971.

Kenyon, K. E., Edge waves with current shear, *J. Geophys. Res., 77,* 6599-6603, 1972.

Kirby, J. T., R. A. Dalrymple, and P. L.-F. Liu, Modification of edge waves by barred beach topography, *Coastal Engineering, 5,* 35-49, 1981.

Lippmann, T. C. and R. A. Holman, The spatial and temporal variability of sand bar morphology, *J. Geophys. Res., 95,* 11575-11590, 1990.

Oltman-Shay, J. and R. T. Guza, Infragravity edge wave observations on two California beaches, *J. Phys. Ocean., 17,* 644-663, 1987.

Oltman-Shay, J., P. A. Howd, and W. A. Birkemeier, Shear instabilities of the mean longshore current, 2: Field data, *J. Geophys. Res., 94,* 18031-18042, 1989.

Press, W. H., B. P. Flannery, S. A. Teukolsky, and W. T. Vetterling, Numerical Recipes: The Art of Scientific Computing, Cambridge Univ. Press, New York, 1986

Sallenger, A. H., R. A. Holman and W. A. Birkemeier, Storm-induced response of a nearshore-bar system, *Marine Geology*, *64*, 237-257, 1985.

Short, A. D., Multiple offshore bars and standing waves, *J. Geophys. Res.*, *80*, 3838-3840, 1975.

CHAPTER FOUR:
INFRAGRAVITY WAVES, LONGSHORE CURRENTS,AND LINEAR SAND BAR FORMATION

Abstract

A new hypothesis regarding the role of infragravity waves in controlling the formation and offshore migration of linear (2-dimensional) sand bars is presented. The hypothesis is dependent on the modification by strong longshore currents of the apparent beach profile felt by edge waves A simple formulation for this effective beach profile is presented. An initial test of the hypothesis that the true profile responds to the effective profile is accomplished using data collected at the DELILAH experiment. The results are encouraging.

Introduction

The formation and subsequent migration of linear bars and bar systems is a problem that coastal researchers have pondered for many decades. Numerous theories have been proposed, and can be roughly broken into two groups: those relying on incident wave characteristics and their related cross-shore flow structure [*Miller*, 1976; *Dally*, 1987, among many], and a second group focussing on the role of infragravity waves [for instance *Bowen*, 1980; *Holman and Bowen*, 1982].

The most attractive of the incident wave theories rely on the wave-driven mean cross-shore flow, the 'undertow', to transport sediment to the breakpoint where the current disappears and a sand bar should form. Studies of sand bar formation in wave flumes tend to support this theory [*Sunamura and Maruyama*, 1987; *Dally*, 1987, among many others), however, field studies have indicated that the bar crest location does not appear to be consistently tied to the 'breakpoint' position [*Sallenger and Howd*, 1989]. The possible role of incident wave skewness and asymmetry changes across the surf zone is an interesting, and ongoing topic of investigation.

Theories linking infragravity waves to bar formation began with the recognition that both the cross-shore and alongshore length scales of the bars and the waves were similar. Unlike reflected incident waves, which have nodes every 10-20 m in the cross-shore, infragravity wave nodes are typically spaced at 100-200 m intervals, closely matching the observed scales of sand bar spacing [*Short*, 1975; *Bowen*, 1980]. The results of *Holman and Bowen* [1982] convincingly show how many of the naturally occurring beach topographies may be explained in terms of the drift velocity pattern of interacting edge waves.

Introduction of barred topography produces kinematic changes in edge waves [*Holman and Bowen*, 1979; *Kirby et al.*, 1981). *Kirby et al.* [1981] present numerical solutions which show two kinematic effects, the relative amplification of edge wave amplitudes away from the shoreline (compared to the plane beach case) and distortion of edge wave shapes so that nodes in the cross-shore current are attracted to the bar crest. Their results provide a mechanism for the stabilization of the bar crest in a preferred cross-shore location (the node of cross-shore velocity).

In the next section we will briefly, and to a large extent conceptually, explore the role of the cross-shore structure of the mean longshore current, $V(x)$, in modifying the structure of edge waves in the nearshore. We will show that the effect of the current is to produce an easily calculated 'effective profile' which we hypothesize to be responsible for evolution of the true topography. A first test of this hypothesis is presented in the Results section.

Theory

One conceptual approach to understanding low frequency waves in the nearshore is through the concept of a wave guide. A wave guide, either in a fluid such as the ocean, or in a solid such as the earth's crust, is simply a zone which contains a celerity minimum. The nearshore, where wave celerities are a function of the water depth, has a velocity minimum at the shoreline. The simplest nearshore wave guide, mathematically and otherwise, is a plane sloping beach (Figure IV.1). How low frequency waves behave in this wave guide differentiate two types of surface gravity waves. Edge waves are the discrete set of resonant motions trapped in the nearshore wave guide by reflection at the shoreline and refraction offshore. Leaky waves are those free waves which escape from the nearshore wave guide to deep water upon reflection from the shoreline. A critical alongshore wavenumber, $\kappa = 2\pi/L$, of the motion separates the two regimes with leaky waves satisfying $|\kappa| < \sigma^2/g$ and edge waves falling in the range $\sigma^2/g < |\kappa| < \sigma^2/g\beta$ on a plane beach (σ is the radial frequency, g is the acceleration of gravity, and β the beach slope). The sign of κ determines the direction of wave progression.

There are two common properties of the nearshore which act to modify the wave guide, sand bars and longshore currents (Figure IV.2). Sand bars modify the wave guide by changing the water depth, thus modifying the celerity of waves. The sand bar crest, a depth minimum, is also the location of a local celerity minimum. This can be thought of as providing a focussing of wave rays at that location regardless of the direction of wave propagation. A longshore current modifies the wave guide in a more complicated manner. Those infragravity waves travelling into the current experience 'refractive focussing' at the cross-shore location of the maximum longshore current. This response is very similar to the sand bar case. Infragravity waves travelling with

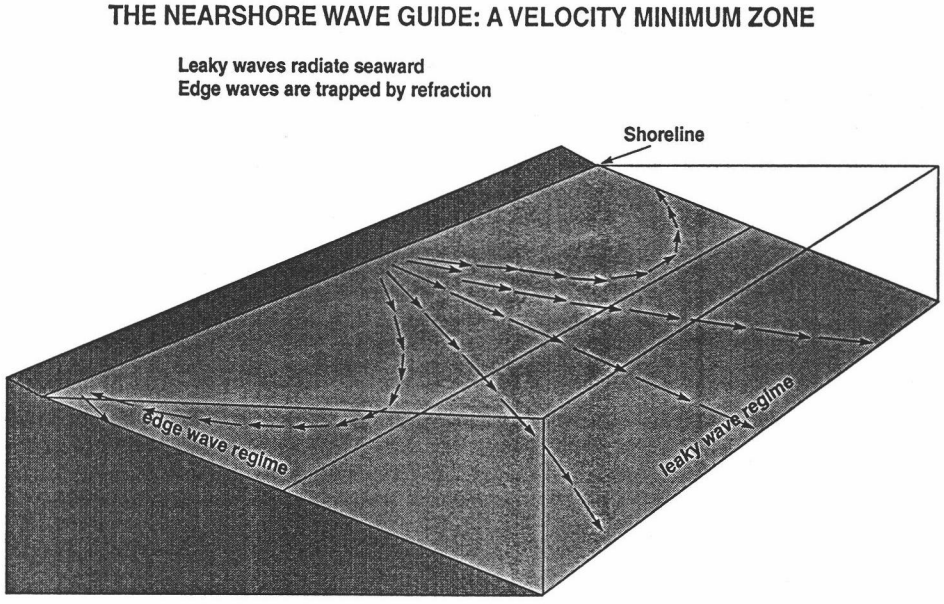

Figure IV.1. The nearshore wave guide for the simple case of a plane sloping beach. Edge waves are trapped to the shoreline by refraction while leaky waves escape seaward.

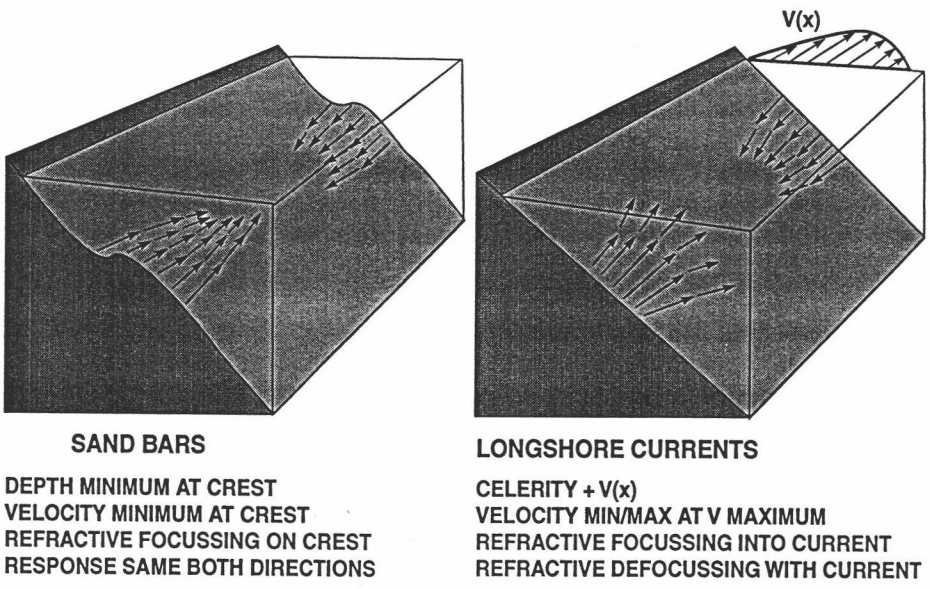

Figure IV.2. Modification of the nearshore wave guide by either sand bars or longshore currents.

the current are defocussed at the longshore current maximum.

This conceptual treatment of the nearshore as a wave guide can be formalized in a theoretical description of edge wave behavior by inclusion of variable topography and longshore currents in the relevant governing equations. *Holman and Bowen* [1979] previously included the effects of arbitrary topography as have *Kirby et al.* [1981]. *Howd et al.* (in prep.) were the first to include the effect of arbitrary longshore current as well. They make three assumptions in their derivation. First, that the total velocity vector can be written as $U = (u, v+V)$, where the lower case variables, u and v, refer to the edge wave orbital velocities in the cross-shore and alongshore directions, V to the longshore current and $u,v<<V$. Second, they keep the resulting equations linear in u and v; and third, they assume a wavelike solution of the form $f(x,y,t) = \phi(x)e^{i(\kappa y-\sigma t)}$.

Applying these assumptions and definitions, and substituting in the equations for conservation of mass and momentum results in the equation

$$\left[\frac{gh\eta_x}{(-\sigma+\kappa V)^2}\right]_x + \eta\left[1-\frac{\kappa^2 gh}{(-\sigma+\kappa V)^2}\right] = 0 \qquad \text{(IV.1)}$$

where η is the surface elevation of the edge wave, h is the water depth, and g is gravity. Subscripts indicate differentiation. It is understood that η, V, and h are all functions of the cross-shore direction, x. In the case of V(x) = 0, this reduces to the classical edge wave equation (*Eckart*, 1951)

$$\left[\frac{gh\eta_x}{\sigma^2}\right]_x + \eta\left[1-\frac{\kappa^2 gh}{\sigma^2}\right] = 0 \qquad \text{(IV.2)}$$

Of particular interest to this paper is the observation that if we make the substitution in (1) of

$$h'(x) = \frac{h(x)}{\left[1-\frac{V(x)}{c}\right]^2} \qquad \text{(IV.3)}$$

where $h'(x)$ is defined as the effective beach profile and $c = \sigma/\kappa$ is the edge wave celerity, we get the result

$$\left[\frac{gh'\eta_x}{\sigma^2}\right]_x + \eta\left[1 - \frac{\kappa^2 gh'}{\sigma^2}\right] = 0 \qquad \text{(IV.4)}$$

which is functionally identical to the classical edge wave solution of (2). This shows that the effective beach profile, $h'(x)$ as given by (3), is the beach profile which determines the modification of the edge wave dispersion relation and cross-shore dependence of u, v, and η. It is important to note that $h'(x)$ derives its x-dependence from the true beach profile, $h(x)$, and the cross-shore structure of the longshore current, $V(x)$, not from the magnitude of the celerity. The magnitude of the celerity does influence the degree of amplification of features in the effective profile. The form of the effective profile is influenced by the sign of the celerity, as one might guess from the discussion of Figure IV.2.

Figure IV.3 shows the effective beach profiles for two edge waves on a plane beach in the presence of a longshore current along with the solution for the cross-shore shape of the cross-shore component of edge wave orbital velocity. There are two points to be made with this figure; that effective beach profiles may take familiar looking shapes, and that these shapes modify edge waves in an identical manner as true topography. For the edge wave progressing into the current (the dashed lines) the effective profile shows what could be interpreted as a bar crest or terrace edge at the location of the maximum of the longshore current, and the second node of the cross-shore flow is attracted to that location as well. For the edge wave progressing with the current (solid lines) the effective profile shows a 'trough' at the location of the current maximum and a 'bar crest' further offshore. Again the node is attracted to the bar crest as predicted by *Kirby et al.*, [1981].

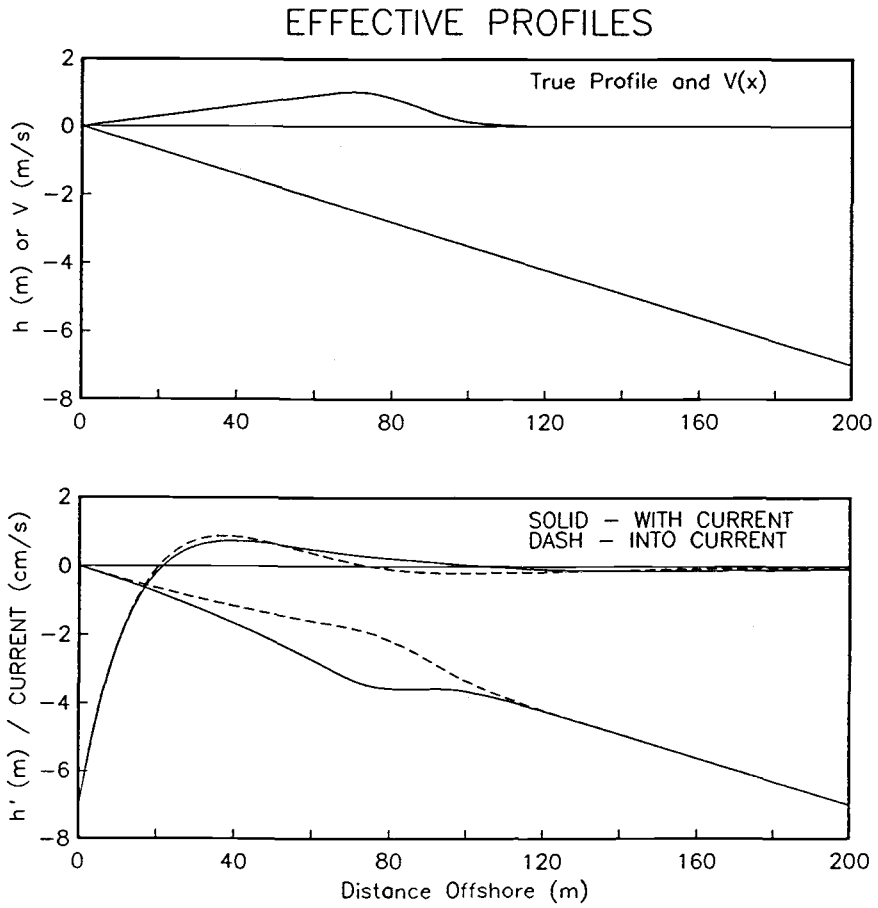

Figure IV.3. Effective beach profiles for a mode 2 edge wave in the presence of a longshore current. The current and true beach profile are shown in the top panel. The current reaches a maximum of 1 ms^{-1} 70 m offshore. The bottom panel shows the effective beach profiles and the shape of the cross-shore component of the edge wave velocity field.

It was the observation of these familiar looking effective profiles and the resulting modification of the edge waves which lead us to hypothesize the following scenario. Strong longshore currents and a dominant direction of edge wave progression combine to produce an effective beach profile significantly different from the true profile. The edge waves are modified by the current such that the result is the true profile moving toward the configuration of the effective profile. Thus we hypothesize that offshore migration of linear sand bars is due (at least in part) to the modification of progressive edge waves by the longshore current. We will test this hypothesis in the next section, but first it is instructive to give the conditions which need to be met by the field data in order to test this hypothesis. First, we need the profile to evolve in the presence of strong longshore currents. Next, the infragravity wave field should be dominated by edge waves (as opposed leaky waves) and they should be dominated by one direction of progression. This will result in a dominant effective beach profile, rather than a mix of two shapes (refer to Figure IV.3). Finally, we clearly desire a period of two-dimensional profile change as the theory does not address alongshore gradients of topography or mean currents.

Field Study

The data used for this study were collected as part of DELILAH, a large multi-agency experiment hosted by the Coastal Engineering Research Center's Field Research Facility (FRF) in Duck, North Carolina during October, 1990. This beach is located on the mid-Atlantic coast of the United States in the center of a 100-km long barrier spit. The mean foreshore slope is approximately 1:10 and decreases offshore to 1:100. Sand bars are common, are usually three-dimensional, but become linear during storms [*Lippmann and Holman*, 1990]. Storms are also commonly accompanied by strong longshore currents [*Oltman-Shay et al.*, 1989].

The primary source of data for this work was an array of bidirectional electromagnetic current meters deployed in the surf zone (Figure IV.4). Sensors were oriented such that $+V$ currents (alongshore) flow 'south' parallel to the beach. The gages were hard wired to a computer-based collection system and were sampled at 8 Hz nearly continuously for a three week period. The inner alongshore array of current meters (approximately 55m offshore in 2m water depth, hereafter referred to as the 2m array) remained submerged at all stages of the tide. The incident wind wave climate was sampled in 8 m depth using a 255 m long array of 9 bottom mounted pressure sensors (the 8m array). The FRF provided daily surveys of the nearshore zone.

The 2m array current meter data were used to calculate the alongshore wavenumber-frequency spectra for both the cross-shore and alongshore components of flow. First, 3-hour time series were extracted from the original longer records in order to bracket either high or low tide. Following routine processing, alongshore wavenumber-frequency spectra were estimated using the Iterative Maximum Likelihood Estimator (IMLE) previously applied to surf zone data by *Oltman-Shay and Guza* [1987] and *Olt-*

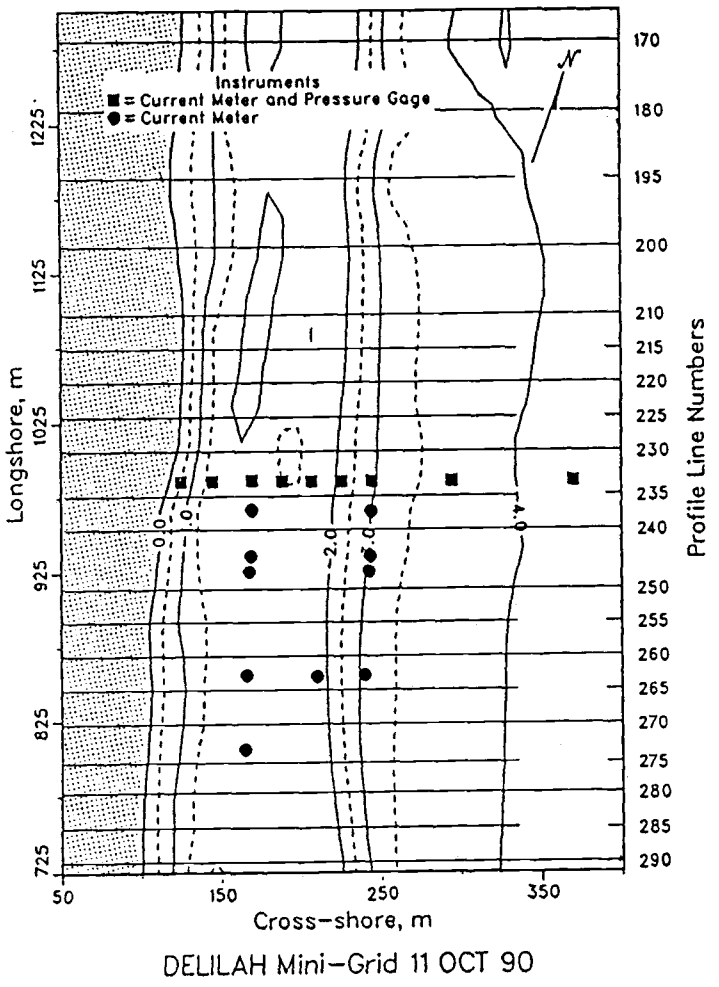

Figure IV.4. Layout of the DELILAH instrument array at the FRF. The FRF pier is located at x=560 m, well south of the instrument locations.

man-Shay et al. [1989]. The cross-shore array of current meters has allowed us to define the $V(x)$ profile. The 8m pressure sensor array allowed similar alongshore wavenumber-frequency analysis and provided estimates of incident wave height, direction, and period.

Results

For the purposes of this paper we will concentrate on the period from late on October 9 to early in the day on October 12. This roughly 3 day period was the time of most active bar migration during the DELILAH experiment. Figure IV.5 presents time series of relevant offshore wave and wind characteristics. Wave height at the 8m array reached a maximum of 2.0 m early in the morning of the 11^{th}. The peak direction at that time was 40 degrees south of shore normal, and the peak period was 7.6 s.

Accompanying the increase in wave height and wind speed was the formation and migration of a linear bar. Figure IV.6 shows the evolution of profile line 235, located near the cross-shore array of sensors. There is little change in the profile between the mornings of the 9^{th} and 10^{th}, active offshore migration between the 10^{th} and 11^{th}, with lesser change again by the morning of the 12^{th}. In all, the bar migrated 21 m seaward during this period

In order to evaluate our hypothesis for this example of bar migration, several conditions must be shown to exist. First, we will show strong longshore currents were present; second, the infragravity wave field was dominated by unidirectional edge waves; and third, while not shown, the evolution of the beach profile was essentially a two-dimensional process. We will now turn our attention to these points. If the effective profile shows evolution which precedes the evolution of the true profile, then further, more detailed testing of the hypothesis should be undertaken.

Throughout this time period the longshore current was strong (O 1m/s) and from the south. Figure IV.7 shows the 3-hour mean V(x) at selected times during the period of bar migration. The data from the working cross-shore current meters were horizon-

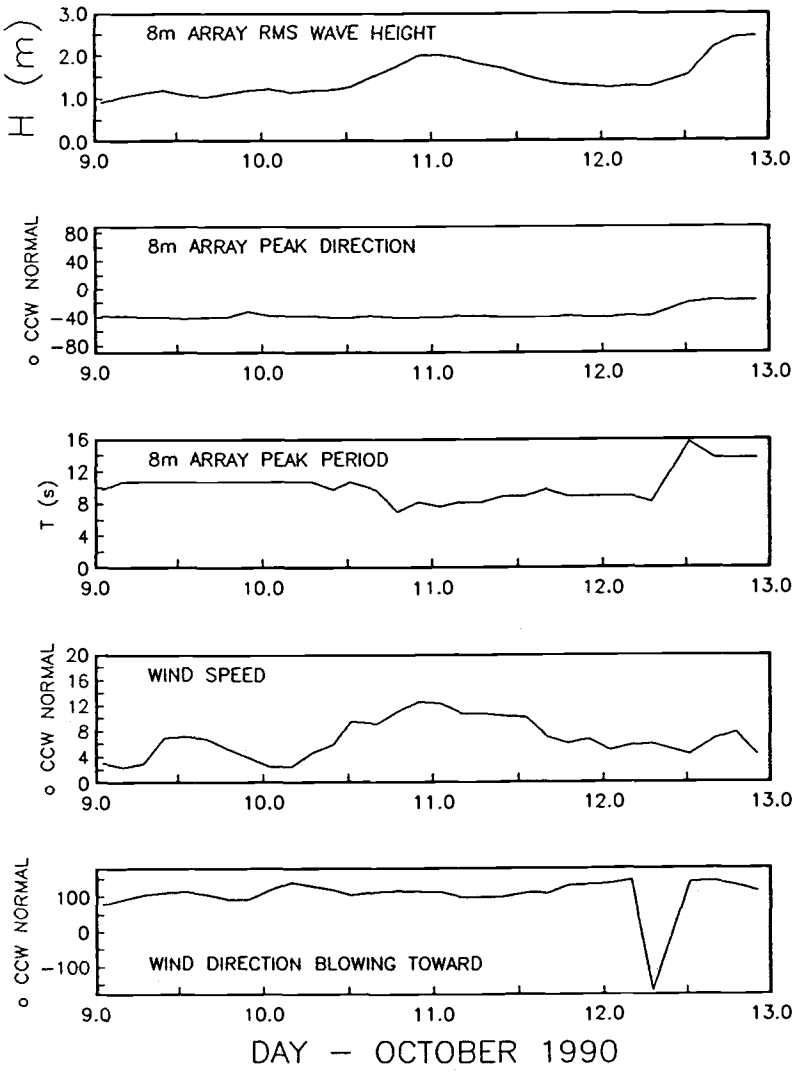

Figure IV.5. Time series of incident wave parameters and wind speed and direction. The wave measurements are from pressure sensors in the 8m array. The anemometer was located above the FRF building. All directions are reported in degrees counterclockwise from shore-normal and are the direction from which the waves are coming and toward which the wind is blowing. Measurements courtesy of Chuck Long, FRF.

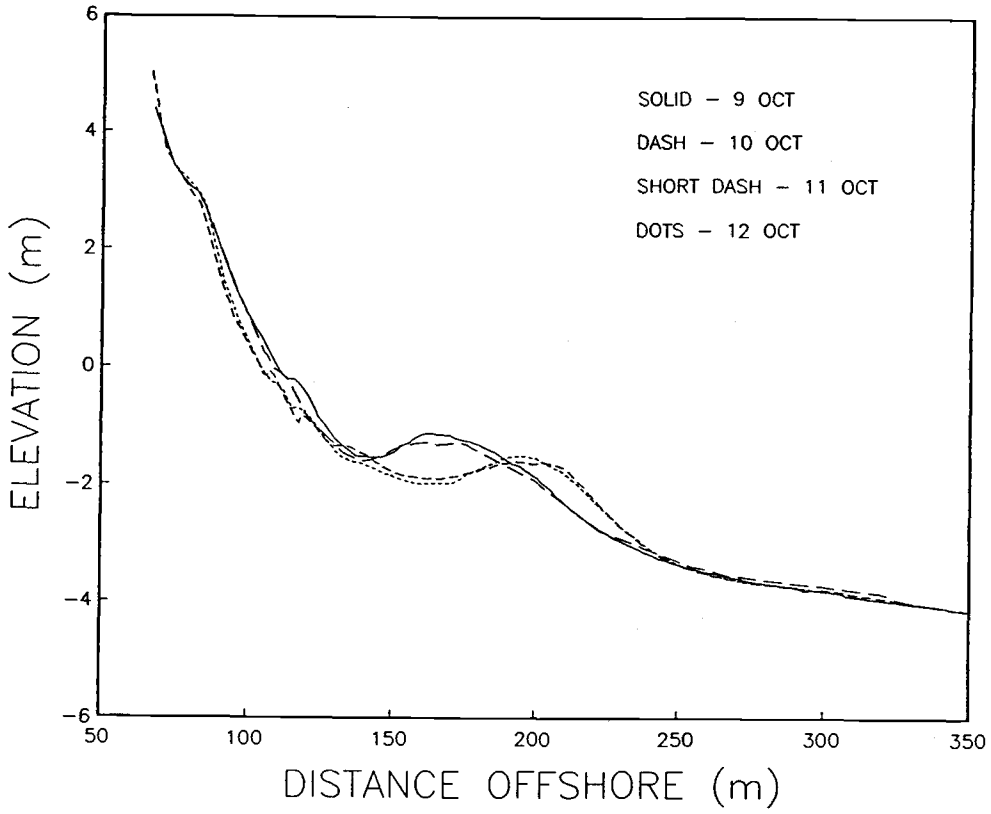

Figure IV.6. Beach profile evolution. Survey data courtesy Bill Birkemeier, FRF.

tally shifted (based on the tide) to a common shoreline at x=0. Shifts were typically in the range of 115-125 m. Interestingly, the maximum longshore current was always located in the bar trough.

The infragravity wave field was found to be strongly directional and dominated by edge waves. The direction of progression was north, as was the current. The dominance of edge waves over leaky waves is most vividly seen in data from the 8m array, but is also visible in k-f spectra calculated using the 2m array data. Typical examples are shown in Figure IV.8. Spectra dominated by leaky waves would have concentration of energy about k = 0. This is clearly not the case for these data.

The final check in this preliminary evaluation of this hypothesis is to look at the evolution of the effective profile as defined by (3). This is shown in Figure IV.9. As the infragravity wave field is dominated by edge waves progressing in the direction of the current, a representative frequency (f = 0.02 Hz) and wavenumber ($k = 1/L$ = -0.0025) were chosen for presentation. Remember, the form of the effective profile, that is, the location of the effective trough and crest, are determined by the cross-shore variability of the longshore current and the true profile, not by the magnitude of the edge wave celerity. It is clear that as the storm progresses, the effective profile evolves in much the same manner as the true profile (Figure IV.6). The initial response of the effective profile is for the trough to deepen as the current increases late on the 10th, and for clear offshore migration of the effective bar crest on the 11th and early on the 12th.

Figure IV.10 shows the relationship between the offshore distances to the effective bar crest and to the true bar crest. In all cases the bar crest was defined as the cross-shore location of the local depth minimum associated with the bar topography. We made 8 estimates of the effective bar crest location, and there were four surveys of the

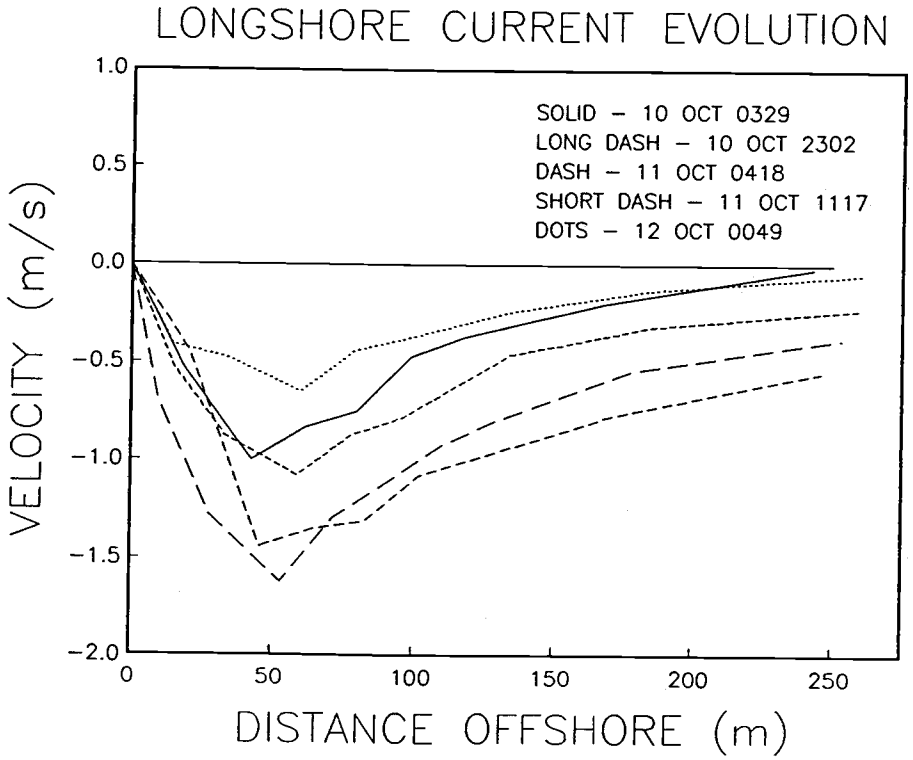

Figure IV.7. Evolution of the mean longshore current during the period of active sand bar migration. Times indicate the start time of the 3 hour averages.

Figure IV.8. Frequency-wavenumber spectra from late on October 10. From the left, the data are from the 8m pressure array, the alongshore flow component of the 2m array, and from the cross-shore flow component of the 2m array. The shaded boxes represent concentrations of variance in f-k space, with darker shading indicating a greater percentage. The solid lines mark the dispersion curve for mode 0 edge waves on a plane beach of slope 0.05, while the dots mark the numerical solutions for modes 0 and 1 taking into account the true profile and $V(x)$. The two solid-line dispersion curves closely bracketing $k = 0$ mark the leaky-edge wave cutoff. Clearly, the dominant infragravity wave energy falls in the edge wave regime, with the negative wavenumbers indicating nothward progression (in the direction of the longshore current). Also visible in the 2m array data at negative wavenumbers with magnitudes larger than the mode 0 edge wave is the distinctive shear wave pattern.

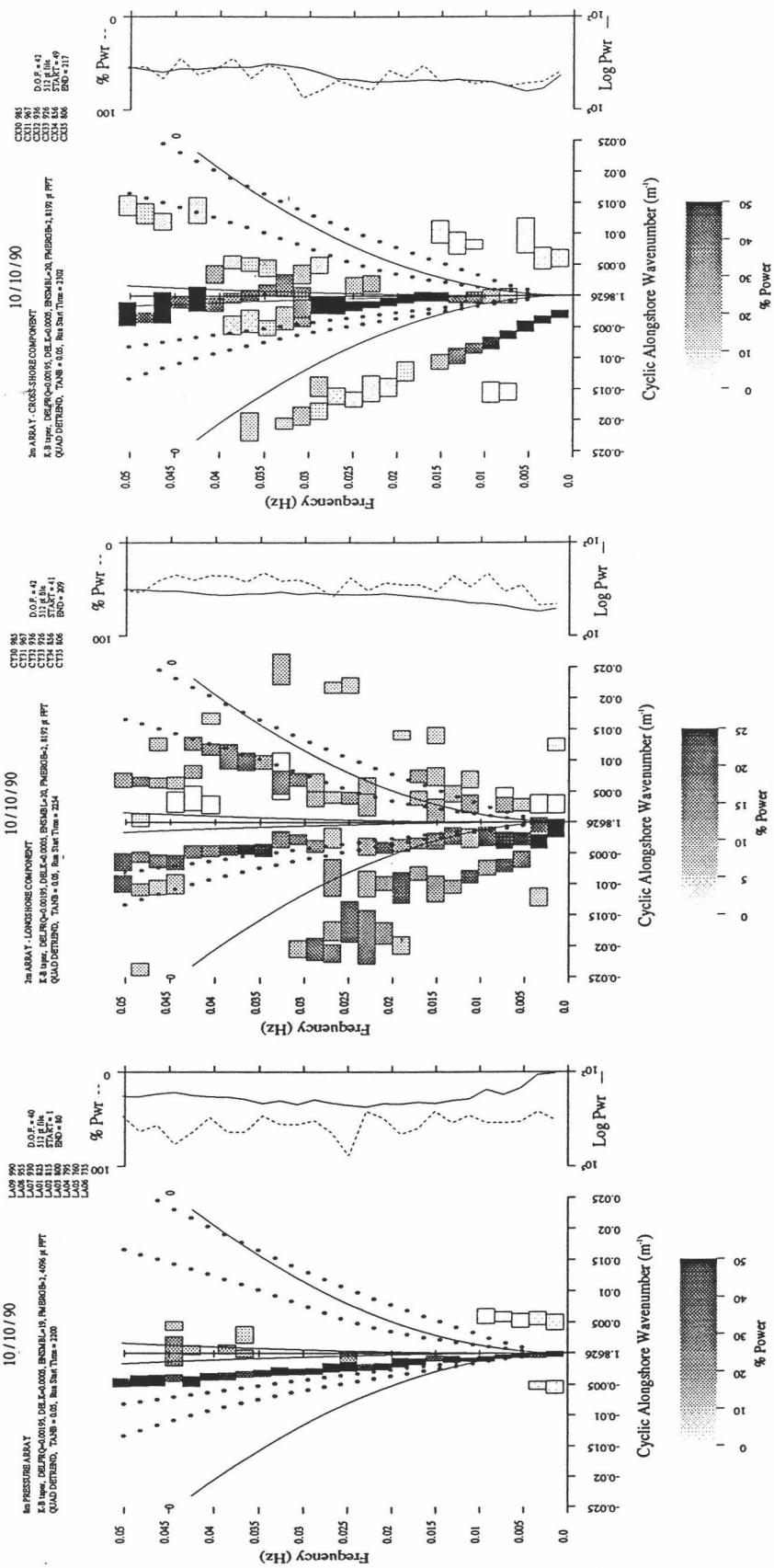
10/10/90
Cyclic Alongshore Wavenumber (m⁻¹)
Frequency (Hz)
% Power
% Pwr
Log Pwr

Figure IV.8.

true morphology during this period. It is clear that while the current remained large, the effective bar crest was located seaward of the true bar crest position and bar migration was in the direction of the effective bar crest.

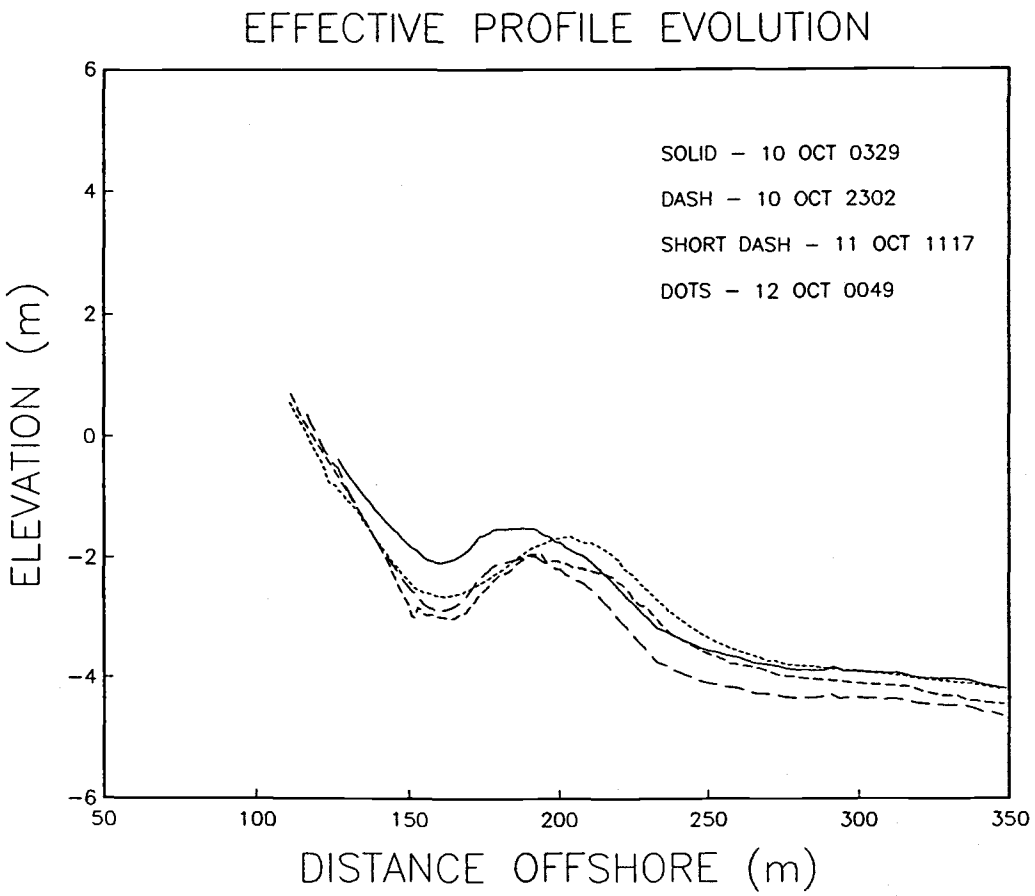

Figure IV.9. Evolution of the effective beach profile through the storm. The response clearly mimics the evolution of the true profile.

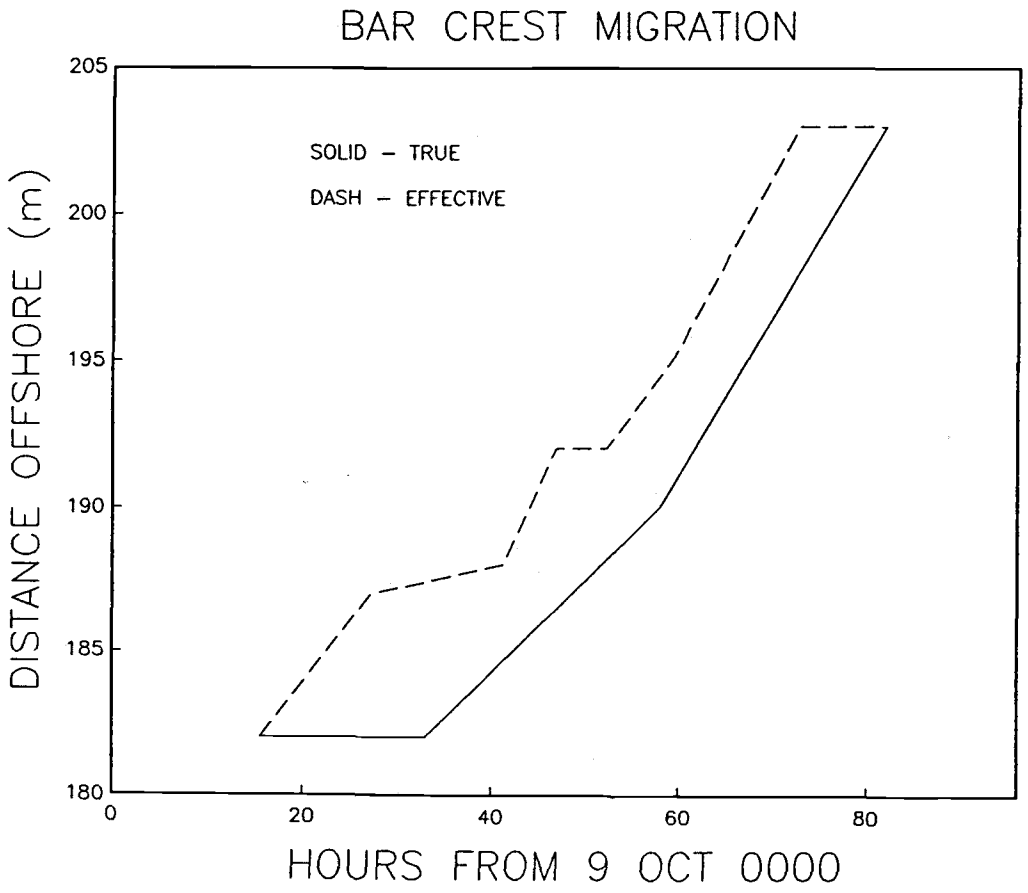

Figure IV.10. The offshore migration of the effective bar crest clearly leads the offshore migration of the true bar crest.

Summary

We have demonstrated that the concept of the effective beach profile may be useful in examining the cause and effect of nearshore morphological evolution. The preliminary results of this analysis suggest that the true profile evolves in a direction toward the effective profile. This is in agreement with earlier results, particularly those of *Kirby et al.* [1981] that suggested bars may well modify edge waves in a manner consistent with enhancement of the bar shape. In this case, the bar shape is that provided by the effective beach profile. A clear goal of future work will be a careful examination of the modification of edge wave drift velocities by mean longshore currents, much in the manner of *Holman and Bowen* [1982]. If the proposed hypothesis is found to withstand further scrutiny, it may well be that longshore currents are responsible for the formation and evolution of nearshore bar systems in ways we had not imagined.

References

Bowen, A.J., Simple models of nearshore sedimentation; Beach profiles and longshore bars, in *The Coastline of Canada*, S.B. McCann, ed.; Geological Survey of Canada, p 1-11., 1980.

Dally, W.R., Longshore bar formation - surf beat or undertow?, *Proc. Coastal Sediments '87*, ASCE, New York, pp 71-86, 1987.

Eckart, C., Surface waves in water of variable depth, *Scripps Inst. of Oc. Ref. 51-12*, Scripps Institute of Oceanography, La Jolla, CA., 1951.

Holman, R.A. and A.J. Bowen, Edge waves on complex beach profiles, *J. Geophys. Res.* 84: 6339-6346, 1979.

Holman, R.A. and A.J. Bowen, Bars, bumps and holes: Models for the generation of complex beach topography, *J. Geophys. Res.*, 87: 457-468, 1982.

Howd, P.A., A.J. Bowen, and R.A. Holman, in prep., Edge waves in the presence of strong longshore currents, 1991.

Kirby, J.T., R.A. Dalrymple, and P. Liu, Modification of edge waves by barred-beach topography, *Coastal Engineering*, 5: 35-49, 1981.

Lippmann, T.C. and R.A. Holman, The spatial and temporal variability of sand bar morphology, *J. Geophys. Res.*, 95: 11575-11590, 1990.

Miller, R.L., Role of vortices in surf zone prediction: sedimentation and wave forces. In: R.A. Davis and R.L. Ethington (editors), *Beach and Nearshore Sedimentation, Soc. Econ. Paleon. Mineral., Spec. Pub., 24*: 92-114, 1976.

Oltman-Shay, J., P.A. Howd, and W.A. Birkemeier, Shear instabilities of the mean longshore current; II. Field observations, *J. Geophys. Res.* 94: 18031-18042, 1989a.

Oltman-Shay, J. and R.T. Guza, Infragravity wave observations on two California

beaches, *J. Physical Oc.*, 17: 644-663, 1987.

Sallenger, A.H., and P.A. Howd, 1989, Nearshore bars and the breakpoint hypothesis, *J. Coastal Engineering*, 12: 301-313, 1989.

Short, A.D., Multiple offshore bars and standing waves, *J. Geophys. Res.*, 80: 3838-3840, 1975.

Sunamura, T. and K. Maruyama, Wave induced geomorphic response of eroding beaches with special reference to seaward migrating bars. *Proc. Coastal Sediments '87*, ASCE, pp. 788-801, 1987.

CHAPTER FIVE: GENERAL CONCLUSIONS

The wave-induced velocity field in the nearshore is composed of contributions from incident wind waves ($f > 0.05$ Hz), surface infragravity waves ($f < 0.05$ Hz, $|\kappa| < (\sigma^2/g\beta)$ and shear waves ($f < 0.05$ Hz, $|\kappa| > \sigma^2/g\beta$), where f is the frequency, $\sigma = 2\pi f$, κ the radial alongshore wavenumber ($2\pi/L$, L being the alongshore wavelength), β is the beach slope, and g is the acceleration due to gravity. Using an alongshore array of current meters located in the trough of a nearshore bar (mean depth $\approx$ 1.5 m), we investigated the bulk statistical behaviors of these wave bands over a wide range of incident wave conditions. The behavior of each contributing wave type was parameterized in terms of commonly measured or easily predicted variables describing the beach profile, wind waves, and current field.

Over the 10 day period, the mean contributions (to the total variance) of the incident, infragravity and shear wave bands were 71.5%, 14.3% and 13.6% for the alongshore component of flow (mean rms values of 44 cm s^{-1}, 20 cm s^{-1}, and 19 cm s^{-1} respectively), and 81.9%, 10.9%, and 6.6% for the cross-shore component (mean rms oscillations of 92 cm s^{-1}, 32 cm s^{-1}, and 25 cm s^{-1}, respectively). However, the values varied considerably. The contribution to the alongshore (cross-shore) component of flow ranged from 44.8%-88.4%, (58.5%-95.8%) for the incident band, 6.2%-26.6% (2.5%-32.4%) for the infragravity band, and 3.4%-33.1% (0.6%-14.3%) for the shear wave band.

Incident wave oscillations were limited by depth-dependent saturation over the adjacent bar crest and varied only with the tide. The infragravity wave rms oscillations on this barred beach are best parameterized by the offshore wave height, consistent with previous studies on planar beaches. Comparison with data from four other beaches of widely differing geometries shows the shoreline infragravity amplitude to be a near

constant ratio of the offshore wave height. The magnitude of the ratio is found to be dependent on the Iribarren number, $\xi_0 = \beta(H/L_0)^{-1/2}$. Shear waves are, as previous observation and theory suggest [*Oltman-Shay et al.*, 1989*a*; *Bowen and Holman*, 1989], significantly correlated with a prediction of the seaward-facing shear of the longshore current.

It is well known that currents are capable of refracting surface gravity waves in much the same manner as variable water depth. Thus longshore currents are expected to modify refraction in the nearshore wave guide, changing the dynamics and kinematics of edge waves. A form of the linear, inviscid shallow water wave equation which includes arbitrary longshore currents and bathymetry is derived. This formulation provides a continuum between gravity waves (either leaky or edge waves) on a longshore current, and the recently discovered shear waves. In this paper we will concentrate on gravity wave solutions for which $|V/c| < 1$, where V is the longshore current, and c is the edge wave alongshore celerity. Interestingly, for gravity waves, the current effects can be uniquely accounted for in terms of a modification to the true beach profile, allowing the definition of the 'effective beach profile', $h'(x) = h(x)\left[1 - \frac{V(x)}{c}\right]^{-2}$, where $h(x)$ is the true profile. The effective profile is particularly useful in conceptualizing the combined effects of longshore currents and variable bottom topography.

To test the sensitivity of edge waves to mean longshore currents, we have numerically solved for the dispersion relationship and the cross-shore shapes of edge waves on a plane beach under a range of current conditions. Changes to the edge wave alongshore wavenumber, κ, of nearly 100% are found for reasonable current profiles, showing that the departure from plane beach dispersion due to longshore currents can be of the same order as the effect of introducing non-planar topography. These changes are not symmetric as they are for profile changes; $|\kappa|$ increases for edge waves opposing the

current flow (a shallower effective profile), but decreases for those coincident with the flow (a deeper effective profile). The cross-shore structure of the edge waves is also strongly modified. As expected, as $|\kappa|$ increases (decreases), the nodal structure shifts landward (seaward) from the positions found on the test beach in the absence of a current. In addition, the predicted variances away from the nodes, particularly for the alongshore component of edge wave orbital velocity, may change dramatically from the no-current case. Failure to account for these changes can lead to incorrect identification of modes and large errors in the estimation of the corresponding shoreline amplitude.

The magnitudes of many of the edge wave responses are related to the ratio V_{max}/c, where V_{max} is the maximum current, and to the dimensionless cross-shore scale of the current, $|\kappa|x(V_{max})$, where $x(V_{max})$ is the cross-shore distance to V_{max}. This is most easily understood in terms of the effective profile and the strong dependence of the edge waves to the details of the inner part of the beach profile.

Inclusion of the longshore current also has implications regarding the role of edge waves in the generation of nearshore morphology. The modifications to the wavenumbers of any two phase locked edge wave modes will change the morphology of a potentially resulting sand bar. For example, in the absence of a current, two phase locked edge waves of equal frequency and mode progressing in opposite directions are expected to produce a crescentic bar. However, in the presence of a current, the wavenumbers would differ, stretching the expected crescentic bar into a welded bar. A more interesting effect is the possibility that modifications to the edge waves due to the presence of a virtual bar in the effective profile could lead to the development of a real sand bar on the true profile. These modifications appear to be only weakly sensitive to frequency, in contrast to the relatively strong dependence of the traditional model for sand bar generation at infragravity wave nodes.

We have demonstrated that the concept of the effective beach profile may be useful in examining the cause and effect of nearshore morphological evolution. The preliminary results of this field data analysis suggest that the true profile evolves in a direction toward the effective profile. This is in agreement with earlier results, particularly those of *Kirby et al.* [1981] that suggested bars may well modify edge waves in a manner consistent with enhancement of the bar shape. In this case, the bar shape is that provided by the effective beach profile. A clear goal of future work will be a careful examination of field data for the modification of edge wave drift velocities by mean longshore currents, much in the manner of the methods of Chapter Three. If the proposed hypothesis is found to withstand further scrutiny, it may well be that longshore currents are responsible for the formation and evolution of nearshore bar systems in ways we had not imagined.

BIBLIOGRAPHY

Ball, F. K., Edge waves in an ocean of finite depth, *Deep Sea Res.,14*,79-88, 1967.

Birkemeier, W.A. and C. Mason, The CRAB: a unique nearshore surveying vehicle, *J. Surv. Eng.*, Am. Soc. Civ. Eng. 110, 1-7, 1984.

Bowen, A., D. Inman, and V. Simmons, Wave setdown and setup, *J. Geophys. Res.*, 37, 206-215, 1968.

Bowen, A. J., and D. L. Inman, Rip currents: 2. Laboratory and field observations, *J. Geophys. Res., 74*, 5479-5490, 1969.

Bowen, A. J. and D. L. Inman, Edge waves and crescentic bars, J. *Geophys. Res., 76,* 8662-8671, 1971.

Bowen, A. J., Simple models of nearshore sedimentation; beach profiles and longshore bars, in *Proceedings of the Coastlines of Canada Conference*, p. 1-11, 1980.

Bowen, A. J. and R. A. Holman, Shear instabilities of the mean longshore current: 1. Theory, *J. Geophys. Res., 94,* 18023-18030, 1989.

Crowson, R., W. Birkemeier, H. Klein, and H. Miller, SUPERDUCK nearshore processes experiment: Summary of studies CERC Field Research Facility, *US Army Tech. Report CERC-88-12,* 1988.

Dally, W.R., Longshore bar formation - surf beat or undertow?, *Proc. Coastal Sediments '87*, ASCE, New York, pp 71-86, 1987.

Eckart, C., Surface waves in water of variable depth, *Wave Rep. 100, Ref. 51-12*, 99 pp., Scripps Inst. of Oceanogr., Univ. of Calif., La Jolla, 1951.

Elgar, S. and R.T Guza, Observations of bispectra of shoaling surface gravity waves, *J. Fluid Mech.*, 161, 425-448, 1985.

Elgar, S., J. Oltman-Shay, and P.Howd, Observations of infragravity-frequency long waves; I. Coupling to wind waves, *EOS, Trans., Am. Geophys. Union*, 70, 1333, 1989.

Gallagher, B., Generation of surf beat by non-linear wave interactions, *J. Fluid Mech., 49*, 1-20, 1971.

Galvin, C. and P. Eagleson, Experimental study of longshore currents on a plane beach, *US Army CERC Tech. Memo. 10*, 1965.

Guza, R. T. and D. L. Inman, Edge waves and beach cusps, *J. Geophys. Res., 80,* 2997-3012, 1975

Guza, R. and A. Bowen, Resonant interactions for waves breaking on a beach, *Proc. 15th Conf. Coastal Eng.* 560-579, 1976.

Guza, R. T. and E. B. Thornton, Observations of surf beat, *J. Geophys. Res., 90*, 3161-3172, 1985.

Guza, R., E. Thornton, and R. Holman, Swash on steep and shallow beaches, *19th Coastal Engineering Conference Proceedings*, p. 708-723, 1985.

Haines, J. and A. J. Bowen, Phase-locking of modes in the nearshore: Field evidence, *Proc. 21st Conf. Coastal Eng.*, 1522-1534, 1988.

Holman, R.A. and A. J. Bowen, Edge waves on complex beach profiles, *J. Geophys. Res., 84,* 6339-6346, 1979.

Holman, R. A., Infragravity wave energy in the surf zone, *J. Geophys. Res.*, *86,* 6422-6450, 1981.

Holman, R. A. and A. J. Bowen, Bars, bumps, and holes: Models for the generation of complex beach topography, *J. Geophys. Res., 84,* 457-468, 1982.

Holman, R. A. and A. J. Bowen, Longshore structure of infragravity wave motions, *J. Geophys. Res.*, *89*,6446-6452, 1984.

Holman, R. A. and A. H. Sallenger, Setup and swash on a natural beach, *J. Geophys. Res.*, *90,* 945-953, 1985.

Howd, P.A., A.J. Bowen, and R.A. Holman, in prep., Edge waves in the presence of strong longshore currents.

Howd, P. A., J. Oltman-Shay, and R. A. Holman, Wave variance partitioning in the trough of a barred beach, *J. Geophys. Res., in press,* 1991a.

Howd, P. A., A. J. Bowen, R. A. Holman, and J. Oltman-Shay, Infragravity waves, longshore currents and linear sand bar formation, *Proceedings, Coastal Sediments '91*, 1991b.

Hunt, J. N., and B. Johns, Current induced by tides and gravity waves, *Tellus, 15*, 343-351, 1963.

Huntley, D. A., R. T. Guza, and E. B. Thornton, Field observations of surf beat, 1. Progressive edge waves, *J. Geophys. Res., 86,* 6451-6466, 1981.

Huntley, D., Evidence for phase coupling between edge wave modes, *J. Geophys. Res.*, 93, 12393-12408, 1988.

Kenyon, K. E., Wave refraction in ocean currents, *Deep Sea Res., 18*, 1023-1034, 1971.

Kenyon, K. E., Edge waves with current shear, *J. Geophys. Res., 77*, 6599-6603, 1972.

Kirby, J. T., R. A. Dalrymple, and P. L.-F. Liu, Modification of edge waves by barred beach topography, *Coastal Engineering, 5*, 35-49, 1981.

Lippmann, T., The stability and spatial variability of sand bar morphology, MS thesis, 132 p., Oregon State Univ., 1989.

Lippmann, T. and R. Holman, Quantification of sand bar morphology: A video technique based on wave dissipation, *J. Geophys. Res.*, 94, 995-1011, 1989.

Lippmann, T. C. and R. A. Holman, The spatial and temporal variability of sand bar morphology, *J. Geophys. Res., 95*, 11575-11590, 1990.

Long, C. and J. Oltman-Shay, 1989, Directional characteristics of waves in shallow water, *US Army CERC Technical Report*, in press.

Longuet-Higgins, M. and R. Stewart, Radiation stress in water waves; a physical discussion, with applications, *Deep Sea Research*, 11, 529-562, 1964.

Miller, R.L., Role of vortices in surf zone prediction: sedimentation and wave forces. In: R.A. Davis and R.L. Ethington (editors), *Beach and Nearshore Sedimentation, Soc. Econ. Paleon. Mineral., Spec. Pub., 24*: 92-114, 1976.

Oltman-Shay, J. and R. T. Guza, Infragravity edge wave observations on two California beaches, *J. Phys. Ocean., 17*, 644-663, 1987.

Oltman-Shay, J., P. A. Howd, and W. A. Birkemeier, Shear instabilities of the mean longshore current, 2: Field data, *J. Geophys. Res., 94*, 18031-18042, 1989a.

Oltman-Shay, J., S. Elgar, and P.Howd, Observations of infragravity-frequency long waves; II. Comparisons with a 2-D wave group generation model, *EOS, Trans., Am. Geophys. Union*, 70, 1333, 1989b.

Pawka, S., Wave directional characteristics on a partially sheltered coast, Ph.D. dissertation, 246 p. Scripps Inst. of Oceanography, UCSD, 1982.

Pawka, S., Island shadows in wave directional spectra, *J. Geophys. Res.*, 88, 2579-2591, 1983.

Press, W. H., B. P. Flannery, S. A. Teukolsky, and W. T. Vetterling, Numerical Recipes: The Art of Scientific Computing, Cambridge Univ. Press, New York, 1986

Sallenger, A. and R. Holman, On predicting infragravity energy in the surf zone, *19th Coastal Engineering Conference Proceedings*, p. 1940-1951, 1985a.

Sallenger, A. and R. Holman, Wave energy saturation on a natural beach of variable slope, *J. Geophys. Res.*, 90, 11939-11944, 1985b.

Sallenger, A. H., R. A. Holman and W. A. Birkemeier, Storm-induced response of a nearshore-bar system, *Marine Geology*, *64*, 237-257, 1985c.

Sallenger, A. and R. Holman, Infragravity waves over a natural barred profile, *J. Geophys. Res.*, 92, 9531-9540, 1987.

Sallenger, A.H., and P.A. Howd, 1989, Nearshore bars and the breakpoint hypothesis, *J. Coastal Engineering*, 12: 301-313, 1989.

Short, A. D., Multiple offshore bars and standing waves, *J. Geophys. Res.*, *80,* 3838-3840, 1975.

Suhayda, J., Standing waves on beaches, *J. Geophys. Res.*, 72, 3065-3071, 1974.

Sunamura, T. and K. Maruyama, Wave induced geomorphic response of eroding beaches with special reference to seaward migrating bars. *Proc. Coastal Sediments '87*, ASCE, pp. 788-801, 1987.

Thornton, E. and R. Guza, Energy saturation and phase speeds measured on a natural beach, *J. Geophys. Res.*, 87, 9499-9508, 1982.

Thornton, E. and R. Guza, Surf zone currents and random waves: Field data and models, *J. Phys. Oc.*, 16, 1165-1178, 1986.

Weishar, L. and R. Byrne, Field study of breaking wave characteristics, *Proc. 16th Coastal Eng. Conf.*, 1978

Wright, L.D. and A.D. Short, Morphodynamics of beaches and surf zones in Australia, in *CRC Handbook of Coastal Processes and Erosion*, Ed. by P.D. Komar, CRC Press, Boca Raton, FL., 1983.

Wright, L.D., P. Nielsen, N.C. Shi, and J.H. List, Morphodynamics of a bar-trough surf zone, *Marine Geology*, 70, 251-285, 1986.